

THE QUANTUM ELECTRONIC TRANSPORT IN STRONGLY CORRELATED QUANTUM DOT SYSTEM

BY

KAO-CHIN, LIN

A Dissertation submitted to the Graduate School
in partial fulfillment of the requirements
for the Degree

Doctor of Philosophy



Major Subject: Physics

National Chiao-Tung University, Hsinchu 300, Taiwan

May 2005

Copyright 2005 by Kao-Chin, Lin

“ The Quantum Electronic Transport in Strongly Correlated Quantum Dot System ,” a dissertation prepared by Kao-Chin, Lin in partial fulfillment of the requirements for the degree, Doctor of Philosophy , has been approved and accepted by the following:

D.S. Chuu



ABSTRACT

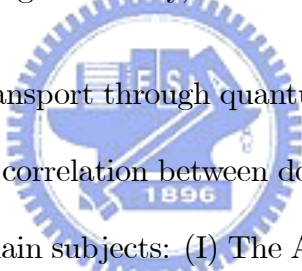
THE QUANTUM ELECTRONIC TRANSPORT IN STRONGLY CORRELATED QUANTUM DOT SYSTEM

BY

KAO-CHIN, LIN

Doctor of Philosophy

National Chiao-Tung University, Hsinchu 300, Taiwan, 1998



The electron quantum transport through quantum dot(s) system is studied in this dissertation. The strong correlation between dot and lead is considered. The dissertation consists of two main subjects: (I) The Anderson impurity model with spin flip associated tunneling in quantum dot system. (II) The electron-photon interaction inducing correlation of dot-nonconnected-lead in double-dot-system in which each dot is coupled to leads individually. In order to calculate the interaction system, the non-equilibrium Green function technique is used. The non-equilibrium electron transport formula is used to calculate the conductance due to electron transport through the interacting quantum dot. In subject (I), we find the spin flip associated tunneling causes enhancement and blue shift of Kondo resonance peak. The net effect suppresses the conductance as the strength

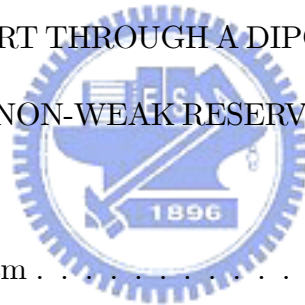
of spin-flip associated tunneling is increased. In subject (II), it is found that the dipole-like electron-photon interaction induces the correlation between dot and nonconnected-lead under non-weak-coupling approximation in double-dot-system when the detuning factor $\Delta = \varepsilon_2 - \varepsilon_1 - \omega_{ph}$ is smaller than a critical detuning factor Δ_C and the temperature is below the critical temperature $\pi T_c^{ph} = |\Delta|$. After the dot-nonconnected-lead correlation is constructed, the corresponding peak grows logarithmically at the vicinity of $\omega_m = \varepsilon_{m'}^F - (-1)^m \omega_{ph}$ where $m, m' \in 1, 2$, $m \neq m'$, and $m = 1, 2$ indicates the lower energy ($m = 1$) and higher energy ($m = 2$) dot, respectively.



CONTENTS

| | | |
|---------|--|----|
| 1 | INTRODUCTION | 1 |
| 1.1 | The Quantum Dot | 1 |
| 1.1.1 | Electron Transport through the Quantum Dot System | 8 |
| 1.1.2 | The Photon Associated Transport | 12 |
| 1.1.3 | The Anderson Impurity Model in Quantum dot system | 18 |
| 1.1.3.1 | Electron transport at low temperature | 18 |
| 2 | THE NONEQUILIBRIUM GREEN FUNCTION AND CURRENT FORMULA | 26 |
| 2.1 | The Green function method | 26 |
| 2.1.1 | Equilibrium Green function (time ordered Green function) | 26 |
| 2.1.1.1 | Definition of Green functions | 26 |
| 2.1.1.2 | Fluctuation-Dissipation theorem | 29 |
| 2.1.1.3 | Perturbation Expansion of the Green function | 30 |
| 2.1.1.4 | The interaction and self energy | 34 |
| 2.1.2 | The nonequilibrium Green function | 36 |
| 2.1.2.1 | The Langreth theorem | 39 |
| 2.2 | The Nonequilibrium transport Formula in the interacting resonant tunneling | 44 |

| | | |
|-----|---|-----|
| 2.3 | The Equation of Motion Method and The Lacroix's Decoupled Scheme | 50 |
| 3 | ANDERSON MODEL WITH SPIN-FLIP ASSOCIATED TUNNELING | 52 |
| 3.1 | Model and Formalism | 56 |
| 3.2 | Result and Discussion | 62 |
| 3.3 | Summary | 72 |
| 3.4 | Appendix A | 75 |
| 3.5 | Appendix B | 76 |
| 3.6 | Appendix C | 78 |
| 4 | ELECTRON TRANSPORT THROUGH A DIPOLE-INTERACTION-DOUBLE-DOT SYSTEM UNDER NON-WEAK RESERVOIR COUPLING APPROXIMATION | 82 |
| 4.1 | Model and Formalism | 84 |
| 5 | SUMMARY | 101 |
| 6 | FUTURE WORKS | 104 |



CHAPTER 1

INTRODUCTION

1.1 The Quantum Dot

With the advent of the modern semiconductor technologies, artificial heterostructures with layer width of only a few nanometers, i.e. the superlattice, have been grown. The heterostructure layers confine the free electron gas in a 2D plane to form a two-dimensional electron gas (2DGE). Using the additional metallic lateral patterning by lithographic (such as the electron-beam) or etching techniques (ion beam, x-ray, scanning probe microscopies) on the heterostructure layer, the electron can be confined in a very small region with nanometer scale by the applied electric field on the metallic patterning. Thus, it is possible to make a nanometer scale zero-dimension device whose vertical and lateral dimensions are controlled in the order of de Broglie wavelength of the electron in semiconductor as shown in Fig.1.1, Fig.1.2 and Fig.1.3). Such a zero dimension device is called as "quantum dot".

Besides the lateral patterning confinement, the quantum dot can also be made by the cluster of the atoms called "assembled quantum dot". The assembled quan-



Figure 1.1: A scanning electron micrograph of various size GaAs nanostructures containing quantum dots. The dark region on top of the column is the electron-beam defined Ohmic contact and etch mask



Figure 1.2: A. Schematic diagram of an artificial atom located between two capacitor plates. The artificial atom is actually two-dimensional; the bowl like shape represents the force tending to move electrons to the center of the atom. B. Diagram of the sample used in single-electron capacitance spectroscopy (SECS) experiments in a crystal grown using molecular-beam epitaxy. The artificial atom is the black disk in the quantum well. C. Capacitance of the sample containing the artificial atom as a function of the top plate (gate) voltage. The first peak on the left represents the first electron entering the artificial atom.



Figure 1.3: The quantum dot structure studied at Delft and NTT in Japan is fabricated in the shape of a round pillar. The source and drain are doped semiconductor layers that conduct electricity, and are separated from the quantum dot by tunnel barriers 10 nm thick. When a negative voltage is applied to the metal side gate around the pillar, it reduces the diameter of quantum dot.



Figure 1.4: The self-assembled quantum dot. (a) and (b) are plane view. (c) is the cross-sectional view of a typical island sample (a). The wetting layer and underlying 60 Å reference InGaAs quantum well.

tum dot is constructed during the growth of highly lattice mismatched semiconductor layer onto a substrate, leading to spontaneous formation of small islands. (as shown in Fig.1.4).

The semiconductor quantum dot is constructed by a million atoms with an equivalent number of electrons. But almost all of the electrons are bound to the nuclei of atoms and do not affect the properties of quantum dot. In fact, there are only few free electrons confined in quantum dot which dominate the properties of quantum dot.

Since the dimension of confinement is in the order of the electron wavelength, the energy level of quantum dot is discrete due to the quantization of electron energy in quantum dot. In 1988, Reed et al. used the electron-beam lithography to define an ensemble of AuGe/Ni/Au Ohmic metallization dots with 100~250 nm diameter[1]. (Fig.1.1) They studied the current-voltage characteristics of a single quantum dot and observed resonance corresponding to the discrete density of state of quantum dot. Owing to the quantization of energy, the quantum dot is regarded as an "artificial atom" [2]. Similar to the natural atom, the shell structure is found in quantum dot[3].(Fig.(1.5) But instead of the optical spectroscopic study in natural atom system, the periodic table of quantum dot system is constructed via measuring the electron transport through quantum dot, i.e. the single-electron capacitance spectroscopy[3][4]. By the way of single-electron capacitance spectroscopy, the energy levels of a N -electron dot can be directly measured as a

function of the magnetic field. In 1993, Ashoori et al. used the electrode confined electron in AlGaAs/GaAs/AlGaAs superlattice and studied the electronic state of quantum dot via observing of the relationship between capacitance and gate voltage. They also studied the N-electron ground state energies of quantum dot in magnetic field.[4](Fig.1.2) In 1998, Tokura et al. found the atom like property such as a shell structure and they found that Hund's rule is obeyed in the vertical quantum dot[5].(Fig.1.3 and Fig.1.5) They also used the vertical quantum dot which contains double-barrier structure to observe the electron states in quantum dot molecules[3]. Besides the periodic table, as the ionization energy in natural atom, the quantum dot has the charge energy which is the energy required to add or remove a single electron from quantum dot. The quantum dot coupled to lead is analogy to the impurity in electron gas. The electron transport problem in impurity embedded electron gas, such as Anderson impurity model, Kondo effect and localization effect etc., is also found in the quantum dot system[6][7][8]. Since there are many atom-like properties, the quantum dot is naturally regarded as the artificial atom. But unlike the real atom, the quantum dot is constructed by hundreds or thousands atoms. The dimension of the quantum dot is in mesoscopic scale. Since the dimension of atom is in microscopic scale, the bias voltage may be considered as zero and the electron transport problem can be treated as equilibrium case. However, the applied bias is actually able to drop over a mesoscopic length ,i.e. the bias voltage may be finite. Thus, the transport problem in QD

system might be a nonequilibrium problem[9]. For the dimensional size of the quantum dot, it is easy to apply the external field on the quantum dot and hence the properties of quantum dot maybe modified. Thus, the physics of quantum dots has been a very active and fruitful research topic.

1.1.1 Electron Transport through the Quantum Dot System

Besides the discrete energy, the small dimension confinement of quantum dot causes the strong intradot Coulomb interaction. In addition to these two effects, the temperature strongly affects the essential characters of electron transport through the quantum dot. The intradot Coulomb interaction depends on the particle number in QD and is hardly to be calculated by the way of first principle. A compact way is the equivalent circuit model which suggests the Coulomb interactions to be expressed in terms of the circuit diagram as shown in Fig.1.6[10].

Using the capacity model, the additional energy of quantum dot is found as

$$\mu_{dot}(N + 1) - \mu_{dot}(N) = \Delta E + \frac{e^2}{C} \quad (1.1)$$

where $\Delta E = E_{N+1} - E_N$ is the quantum level spacing, e^2/C is the charge energy and N is the particle number. C is the total capacitance, i.e. the capacitance between the dot and all other pieces of metal around it, plus the contribution from self-capacitance. The total capacitance $C = C_l + C_r + C_g$ consists of capacitances across the barriers, C_l and C_r , and a capacitance between the dot and gate, C_g .



Figure 1.5: Current flowing through a two-dimensional circular quantum dot on varying the gate voltage. (a) The first peak marks the voltage where the first electron enters the dot and the number of electron, N , increases by one at each subsequent peak. The distance between adjacent peaks corresponds to the addition energies (see inset). (b) The addition of electrons whereas the second shell can contain up to four electrons. It therefore costs extra energy to add the third and seventh electron. (c) The electronic properties following from a two-dimensional shell structure can be summarized in a periodic table for two-dimensional elements. (The elements are named after team members from NTT and Delft.)



Figure 1.6: Circuit diagram for electron transport through a quantum dot. The tunneling barriers are represented as a parallel capacitor and resistor. The different gates are represented by a single capacitor $\sum C_g$. The charging energy in this circuit is $e^2/(C_l + C_r + \sum C_g)$

This simple model is valid at the linear response regime (i.e. $(\mu_{left} - \mu_{right})/e \ll \Delta E/e, e/C$). The requirement for electron being able to transport through QD is when there are available states in the dot within the energy window between μ_{left} and μ_{right} . Thus, for $\mu_{dot}(N) < \mu_{left}, \mu_{right} < \mu_{dot}(N + 1)$ the electron transport is blocked, which is known as the Coulomb blockade.

Since the temperature effect broadens the profile of Fermi distribution of the electron in lead with energy in the vicinity of Fermi level of lead. The role of temperature will divide the transport problem in QD system into three regimes:

- (i) $e^2/C \ll k_B T$, where the discreteness of charge cannot be discerned.
- (ii) $\Delta E \ll k_B T \ll e^2/C$, the classical or metallic Coulomb blockade regime, where many levels are excited by thermal fluctuations.
- (iii) $k_B T \ll \Delta E < e^2/C$, the quantum Coulomb blockade regime, where only one or a few levels participate in transport.

The quantum electron transport appears in regime (iii). In situation of regime (iii), since the large intradot Coulomb interaction and energy spacing, the electron can transport through QD via channels (energy levels) with energy between the bias window $eV_{sd} = \mu_{high} - \mu_{low}$ which is called "conduction channel" in this dissertation (Fig.1.7). The channels with energy below the lower Fermi level of the lead μ_{low} are occupied and do not contribute current. The channels above the higher Fermi level of lead are unoccupied and the electron in the transport channel can be excited to these unoccupied channel. Thus, at the regime of the

Figure 1.7: The sketch of the quantum transport

quantum transport, the channel coupled to the bias window is similar to the most outshell electron in natural atom which interacts with external field and dominates the properties of the system. The sketch is shown in Fig.1.7. In this dissertation, the quantum electron transport is considered. We study the electron tunneling through the conduction channels which interacts with each other or with unoccupied channel via electron-photon interaction.

1.1.2 The Photon Associated Transport

The photon associated transport means that the electron transport through a region coupled with an AC field (or photon field) . The frequency regime of the applied AC field is much lower than that of the visible light. The important frequency scales are listed in table I.

Table I. A list of the important energy/frequency scales for transport through quantum dots. For $\omega_{ph} = 10GHz$ the photon energy, $\sim\omega_{ph}$, is $40 \mu eV$. [11]

| Quantity | Equivalent frequency | Typical frequency |
|---|-----------------------|-----------------------|
| thermal broadening | $\sim 4k_B T/h$ | $10GHz$ (at $100mK$) |
| Tunneling rate on/off the dot | Γ | $0 \sim 100GHz$ |
| Level spacing (or inverse traversal time) | $\Delta\varepsilon/h$ | $10 \sim 100GHz$ |
| Charge energy | e^2/hC | $40 \sim 400GHz$ |
| Tunnelling time | $1/\tau_{tunnel}$ | $200GHz \sim 1THz$ |

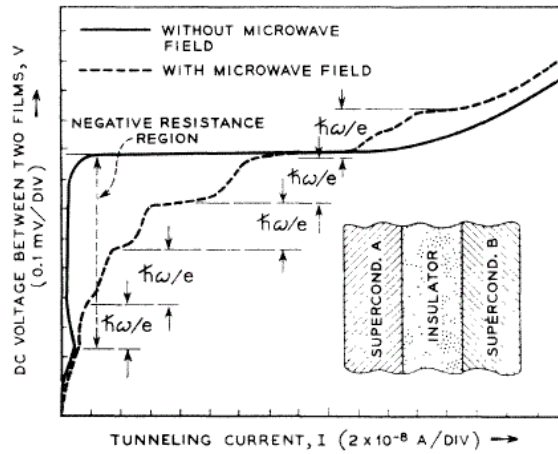
For the typical quantum dot, the level spacing $\Delta\varepsilon$ is $0.05 \sim 0.5 meV$ and the charge energy, e^2/C , is about $0.2 \sim 2meV$. To observe the discreteness of the energy (level) in quantum dot, the thermal broadening $4k_B T/h$ can not exceed the level spacing and charge energy e^2/C . Γ is the rate for tunneling in/off the dot and can be very small. In order to keep the transport process in quantum transport regime, Γ should be smaller than $\Delta\varepsilon$ otherwise the level broadening will exceed the spacing between the single states. The tunneling time is the actual time spent during tunneling through the barrier. AC signals can be applied and the effects on DC transport can be observed when the AC signal time scale exceeds the tunneling time scale.

If the frequency of AC field is much smaller than the tunneling rate Γ , i.e. $\omega_{ph} \ll \Gamma$ the electron is acted by an static potential [12]. If $\omega_{ph} \gg \Gamma$, the electron will interact many cycles with AC field in interaction region. In order to

observe the effect of AC field, the energy of AC field must be larger than the thermal broadening, otherwise the photon process will be covered by the thermal fluctuations. Since that, the frequency of AC field for PAT is set in the condition $h\omega_{ph} \gg 4k_B T$ and $h\omega_{ph} \gg 4k_B T$. [13]

The photon associated transport has been studied for a long time since 1960. In 1963, Dayem and Martin observed the multiphoton associate tunneling in superconductor diode (superconductor-insulator-superconductor) [14]. In their work, microwave is coupled to the superconductor diode and found that (1) an excess of tunneling current in the region below the knee of the current (if microwave is turned off) and a reduction of the tunneling current in the region above the knee of the current if microwave is turned on, and (2) the tunneling current appears at voltage of $n\hbar\omega_{ph}/e$, $n \in \text{integer}$ and ω_{ph} is the frequency of microwave. As shown in Fig.1.8, Tien and Gordon employed a time dependent potential difference

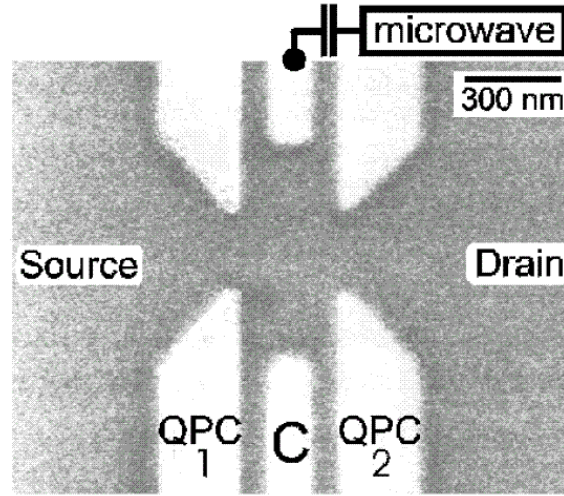
$V \cos \omega_{ph} t$ between two films to model the experiment of Dayem and Martins. They found that the wave function contains components which have energies, E_0 , $E_0 \pm \hbar\omega_{ph}$, $E_0 \pm 2\hbar\omega_{ph}$,, etc., respectively when the microwave is applied. The additional energies $E_0 \pm \hbar\omega_{ph}$, $E_0 \pm 2\hbar\omega_{ph}$,, are called photonic sidebands which provide the additional channels for electron tunneling. Each component with energy $E_0 \pm n\hbar\omega_{ph}$ corresponding to absorbing n photons for sign "+" and emitting n photons for sign "-". And the amplitude of n - photon absorption (emission) component is proportional to the n th order Bessel function $J_n(\frac{V}{\hbar\omega})$, and the effective



Bias voltage vs tunneling current of a superconducting Al-Al₂O₃-In diode as measured by Dayem and Martin with and without the microwave field. $\hbar\omega/e=0.16$ mV.



Figure 1.8: The multi-photon associated tunneling in superconductor diode (superconductor-insulator-superconductor) observed by A.H. Dayem and R.J. Martin.



SEM photo of the sample. The lithographic size of the dot is $(600 \times 300) \text{ nm}^2$. Current can flow when we apply a voltage between source and drain. The microwave signal is capacitively coupled to one of the center gates.

Figure 1.9: The SEM photo of sample for PAT experiment in quantum dot system.

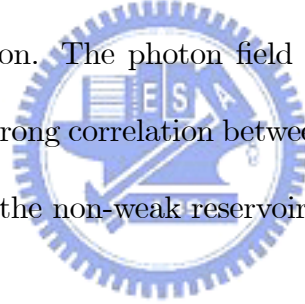
density is proportional to $J_n^2(\frac{V}{\omega})$. Thus the current due to the electron tunneling via the channel with energy $E_0 \pm n\omega_{ph}$ is proportional to $J_n^2(\frac{V}{\omega})$. In 1994, the electron transport via the photon sideband was also found and studied in quantum dot system[15]. L. P. Kouwenhoven et al. applied microwave to a quantum dot defined by metallic gates (Fig.1.9) in a GaAs/AlGaAs heterostructure containing a 2-DEG dimensional electron gas (2DEG) 100nm below the surface. The current due to the electron transport via photonic sideband $E_0 \pm \omega_{ph}$, $E_0 \pm 2\omega_{ph}$ was observed in the experiment. Almost all of the studies in PAT topics treated the photon field as the semi-classical model, i.e. treated the photon field as the AC gate voltage[16][17]. The quantum electrodynamic treatment of PAT was studied

by Foden and Whittaker. Foden and Whittaker treated the photon field as a quantum field and used the canonical transformation to solve the PAT problem. They pointed out that the classical field approximation is a valid one, not because the field intensities are high but because the coupling between the electrons and field is weak[18].

In the above introduction about PAT, the electron interacts with photon and without inter-state transition. But for the two level system (ground state and excited state), the electron may transit between the ground state and excited state via electron-photon interaction. In the atomic optical topic, this is the dipole interaction. In the case of dipole interaction, the atom can transit between lower energy state and higher energy state due to the photon absorption or emission process. It is known that the transition cycle between two states is called Rabi oscillation with Rabi frequency Ω_R . The Rabi frequency is defined as $\Omega_R = \sqrt{\Delta^2 + 4g^2n_{ph}}$ where $\Delta = \omega_{ph} - (\varepsilon_2 - \varepsilon_1)$ is the detuning factor, where n_{ph} , ω_{ph} are the photon number and photon frequency, respectively[19]. Since the properties of quantum dot is similar to the atom, the dipole interaction may appear in the quantum dot system. The two-level quantum dot system with intradot transition due to AC field was considered by Brune et al..[20] They found that the photonic sideband locates at $\varepsilon = (\varepsilon_2 + \varepsilon_1 \pm \sqrt{\omega_{ph}^2 \pm \Omega_R^2})/2$ where Rabi frequency is $\Omega_R = \sqrt{\Delta^2 + |\Delta f|^2}$, and Δf is the coupling strength of the electron-field interaction.[15]

Besides the semi-classical treatment of photon field, most of the theoretical models treated the PAT problem in the frame work of weak reservoir coupling limit. In the weak reservoir approximation, the electron-photon interaction is assumed much stronger than the tunneling effect.[17] Hence, the AC field applied on the quantum dot is firstly treated as an electron-photon interaction quasi-particle and then the interaction quasi particle is coupled to lead. In the weak reservoir coupling limit, the higher order tunneling effects, such as Kondo effect and co-tunneling effect, are ignored.

In chapter 4 of this dissertation, the electron transport through the AC field-applied-two-level quantum dot is studied. The electron-photon interaction is treated as a dipole interaction. The photon field will be treated as a quantum field. In order to study the strong correlation between dot and lead induced by the electron-photon interaction, the non-weak reservoir coupling limit is considered.



1.1.3 The Anderson Impurity Model in Quantum dot system

1.1.3.1 Electron transport at low temperature

For normal metal or free electron gas, the property of electron transport or the electrical conductivity (resistivity) can be explained by Ohm's law. In Ohm's law, the electrical conductivity σ is defined as $\sigma = ne^2\tau/m$ where n is the electron number, e is electronic charge, τ is the collision time and m is the electronic mass. The net collision time τ can be recognized as the phonon scattering part τ_L and

the imperfection scattering part τ_i and $\frac{1}{\tau} = \frac{1}{\tau_L} + \frac{1}{\tau_i}$. The net resistivity is given by $\rho = \rho_L + \rho_i$ where ρ_L is the resistivity caused by the thermal phonons, and ρ_i is the resistivity caused by scattering of the electron waves by static defects that disturb the periodicity of the lattice. The collision time τ_L and resistivity ρ_L can be estimated by the Drue model. In Drue model, the resistivity is originated by the collision of conduction electron which alters the velocity of conduction electron. The electron-electron interaction between collisions is neglected which is known as the independent electron approximation. The electron-ion interaction is also ignored and that is known as the free electron approximation. The electrons are assumed to achieve thermal equilibrium with their surrounding only through collision. The average time between the collision events is assumed as τ_L . The time τ_L is called as the relaxation time, the collision time, or the mean free time, and it plays a fundamental role in the theory of metallic conduction. The mean free path l_L can be expressed by the mean free time as $l_L = v_0\tau_L$ where v_0 is the average electronic speed. The mean free path measures the average distance of an electron travelling between two successive collisions. The average electronic speed is estimated from classical equipartition principle of energy: $\frac{1}{2}mv_0^2 = \frac{3}{2}k_B T$. For a given sample, the mean free path is constant and the mean free time is $\tau_L = l_L/\sqrt{3k_B T/m}$. The resistance can be estimated as $\rho_L = \frac{m}{ne^2\tau_L} = \frac{m\sqrt{3k_B T/m}}{ne^2 l_L}$. The resistivity originated by the phonon (or electron) scattering is proportional to the square root of temperature. The resistivity ρ_i is often independent of temperature.

Thus, the resistivity of metal is decreased with decreasing of temperature at high temperature region and approximates to a constant residual resistivity, $\rho(0)$, when the temperature is low.

But, for many years experimentalists noticed that magnetic impurities in non-magnetic metals caused anomalous behavior in low-temperature resistivity $\rho(T)$. Magnetic impurities are those with a net spin caused by partially filled d- or f-electron shells. An example is manganese impurities in copper. The magnetic impurity causes a resistance minimum at nonzero temperature. Kondo explained this behavior as due to spin-flip scattering between the conduction electrons and localized spin. The resistance minimum is called Kondo effect. The Anderson model is another model for a system of conduction electrons that interact with a local spin[21]. Many early works regarded that these two models can make very similar predictions. Schrieffer and Wolff gave the transformation which shows that the two models are very similar[22]. Now it is known that the Anderson model has a greater variety of behavior. It contains more interesting physics.

The Anderson impurity model describes the strong correlation between electron in magnetic impurity and electron reservoir (electron gas) via the Coulomb interaction and direct tunneling between impurity and metal. Consider an electron with spin σ_1 which occupies an impurity state with energy ε_0 . It is intuitive that the second electron with spin σ_2 will occupy the impurity state with energy $\varepsilon_0 + U$.(Fig.(1.10.a)) But Anderson regarded that this is not the ground state of



Figure 1.10: (a) Unperturbed energy levels (b) Density of state distribution, The "humps" at $\varepsilon_0 + \langle n_{\sigma_1} \rangle U$ and $\varepsilon_0 + \langle n_{\sigma_2} \rangle U$ are virtual states in impurity. The number of electrons $\langle n_{\sigma_1} \rangle$ and $\langle n_{\sigma_2} \rangle$ occupied is computed from the area of unshaded portion, below Fermi surface.



the two-electron-system in impurity under Coulomb interaction and tunneling perturbation. The ground state is the virtual state constructed by the electron with energy $\varepsilon_0 + \langle n_{\sigma_2} \rangle U$ and $\varepsilon_0 + \langle n_{\sigma_1} \rangle U$ and lies near the Fermi level[21].(Fig.(1.10.b))

In this case, the electron can tunnel from the impurity and escape provided its energy lies above the Fermi level, otherwise it will remain to be trapped. In the picture, the defect has a spin of $1/2$ and its z-component is fixed as either "spin up" or "spin down". The so-called exchange processes can effectively flip the spin of the impurity from spin up to spin down, or vice versa, which simultaneously

creates a spin excitation in the Fermi sea.

The Kondo effect is a quantum mechanical phenomenon. The energy needed for the electron is taken from the magnetic impurity state and put into an unoccupied state at the Fermi surface of Fermi level is about $1 \sim 10eV$, this process is forbidden for classical situation. But it is possible to take place in quantum mechanics. The uncertainty principle allows such a configuration to exist for a very short time $\tau_K = h/|\varepsilon_0|$ (h is the Plank constant.) Within this time scale, another electron must tunnel from the Fermi sea back towards the impurity. The spin of impurity is changed via this quantum mechanics process. As many spin exchange processes take place together, the new state (the virtual state), known as the Kondo resonance, is constructed with the energy near the Fermi level. Since many electrons need to be involved, the Kondo effect is a many body phenomenon.

Note that, the Kondo state is always "on resonance" since it is fixed to Fermi level. The Kondo effect alters the energy of the system so that it is always on resonance. The only requirement for the effect to occur is that the sample has to be cooled to sufficiently low temperature to be below Kondo temperature T_K . Duncan Haldane showed that T_K is related to the parameters of the Anderson model by $T_K = 1/2(\Gamma U)^{1/2} \exp[\pi\varepsilon_0(\varepsilon_0 + U)/\Gamma U]$, where Γ is the width of impurity state due to the direct tunneling from it, and U is the on-site Coulomb repulsion energy[23]. The Kondo temperature can vary from $1 \sim 100K$.

When temperature is near or below the critical temperature T_K (Kondo tem-

perature), the virtual state is constructed and the density of state of electron in the impurity grows logarithmically in the vicinity of Fermi surface to form Kondo resonance peak. In a magnetic bulk, the virtual state causes more scattering, hence the resistance is increased logarithmically as temperature is decreased. As a result to cause a minimum resistance at nonzero temperature.

Since the quantum dot can be controlled more conveniently than natural impurity. This property provides a way to control the Kondo effect experimentally. Therefore, the non-equilibrium (i.e. nonzero bias, Kondo effect) is naturally studied in quantum dot system.[24] The spin state of quantum dot can be modified by applying an external magnetic field. The Kondo effect can also be found in singlet ($S = 1/2$) and triplet ($S = 1$) states in quantum dot system by applying a magnetic field around 1 tesla. This experiment is hardly to implement in the natural magnetic impurity since the required magnetic field is about 10^6 tesla and can not be generated in the laboratory. The quantum dot is a powerful system for the research in Kondo effect which provides wider regime to be inaccessible with magnetic impurities. In the quantum dot system, unlike the bulk system, the virtual state provides a channel in the vicinity of Fermi energy of lead for electron tunneling between quantum dot and lead. Thus the conductance is increased logarithmically as temperature is decreased.

The Kondo effect is a many-body problem and needs more skills to solve. There are many methods to solve Kondo problem. The equation of motion method

(EOM)[25][26][27][28], slave boson technique[29] and renormalization group theory[30] are often used to solve the Kondo effect problem. The EOM is a compact way for the Kondo problem and widely employed to describe an interacting QD coupled to normal or superconducting electrodes. The EOM generates two-particle Green functions, which have to be decoupled and truncated. The preciseness of the EOM depends on the way of decoupled scheme. The two-particle Green function corresponding to the Anderson impurity model is $G^{(2)} = \langle\langle T d_\sigma n_{\sigma'}, d_\sigma \rangle\rangle$. If one takes $G^{(2)} = n_{\sigma'} \langle\langle T d_\sigma, d_\sigma \rangle\rangle$, this approximation is effective to the Hartree-Fock approximation which gives the Coulomb Blockade effect. For the higher order perturbation due to the tunneling between dot and lead, two-particle Green function contains two lead electronic operators and two dot electronic operators which maybe decoupled as $\langle\langle c_{k\sigma} c_{q-\sigma} d_{-\sigma}^+, d_\sigma^+ \rangle\rangle \simeq -\langle c_{q-\sigma} d_{-\sigma}^+ \rangle, \langle\langle c_{q-\sigma}^+ c_{k\sigma} d_{-\sigma}, d_\sigma^+ \rangle\rangle \simeq -\langle c_{q-\sigma}^+ d_{-\sigma} \rangle \langle\langle c_{k\sigma}, d_\sigma^+ \rangle\rangle, \langle\langle c_{q-\sigma}^+ c_{k-\sigma} d_\sigma, d_\sigma^+ \rangle\rangle \simeq \langle c_{q-\sigma}^+ c_{k-\sigma} \rangle \langle\langle d_\sigma, d_\sigma^+ \rangle\rangle$. Lacroix (1981) suggested that the decoupled approximation $\langle c_{q-\sigma} d_{-\sigma}^+ \rangle = \langle c_{q-\sigma}^+ d_{-\sigma} \rangle = 0$ and $\langle c_{q-\sigma}^+ c_{k-\sigma} \rangle = \delta_{q,k} \langle n_{k-\sigma} \rangle$ are correct only at high temperature (above the Kondo temperature). These decouple scheme will be called as Lacroix's high temperature decoupled scheme in this dissertation. When temperature is below Kondo temperature T_K , Lacroix pointed out that the approximations $\langle c_{q-\sigma} d_{-\sigma}^+ \rangle = \langle c_{q-\sigma}^+ d_{-\sigma} \rangle = 0$ and $\langle c_{q-\sigma}^+ c_{k-\sigma} \rangle = \delta_{q,k} \langle n_{k-\sigma} \rangle$ do not correct exactly and have to be solved in higher order expansion and calculated self-consistently (This decoupled approximation is called as the Lacroix's low temperature decoupled scheme). Luo et al.

(1999) included the higher order term (compares to the Lacroix's low temperature decoupled scheme) and got the result very closed to the one calculated by numerical renormalization group[31]. Although the Lacroix's high temperature decoupled scheme is not correct exactly (quantitatively) but it can give reasonably qualitative result. For simplicity, the Lacroix's high temperature decoupled scheme will be adopted.



CHAPTER 2

THE NONEQUILIBRIUM GREEN FUNCTION AND CURRENT FORMULA

2.1 The Green function method

In this dissertation, one of the interest subjects is to study the current due to the electron transport through the quantum dot which interacts with other particle, i.e. the many body problem. In order to calculate such a many body problem, the current formula which is based on the nonequilibrium Green functions (or contour ordered Green functions) developed by Antti-Pekka Jauho et al. is used. In the following, we will give an brief introduction. For detial review, one can refer to the book "Quantum Kinetics in Transport and Optics of Semiconductors".

2.1.1 Equilibrium Green function (time ordered Green function)

2.1.1.1 Definition of Green functions

There are many ways to treat the many-body interacting system, the Green function method is one of the popular methods. The equilibrium Green function

is defined as

$$G(x, t, x', t') = -i \frac{\langle \Psi_0 | T \{ \psi_H(x, t) \psi_H^\dagger(x', t') \} | \Psi_0 \rangle}{\langle \Psi_0 | \Psi_0 \rangle} \quad (2.1)$$

Here, $T\{\dots\}$ is the time-ordering operator which moves the operator with early time to the right:

$$T\{A(t)B(t')\} = \theta(t - t')A(t)B(t') \mp \theta(t' - t)B(t')A(t) \quad (2.2)$$

where the upper sign refers to Fermions. This negative sign is caused by the interchange of the order of Fermi operator. The operator $\varphi_H(x, t)$ is time dependent and in Heisenberg picture. $H|\Psi_0\rangle = E_0|\Psi_0\rangle$ is the ground system of interacting system. The term $\langle \Psi_0 | \Psi_0 \rangle$ is a normalization factor and relates to density operator of ground state.

For future use, it is necessary to define the retarded, advanced, "lesser" and "greater" Green functions:

$$G^r(x, t; x', t') = -i\theta(t - t') \langle \{ \psi(x, t), \psi^\dagger(x', t') \} \rangle \quad (2.3)$$

$$G^a(x, t; x', t') = i\theta(t' - t) \langle \{ \psi(x, t), \psi^\dagger(x', t') \} \rangle \quad (2.4)$$

$$G^<(x, t; x', t') = i \langle \psi^\dagger(x', t') \psi(x, t) \rangle \quad (2.5)$$

$$G^>(x, t; x', t') = i \langle \psi(x, t) \psi^\dagger(x', t') \rangle \quad (2.6)$$

The retarded Green function G^r is nonzero only for times $t \geq t'$, thus this function can be used to calculate the response at t to an earlier perturbation of the system at time t' . The advanced Green function G^a is only finite for $t \leq t'$. The "lesser"

Green function is also called the particle propagator, while the "greater" Green function, in which the order of the creation and annihilation operators are reversed, is called the hole propagator. These various functions are not independent, they obey

$$G^r - G^a = G^> - G^< \quad (2.7)$$

In Eq.(2.3)~Eq.(2.6), we dropped the normalization factor $\langle \Psi_0 | \Psi_0 \rangle$. Note that the time-ordered, the retarded, and the advanced Green function can be expressed in term of $G^>$ and $G^<$:

$$G(x, t, x', t') = \theta(t - t')G^>(x, t, x', t') + \theta(t' - t)G^<(x, t, x', t') \quad (2.8)$$

$$G^{r,a}(x, t, x', t') = \pm\theta(\pm t \mp t')[G^>(x, t, x', t') - G^<(x, t, x', t')] \quad (2.9)$$

The observables can also be expressed in term of $G^{>,<}$; for example

$$\langle n(x) \rangle = -iG^<(x, t; x, t) \quad (2.10)$$

Although all Green functions can be expressed in terms of each other, each one of them has its own advantage and necessary to introduce:

- (1) $G(x, t, x', t')$ can be obtained by a systematic perturbation theory.
- (2) $G^{r,a}(x, t; x', t')$ has a nice analytic structure (pole in one half-plane) and is convenient to calculate the physical quantities, such as spectral properties, densities of states, and scattering rates.
- (3) $G^{>,<}(x, t; x', t')$ is directly linked to observable physical quantities and kinetic properties, such as particle densities or current.

Another important properties for these Green functions is that Green functions $G, G^{r,a}, G^{>,<}$ are also linked by the fluctuation-dissipation theorem.

2.1.1.2 Fluctuation-Dissipation theorem

The spectral function (or the density of state) is essential and relates to observable quantities. It is defined as:

$$A(k, \omega) = i[G^r(k, \omega) - G^a(k, \omega)] \quad (2.11)$$

and with the property:

$$\int_{-\infty}^{\infty} \frac{d\omega}{2\pi} A(k, \omega) = \int d^3(x - x') e^{-ik(x-x')} \langle \{\psi(x, t), \psi^+(x', t')\} \rangle = 1 \quad (2.12)$$

because of the equal-time anticommutation rule. The density of state can be calculated by $A(k, \omega)$:

$$\rho(\omega) = \int_{-\infty}^{\infty} \frac{d^3k}{(2\pi)^3} A(k, \omega)$$

(Since the vector k is quantized in quantum dot, the spectral function $A(\omega)$ equals to the density of state $\rho(\omega)$). The fluctuation-dissipation theorem $A(k, \omega)$ links the spectral function to the particle propagator $G^<(k, \omega)$:

$$G^<(k, \omega) = if(\omega)A(k, \omega) \quad (2.13)$$

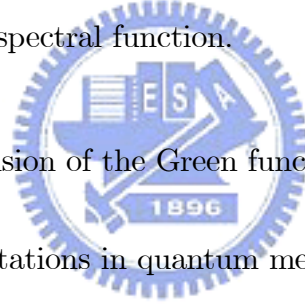
where $f(\omega) = (1 + \exp[\beta(\omega - \mu)])^{-1}$, $\beta = (k_B T)^{-1}$ and μ is the chemical potential. Eq.(2.13) is an useful equation for determinating the particle number in equilibrium system (zero basis system). For the case of quantum dot:

$$N = -i \int \frac{d\omega}{2\pi} G^<(\omega) = \int \frac{d\omega}{2\pi} f(\omega) A(\omega) \quad (2.14)$$

The spectral function is the image part of retarded Green function, and it determines the decay in time-domain, and hence the dissipation. The form of Eq.(2.13) explains the name "fluctuation-dissipation" theorem. It means that the correlation function $G^<$ (which also carries information about the fluctuations) is proportional to the dissipative part and the proportionality factor is the Fermi-Dirac distribution function. For non-interaction system, $A(k, \omega) = 2\pi\delta(\varepsilon_k - \omega)$. The greater Green function (or the hole propagator) also has the similar relation:

$$G^>(k, \omega) = -i(1 - f(\omega))A(k, \omega)$$

The hole propagator is proportional to the probability of finding a hole, i.e. an unoccupied state, times the spectral function.



2.1.1.3 Perturbation Expansion of the Green function

There are three representations in quantum mechanics, i.e.

(a) Schrodinger picture: the wave function is time dependent $i\frac{\partial}{\partial t}\psi(t) = H\psi(t)$;

the operators are constant.

(b) Heisenberg picture: the wave function is constant; the operator is time dependent $\hat{O}(t) = e^{iHt}\hat{O}(0)e^{-iHt}$.

(c) interaction picture: The wave function develops under the influence of the interaction part of Hamiltonian $H = H_0 + V$; $\hat{\psi}(t) = e^{-iVt}\psi(0)$. The operator develops under the influence of the non-interaction part of Hamiltonian $\hat{O}(t) = e^{iH_0t}\hat{O}(0)e^{-iH_0t}$.

The time evolution of wave function in interaction picture can be expressed as:

$$\hat{\psi}(t) = U(t)\hat{\psi}(0), \quad U(t) = e^{-iVt}$$

Introduce the S-matrix which describes the time evolution of wave function from t to t' :

$$S(t, t') = U(t)U(t'), \quad \hat{\psi}(t) = S(t, t')\hat{\psi}(t')$$

The S-matrix obeys the property $S(t, t') = S(t, t'')S(t'', t')$. The S-matrix can be expressed as a time ordered product:

$$S(t, t') = T e^{-i \int_{t'}^t dt_1 \hat{V}(t_1)} \quad (2.15)$$

Thus the relation between the exact ground state of interaction system $|\Psi_0\rangle$ and noninteracting system $|\Phi_0\rangle$ is:

$$|\Psi_0\rangle = S(0, -\infty) |\Phi_0\rangle \quad \text{and} \quad \langle \Psi_0 | = \langle \Phi_0 | S(0, -\infty)$$

The term $\langle \Psi_0 | \Psi_0 \rangle = \langle \Phi_0 | S(0, -\infty) S(0, -\infty) | \Phi_0 \rangle$ is an ill-defined phase and is cancelled with numerator in Eq.(2.1) under the "adiabatic switch on" interaction, i.e. the cancellation theorem[32][33]:

$$\begin{aligned} G(x, t, x', t') &= -i \frac{\langle \Psi_0 | T \{ \hat{\psi}_H(x, t) \hat{\psi}_H^+(x', t') \} | \Psi_0 \rangle}{\langle \Psi_0 | \Psi_0 \rangle} \quad (2.16) \\ &= -i \frac{\langle \Phi_0 | T \{ S(-\infty, \infty) \hat{\psi}_i(x, t) \hat{\psi}_i^+(x', t') \} | \Phi_0 \rangle}{\langle \Phi_0 | S(-\infty, \infty) | \Phi_0 \rangle} \\ &= -i \frac{\langle \Phi_0 | S(-\infty, \infty) | \Phi_0 \rangle_{non-connected} \langle \Phi_0 | T \{ S(-\infty, \infty) \hat{\psi}_i(x, t) \hat{\psi}_i^+(x', t') \} | \Phi_0 \rangle_{connected}}{\langle \Phi_0 | S(-\infty, \infty) | \Phi_0 \rangle_{non-connected}} \\ &= -i \langle \Phi_0 | T \{ S(-\infty, \infty) \hat{\psi}_i(x, t) \hat{\psi}_i^+(x', t') \} | \Phi_0 \rangle_{connected} \end{aligned}$$

Figure 2.1: The sketch of Feynmann diagram corresponding to connected term, non-connected term and Green function



The subscript connected in the term $\langle \Phi_0 | \dots | \Phi_0 \rangle_{connected}$ presents that the interaction line connects with the particle line. The subscript non-connected in the term $\langle \Phi_0 | \dots | \Phi_0 \rangle_{non-connected}$ presents that the interaction line does not connect with the particle line. The $\langle \Phi_0 | \dots | \Phi_0 \rangle_{non-connected}$ is the vacuum bubble and does not affect the system. The sketch is shown in Fig.2.1. This result generates the systematic perturbation scheme for Green function. The S-matrix can be expanded in $V(t)$:

$$S(\infty, -\infty) = \sum_{n=0}^{\infty} \frac{(-i)^n}{n!} \int_{t_1}^{\infty} \dots \int_{-\infty}^{t_n} dt_1 \dots dt_n T\{\hat{V}(t_1) \dots \hat{V}(t_n)\} \quad (2.17)$$

i.e. the Dyson expansion. Since $t_1 \cdots t_n$ are mute variables, the time order of $t_1 \cdots t_n$ have $n!$ possible permutations with the same physical meaning. The factorial $n!$ will be cancelled with the number of possible permutations due to change of the upper limit and lower limit of integral variables to ∞ and $-\infty$ [34]. For example, if $\hat{V}(t_1)$ contains two operators, for the second expansion, i.e. $n = 2$, one needs to evaluate the term:

$$\langle \Phi_0 | T \{ \hat{\psi}(t) \hat{\psi}^+(t') \hat{\psi}^+(t_1) \hat{\psi}^+(t_2) \hat{\psi}(t_2) \hat{\psi}(t_1) \} | \Phi_0 \rangle \quad (2.18)$$

It is constructed by the product of six operators. It can be treated with Wick's theorem, which means that the result of Eq.(2.18) is the sum of all pairwise contractions[35]. There are three time variables and $3!$ possible permutations. All the possible diagrams corresponding to Eq.(2.18) are shown in Fig.(2.2): The diagrams (a) and (b) are vacuum bubbles which are cancelled by the normalization factor in denominator as shown in Fig.(2.1). The diagram (c) equals to (e) and diagram (d) equals to (f) since the time variables are mute. Hence, the factorial $n!(2! = 4$ for Eq.(2.18)) in the denominator of Eq.(2.17) is cancelled by the $n!$ equivalent time ordered arrangement. Thus, in the "adiabatic switch on" limit, the Green function of interaction system can be obtained as:

$$G(t, t') = -i \sum_{n=0}^{\infty} (-i)^n \int_{-\infty}^{\infty} dt_1 \cdots \int_{-\infty}^{\infty} dt_n \langle \Phi_0 | T \{ \hat{\psi}_i(x, t) \hat{\psi}_i^+(x', t') \hat{V}(t_1) \hat{V}(t_2) \cdots \hat{V}(t_n) \} | \Phi_0 \rangle_{connected} \quad (2.19)$$

where the summation includes topologically different connected diagrams only.

Figure 2.2: diagrams correspond to $\langle \Phi_0 | T \{ \hat{\psi}(t) \hat{\psi}^+(t') \hat{\psi}^+(t_1) \hat{\psi}^+(t_2) \hat{\psi}(t_2) \hat{\psi}(t_1) \} | \Phi_0 \rangle$

2.1.1.4 The interaction and self energy



For the interaction system, the Green function can be calculated by Dyson expansion and usually has the form:

$$\begin{aligned}
 G(1, 1') &= G_0(1, 1') + \int dt_2 G_0(1, 2) U(2) G(2, 1') \\
 &+ \int dt_2 \int dt_3 G_0(1, 2) \Sigma(2, 3) G(3, 1')
 \end{aligned}
 \tag{2.20}$$

where $U(2)$ is the one-body external potential U and usually zero in most equilibrium case. The self-energy term $\Sigma(2, 3)$ contains the interaction. Using the

Figure 2.3: The Dyson's equation for $G(\omega)$

Fourier transformation Eq.(2.20) becomes:

$$\begin{aligned}
 G(\omega) &= G_0(\omega) + G_0(\omega)\Sigma(\omega)G(\omega) & (2.21) \\
 &= G_0(\omega) + G_0(\omega)\Sigma(\omega)G_0(\omega) + G_0(\omega)\Sigma(\omega)G_0(\omega)\Sigma(\omega)G(\omega) \\
 &= G_0(\omega) + G_0(\omega)\Sigma(\omega)G_0(\omega) + G_0(\omega)\Sigma(\omega)G_0(\omega)\Sigma(\omega)G_0(\omega) + \dots
 \end{aligned}$$

$$G(\omega) = \frac{1}{\omega - \varepsilon_0 - \Sigma(\omega)} \quad (2.22)$$

where ε_0 is the eigen energy of particle. The diagrams of $G(\omega)$ and $\Sigma(\omega)$ are shown in Fig.(2.3). $\Sigma(\omega)$ is the self energy which maybe a complex quantity. The real part of the self energy is the energy shift and image part is the decay rate (or bandwidth) due to interaction.

2.1.2 The nonequilibrium Green function

The nonzero bias system is an ordinary case in the electron transport problem which is usually nonequilibrium. Consider a quantum dot connecting to the leads of which the right one is a higher Fermi energy level and the left one is a lower Fermi energy level. The electron in state $|R\rangle$ will transport from the right lead through the dot with state $|dot\rangle$ and into the left lead with state $|L\rangle$. The electron does not return to the original lead, i.e. state $|R\rangle$. Hence the process is a nonequilibrium process.

Since the initial state and final state are different states in the nonequilibrium problem. Thus, the final state is not the ground state of the system. The equilibrium Green function (or time ordered Green function) is not suitable for the problem. In order to solve the problem, the contour-ordered Green function is introduced. The contour ordered Green function is defined as

$$G(1, 1') \equiv -i \langle T_C [\psi_H(1) \psi_H(1')] \rangle \quad (2.23)$$

where the contour C begins from t_0 and ends at t_0 ($t_0 \rightarrow \pm\infty$ for the case of adiabatic switch on approximation); the contour starts from t_0 , passes through t_1 and $t_{1'}$ along real axis and finally ends at t_0 again (Fig.2.4). We use the shorthand notation $(1) \equiv (x_1, t_1)$. A typical interesting problem would be the two time Green function. The two time variables would be located on either of two branches of the complex time path, there are four distinct possibilities. Thus Eq.(2.23) contains four different functions:

Figure 2.4: Contour C

$$G(1, 1') = \begin{cases} G_C(1, 1') & t_1, t_{1'} \in C_1 \\ G^>(1, 1') & t_1 \in C_2, t_{1'} \in C_1 \\ G^<(1, 1') & t_1 \in C_1, t_{1'} \in C_2 \\ G_{\tilde{C}}(1, 1') & t_1, t_{1'} \in C_2 \end{cases} \quad (2.24)$$

where $G_C(1, 1')$ is the casual, or time-ordered Green function

$$\begin{aligned} G_C(1, 1') &= -i \langle T[\varphi_H(1)\varphi_H^+(1')] \rangle \\ &= -i\theta(t_1 - t_{1'}) \langle \varphi_H(1)\varphi_H^+(1') \rangle + i\theta(t_{1'} - t_1) \langle \varphi_H^+(1')\varphi_H(1) \rangle \end{aligned} \quad (2.25)$$

$G^>(1, 1')$ is the "greater" Green function

$$G^>(1, 1') = -i \langle \varphi_H(1)\varphi_H^+(1') \rangle \quad (2.26)$$

$G^<(1, 1')$ is the "lesser" Green function

$$G^<(1, 1') = -i \langle \varphi_H^+(1')\varphi_H(1) \rangle \quad (2.27)$$

and $G_{\tilde{C}}(1, 1')$ is the anti-time-ordered Green function

$$\begin{aligned} G_{\tilde{C}}(1, 1') &= -i \langle \tilde{T}[\varphi_H(1)\varphi_H^+(1')] \rangle \\ &= -i - i\theta(t_{1'} - t_1) \langle \varphi_H(1)\varphi_H^+(1') \rangle + i\theta(t_1 - t_{1'}) \langle \varphi_H^+(1')\varphi_H(1) \rangle \end{aligned} \quad (2.28)$$

Since $G_C(1, 1') + G_{\tilde{C}}(1, 1') = G^>(1, 1') + G^<(1, 1')$, there are only four linear independent functions.

The physical quantities related Green functions are $G^{>,<}$ and $G^{a,r}$. In order to calculate the physics quantities, it is necessary to introduce the advanced and retarded Green function. the advanced and retarded Green functions are defined as

$$\begin{aligned} G^a(1, 1') &= i\theta(t_{1'} - t_1) \langle T\{\varphi_H(1), \varphi_H^+(1')\} \rangle \\ &= \theta(t_{1'} - t_1)[G^<(1, 1') - G^>(1, 1')] \end{aligned} \quad (2.29)$$

and

$$\begin{aligned} G^r(1, 1') &= -i\theta(t_1 - t_{1'}) \langle T\{\varphi_H(1), \varphi_H^+(1')\} \rangle \\ &= \theta(t_1 - t_{1'})[G^>(1, 1') - G^<(1, 1')] \end{aligned} \quad (2.30)$$

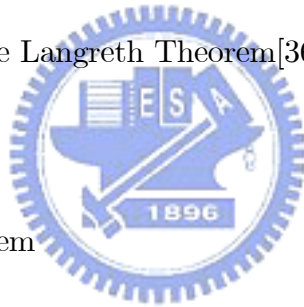
Here the curling bracket denotes an anticommutator. One can observe that $G^r - G^a = G^> - G^<$.

After developing the nonequilibrium Green function, the next problem is: how to obtain the Green function for an interacting system? Fortunately, under the adiabatic "switch on" limit, the equilibrium and nonequilibrium theories are structurally equivalent. The only difference is to replace the real axis integrals by contour integrals.

Since the most interesting problem is related to interacting system. The Green function constructed by the product of Green functions will be needed in the

Figure 2.5: Deformation of contour C

interacting system. One of the key problem in the nonequilibrium problem is: how to obtain the Green function which is structured by the product of Green functions. The solution is the Langreth Theorem[36].



2.1.2.1 The Langreth theorem

Consider the Green function with the structure $C = AB$, or, explicitly,

$$C(t_1, t_{1'}) = \int_C d\tau A(t_1, \tau) B(\tau, t_{1'}) \quad (2.31)$$

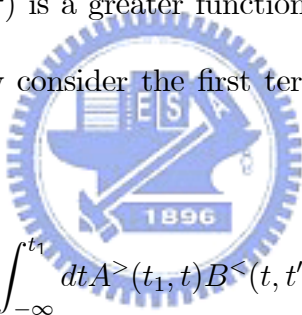
Now, let us evaluate the corresponding lesser Green function $C^<(t_1, t_{1'})$. In order to evaluate $C^<$, let us assume that t_1 is on the first half of C, and $t_{1'}$ is on the latter half, as shown in Fig.(2.5). Hence, the lesser Green function $C^<$ is rewritten

as:

$$C^{\lessdot}(t_1, t_{1'}) = \int_{C_1} d\tau A(t_1, \tau) B^{\lessdot}(\tau, t_{1'}) \quad (2.32)$$

$$+ \int_{C_1'} d\tau A^{\lessdot}(t_1, \tau) B(\tau, t_{1'})$$

The first term at right sight of Eq.(2.32) lies on the contour C_1 on which the variable $t_{1'}$ is always on the later half of C_1 and variable τ runs over all of C_1 . Hence, function $B(\tau, t_{1'})$ is a lesser function on the contour C_1 . In the same way, the function $A(t_1, \tau)$ is a greater function on C_2 . In order to obtain function $A(t_1, \tau)$, we split contour C_1 into two part: $C_{1A} : -\infty < \tau < t_1$ and $C_{1B} : t_1 < \tau < \infty$. The function $A(t_1, \tau)$ is a greater function on the contour C_{1A} and is a lesser function on C_{1B} . Now consider the first term in Eq.(2.32), and split the integration into two parts:



$$\int_{C_1} d\tau A(t_1, \tau) B^{\lessdot}(\tau, t_{1'}) = \int_{-\infty}^{t_1} dt A^{\lessdot}(t_1, t) B^{\lessdot}(t, t_{1'}) + \int_{-\infty}^{t_1} dt A^{\lessdot}(t_1, t) B^{\lessdot}(t, t_{1'}) \quad (2.33)$$

$$\equiv \int_{-\infty}^{\infty} dt A^r(t_1, t) B^{\lessdot}(t, t_{1'})$$

A similar analysis can be applied to the second term in Eq.(2.32). Put two terms together, we have the first of Langreth's result:

$$C^{\lessdot}(t_1, t_{1'}) = \int_{-\infty}^{\infty} dt [A^r(t_1, t) B^{\lessdot}(t, t_{1'}) + A^{\lessdot}(t_1, t) B^a(t, t_{1'})] \quad (2.34)$$

It is easy to generalize the result Eq.(2.34) for a (matrix) product of three

function: If $D = ABC$ is on the contour, then on the real axis, one has:

$$\begin{aligned} D^< &= (AB)^r C^< + (AB)^< C^a \\ &= (AB)^r C^< + (AB)^r C^a + A^< B^a C^a \end{aligned}$$

Now, the next problem is to solve the retarded function $(AB)^r$ which is constructed from the production of A and B. The required expression is derived by repeated use of the definitions Eq.(2.30) and Eq.(2.34). If $E = AB$:

$$\begin{aligned} E^r(t_1, t_{1'}) &= \theta(t_1 - t_{1'})[C^>(t_1, t_{1'}) - C^<(t_1, t_{1'})] \\ &= \theta(t_1 - t_{1'}) \int_{-\infty}^{\infty} dt [A^r(B^> - B^<) + (A^> - A^<)B^a] \\ &= \theta(t_1 - t_{1'}) \left[\int_{-\infty}^{t_1} dt (A^> - A^<)(B^> - B^<) + \int_{-\infty}^{t_{1'}} dt (A^> - A^<)(B^< - B^>) \right] \\ &= \int_{t_{1'}}^{t_1} dt A^r(t, t_1) B^r(t, t_{1'}) \end{aligned}$$

In the compact notation this relation is expressed as $E^r = A^r B^r$. Hence, the lesser function $D^<$ is obtained as:

$$D^< = A^r B^r C^< + A^r B^< C^a + A^< B^a C^a$$

In the interacting system, one may evaluate two Green functions with parallel evolution lines. In this case one needs the "lesser" and/or retarded/advance component of structures like:

$$C(\tau, \tau') = A(\tau, \tau')B(\tau, \tau') \quad (2.35)$$

$$D(\tau, \tau') = A(\tau, \tau')B(\tau', \tau) \quad (2.36)$$

where τ and τ' are contour variables. In similar to the analization presented above, one finds:

$$C^<(t, t') = A^<(t, t')B^<(t, t')$$

$$D^<(t', t) = A^<(\tau, t')B^>(t', t)$$

and

$$C^r(t, t') = A^<(t, t')B^r(t, t') + A^r(t, t')B^<(t, t') + A^r(t, t')B^r(t, t')$$

$$D^r(t, t') = A^r(t, t')B^<(t', t) + A^<(t, t')B^a(t', t)$$

$$= A^<(t, t')B^a(t', t) + A^r(t, t')B^<(t', t)$$

For a quick reference, the rules provided by the Langreth theorem are collective in TableII

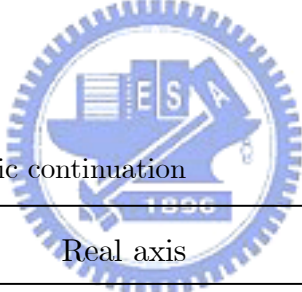


Table II Rules for analytic continuation

| Contour | Real axis |
|---|--|
| $C = \int_C AB$ | $C^< = \int_t [A^r B^< + A^< B^a]$ $C^r = \int_t A^r B^r$ |
| $D = \int_C ABC$ | $D^< = \int_t [A^r B^r C^< + A^r B^< C^a + A^< B^a C^a]$ $D^r = \int_t A^r B^r C^r$ |
| $C(\tau, \tau') = A(\tau, \tau')B(\tau, \tau')$ | $C^<(t, t') = A^<(t, t')B^<(t, t')$ $C^r(t, t') = A^<(t, t')B^r(t, t') + A^r(t, t')B^<(t, t') + A^r(t, t')B^r(t, t')$ |
| $D(\tau, \tau') = A(\tau, \tau')B(\tau', \tau)$ | $D^<(t, t') = A^<(t, t')B^>(t', t)$ $D^r(t, t') = A^<(t, t')B^a(t, t') + A^r(t, t')B^<(t', t)$ |

Using table II, all of possible combinations of product of Contour Green functions can be transformed to Real axis Green function. For example, if a contour function constructed by $D(t, t') = A(t, t')B(t, t')C(t, t')$, the real axis Green function corresponding to $D(t, t')$ can be obtained by following the way:

$$D(t, t') = A(t, t')B(t, t')C(t, t') = [A(t, t')B(t, t')]C(t, t')$$

$$\begin{aligned} D^<(t, t') &= [A(t, t')B(t, t')]^<C^<(t, t') \\ &= A^<(t, t')B^<(t, t')C^<(t, t') \end{aligned}$$

$$\begin{aligned} D^r(t, t') &= [A(t, t')B(t, t')]^<C^r(t, t') + [A(t, t')B(t, t')]^rC^<(t, t') + [A(t, t')B(t, t')]^rC^r(t, t') \\ &= A^<(t, t')B^<(t, t')C^r(t, t') \\ &\quad + A^<(t, t')B^r(t, t')C^<(t, t') + A^r(t, t')B^<(t, t')C^<(t, t') + A^r(t, t')B^r(t, t')C^<(t, t') \\ &\quad + A^<(t, t')B^r(t, t')C^r(t, t') + A^r(t, t')B^<(t, t')C^r(t, t') + A^r(t, t')B^r(t, t')C^r(t, t') \end{aligned}$$

Another useful formula is the Keldysh equation which can be used to calculate the lesser Green function and particle. Assume the lesser Green function of an interaction can be expanded as:

$$G^< = G_0^< + G_0^r \Sigma^< G^< + G_0^r \Sigma^< G^a + G_0^r \Sigma^< G^a \quad (2.37)$$

Proceed by iteration with respect to $G^<$, for one iterating, after regrouping the terms one can obtain

$$G^< = (1 + G_0^r \Sigma^r) G_0^< (1 + \Sigma^a G^a) + (G_0^r + G_0^r \Sigma^r G_0^r) \Sigma^< G^a + G_0^r \Sigma^r G_0^r \Sigma^r G^< \quad (2.38)$$

Repeat the process and rearrange the equation, one can find the second term of 2.38 has the form of $(G_0^r + G_0^r \Sigma^r G_0^r + G_0^r \Sigma^r G_0^r \Sigma^r G_0^r + \dots)$ which equals to the interacting retarded Green function G^r . And the first term of 2.38 becomes $(1 + [G_0^r + G_0^r \Sigma^r G_0^r + G_0^r \Sigma^r G_0^r \Sigma^r G_0^r + \dots] \Sigma^r) G_0^<(1 + \Sigma^a G^a)$ which can be rewritten as $(1 + G^r \Sigma^r) G_0^<(1 + \Sigma^a G^a)$ And the result is:

$$G^< = (1 + G^r \Sigma^r) G_0^<(1 + \Sigma^a G^a) + G^r \Sigma^< G^a$$

2.2 The Nonequilibrium transport Formula in the interacting resonant tunneling

In this section, the nonequilibrium transport formula based on the nonequilibrium Green function is introduced. The derivation processes is followed the ref.[17]. Consider a system that electron transport from lead through the central region which can interact with external field and then transport from the central region into another lead. The Hamiltonian of the system can be written as:

$$H = H_{cen} + H_{lead} + H_T \quad (2.39)$$

where H_{cen} is the Hamiltonian of the central region which contains the noninteracting electron Hamiltonian and the Hamiltonian of interaction part. The Hamiltonian of noninteracting electron with time dependent level is:

$$H_{cen}^0 = \sum_m \varepsilon_m(t) d_m^+ d_m \quad (2.40)$$

Here $d_m^+(d_m)$ is the creation (annihilation) operator in central region.

In this dissertation, the electron-photon interaction is modeled as the dipole interaction, hence the interaction Hamiltonian can be written as:

$$H_{cen}^{int} = Md_1^+ d_2 b^+ + h.c \quad (2.41)$$

where $b^+(b)$ is the photon creator (annihilator) operator. The electron-photon coupling coefficient $M = -\vec{p} \cdot \vec{E}$, where $\vec{p} = e \langle 2 | \vec{r} | 1 \rangle$, is the electron dipole transition matrix element and \vec{E} is the strength of electric field of the photon field. .

The lead Hamiltonian is:

$$H_{lead} = \sum_{k_\alpha \in L, R, m} \varepsilon_{k_\alpha}(t) c_{k_\alpha}^+ c_{k_\alpha} + h.c. \quad (2.42)$$

where $c_{k_\alpha}^+(c_{k_\alpha})$ creates (annihilates) the electron with momentum k at α lead ($\alpha \in L, R$). The electron in lead is assumed to be noninteracting except the applied electrostatic-potential causes a bias voltage. The time dependent bias voltage equivalent to accumulating or depleting charge to form a dipole around the central region. Hence, the particle energy in lead is time dependent, i.e. $\varepsilon_{k_\alpha} \rightarrow \varepsilon_{k_\alpha}(t) = \varepsilon_{k_\alpha}^0 + \Delta_\alpha(t)$. The occupation in each state is not changed by the applied bias and is determined by an equilibrium distribution function. The time dependent Green functions in the leads for the uncoupled system are

$$\begin{aligned} g^<(t, t') &\equiv i \langle c_k^+(t') c_k(t) \rangle \\ &= i f(\varepsilon_{k_\alpha}^0) \exp[-i \int_{t'}^t dt_1 \varepsilon_{k_\alpha}(t_1)] \end{aligned} \quad (2.43)$$

$$\begin{aligned}
g^{r,a}(t, t') &\equiv \mp i\theta(\pm t \mp t') \langle \{c_k(t), c_k^+(t')\} \rangle \\
&= \mp i\theta(\pm t \mp t') \exp[-i \int_{t'}^t dt_1 \varepsilon_{k_\alpha}(t_1)]
\end{aligned} \tag{2.44}$$

The tunneling Hamiltonian H_T is

$$H_T = \sum_{k_\alpha, m \in 1, 2} V_{k_\alpha, m}^*(t) d_m^+ c_{k_\alpha} + h.c. \tag{2.45}$$

where $V_{k_\alpha, m}^*(t)$ is the tunneling matrix between lead α and dot.

The current due to electron transport from left contact into central region can be calculated from time evaluation of the occupation number of the left contact:

$$J_L = -e \left\langle \dot{N}_L \right\rangle = -\frac{ie}{\hbar} \langle [H, N_L] \rangle \tag{2.46}$$

where $N_L = \sum_{k, \alpha \in L} c_{k_\alpha}^+ c_{k_\alpha}$ and $H = H_C + H_T + H_{cen}$. Since N_L commutes with H_C and H_{cen}^0 , one finds:

$$\begin{aligned}
J_L &= \frac{ie}{\hbar} \sum_{k, \alpha \in L} V_{k_\alpha, n} \langle c_{k_\alpha}^+ d_n \rangle - V_{k_\alpha, n}^* \langle d_n^+ c_{k_\alpha} \rangle \\
&= \frac{2e}{\hbar} \text{Re} \left\{ \sum_{k, \alpha \in L} V_{k_\alpha, n}(t) G_{n, k_\alpha}^<(t, t') \right\}
\end{aligned} \tag{2.47}$$

where $G_{k_\alpha, n}^<(t, t) = -[G_{k_\alpha, n}^<(t, t)]^*$, and $G_{k_\alpha, n}^<(t, t') \equiv i \langle c_{k_\alpha}^+(t') d_n(t) \rangle$. In order to obtain the lesser Green function, one must find the contour Green function and then transform it into lesser Green function. The contour Green function can be obtained by the equation of motion or the Dyson expansion technique.

$$G_{k_\alpha, n}(\tau, \tau') = \sum_m \int d\tau G_{nm}(\tau, \tau_1) V_{k_\alpha, m}^*(\tau_1) g_{k_\alpha}(\tau_1, \tau') \tag{2.48}$$

Using the Langreth theorem, one can find the corresponding lesser Green function as:

$$G_{n,k\alpha}^<(t,t') = \sum_m \int dt_1 V_{k\alpha,m}^*(t_1) [G_{nm}^r(t,t_1) g_{k\alpha}^<(t_1,t') + G_{nm}^<(t,t_1) g_{k\alpha}^a(t_1,t')] \quad (2.49)$$

where Green functions are defined in Eq.(2.44) and Eq.(2.43). Combining Eq.(2.44), Eq.(2.43) and Eq.(2.47), one obtains:

$$J_L = -\frac{2e}{\hbar} \text{Im} \left\{ \sum_{\substack{k,\alpha \in L \\ m,n}} V_{k\alpha,n}(t) \int_{-\infty}^t dt_1 e^{i \int_{t_1}^t dt_2 \varepsilon_{k\alpha}(t_2)} V_{k\alpha,m}^*(t_1) \right. \\ \left. \times [G_{nm}^r(t,t_1) f_L(\varepsilon_{k\alpha}) + G_{nm}^<(t,t_1)] \right\} \quad (2.50)$$

Define the generalized linewidth function:

$$[\Gamma^L(\varepsilon, t_1, t)]_{mn} = 2\pi \sum_{\alpha \in L} \rho(\varepsilon) V_{\alpha,n}(\varepsilon, t) V_{\alpha,m}^*(\varepsilon, t_1) \exp[i \int_{t_1}^t dt_2 \Delta_\alpha(\varepsilon, t_2)] \quad (2.51)$$

In terms of the generalized linewidth function, the current can be expressed as:

$$J_L = -\frac{2e}{\hbar} \int_{-\infty}^t dt_1 \int \frac{d\varepsilon}{2\pi} \text{Im} Tr \{ e^{-i\varepsilon(t_1-t)} \Gamma(\varepsilon, t_1, t) \\ \times [G^<(t, t_1) + f_L(\varepsilon) G^r(t, t_1)] \} \quad (2.52)$$

The Eq.(2.52) has rich physical meaning. The first term in square bracket is the lesser Green function which relates the occupation number (the particle number) in the central region. This term expresses the electron tunneling off the central region into the lead with the rate $\Gamma(\varepsilon, t_1, t)$. The second term contains the Fermi-Dirac distribution function which is the occupation number of electron in left and the retarded Green function which relates the density of state in central region.

This term describes the electron tunneling for left lead into central region. Now, the remaining problem is: how to solve the Green function in central region. Without additional interaction except the tunneling between lead and central region, the retarded Green function for central region can be solved by the Dyson expansion:

$$G^r(t, t') = g^r(t, t') + \int dt_1 \int dt_2 g^r(t, t_1) \Sigma^r(t_1, t_2) G^r(t_2, t') \quad (2.53)$$

$$\Sigma_{nn'}^r(t_1, t_2) = \sum_{k, \alpha \in L, R} V_{k\alpha, n}^*(t_1) g_{k\alpha}^r V_{k\alpha, n'}^*(t_2) \quad (2.54)$$

In order to solve Σ^r , the wideband approximation is used[37]. The wideband approximation consists of (i) the energy due to tunneling effect, (ii) energy independent line width and (iii) allowing a single time dependence. Hence, the retarded self-energy in Eq.(2.59) becomes:

$$\begin{aligned} \Sigma_{nn'}^r(t_1, t_2) &= \sum_{k, \alpha \in L, R} u_\alpha^*(t_1) u_\alpha(t_2) e^{-i \int_{t_2}^{t_1} dt_3 \Delta_\alpha(t_3)} \\ &\times \int \frac{d\varepsilon}{2\pi} e^{-i\varepsilon(t_1-t_2)} \theta(t_1 - t_2) [-i\Gamma\alpha] \\ &= -\frac{1}{2} [\Gamma^L(t_1) + \Gamma^R(t_1)] \delta(t_1 - t_2) \end{aligned} \quad (2.55)$$

And the retarded Green function for central region including the perturbation due to tunneling effect is:

$$G^{r,a}(t, t') = g^{r,a}(t, t') \exp\left\{\mp \int_{t'}^t dt_1 \frac{1}{2} [\Gamma^L(t_1) + \Gamma^R(t_1)]\right\} \quad (2.56)$$

with

$$g^{r,a}(t, t') = \mp i \theta(\pm t \mp t') \exp\left[-i \int_{t'}^t dt_1 \varepsilon_0(t_1)\right] \quad (2.57)$$

The lesser Green function $G^<(t, t_1)$ can be calculated by Keldysh equation:

$$G^<(t, t') = \int dt_1 G^r(t, t_1) \Sigma^<(t_1, t_2) G^a(t_2, t') \quad (2.58)$$

where

$$\Sigma^<(t_1, t_2) = i \int \frac{d\varepsilon}{2\pi} e^{-i\varepsilon(t_1-t_2)} f_{L/R}(\varepsilon) \Gamma^{L/R}(\varepsilon, t_1, t) \quad (2.59)$$

Thus, the current formula is obtained as:

$$J_L = -\frac{e}{\hbar} [\Gamma^L(t) N(t) + \int \frac{d\varepsilon}{\pi} f_L(\varepsilon) \int_{-\infty}^{t_1} dt_1 \Gamma^{L/R}(t_1, t) \text{Im}\{e^{-i\varepsilon(t_1-t_2)} G^r(t, t_1)\}] \quad (2.60)$$

In order to give a compact express, the generalized spectral function is introduced:

$$A_{L/R}(\varepsilon, t) = \int dt_1 u_{L/R}(t_1) G^r(t, t_1) \exp[i\varepsilon(t - t_1) - i \int_t^{t_1} dt_2 \Delta_{L/R}(t_2)] \quad (2.61)$$

In term of $A_{L/R}(\varepsilon, t)$, the occupation number can be expressed as

$$N(t) = \sum_{\alpha \in L, R} \Gamma^\alpha(t) \int \frac{d\varepsilon}{2\pi} f_{L/R}(\varepsilon) |A_{L/R}(\varepsilon, t)|^2 \quad (2.62)$$

Thus, the current formula for electron flowing out from central region into left/right lead can be rewritten as a compact form:

$$J_{L/R} = J_{L/R}^{out}(t) - J_{L/R}^{in}(t) \quad (2.63)$$

$$J_{L/R}^{out}(t) = -\frac{e}{\hbar} \Gamma^{L/R}(t) N(t) \quad (2.64)$$

$$J_{L/R}^{in}(t) = -\frac{e}{\hbar} u_{L/R} \int \frac{d\varepsilon}{\pi} f_L(\varepsilon) \text{Im}\{A_{L/R}(\varepsilon, t)\} \quad (2.65)$$

It is evident that $A_{L/R}(\varepsilon, t)$ is just the Fourier transformation of retarded Green function for central region G^r for the time independent case.

2.3 The Equation of Motion Method and The Lacroix's Decoupled Scheme

There are many ways to solve the strong correlation problem. In Anderson model or Kondo problem, equation of motion method (EOM), slave boson, and the renormalization group are often used. The EOM is a compact way. The processes of the EOM method are: (i) calculate the time evolution of the operator by Heisenberg Equation of motion $i\dot{d} = [d, H]$ and take the Fourier transformation into energy representation. (ii) substitute the result of (i) into the operator in Green function. (iii) choose a suitable decoupled approximation scheme to cut off the processes. For the Anderson model, the EOM method needs to calculate the two particle correlation function $\langle d_{\sigma_1} d_{\sigma_2}^+ d_{\sigma_2}; d_{\sigma_1}^+ \rangle$. The suitable decoupled scheme is needed, of which the perturbation order or the interaction bubble for calculation is determined. The correlation function $\langle\langle d_{\sigma_1} d_{\sigma_2}^+ d_{\sigma_2}; d_{\sigma_1}^+ \rangle\rangle$ appears due to electron-electron Coulomb interaction. The decoupled approximation $\langle\langle d_{\sigma_1} d_{\sigma_2}^+ d_{\sigma_2}; d_{\sigma_1}^+ \rangle\rangle \sim \langle n_{\sigma_2} \rangle \langle\langle d_{\sigma_1}; d_{\sigma_1}^+ \rangle\rangle$ is the well-known Hartree-Fock approximation which gives the Coulomb blockade effect in transport problem and is appropriate for the temperature higher than Kondo temperature. When the temperature is near the Kondo temperature, the Kondo effect becomes prominent and the Hartree Fock approximation is not valid. The higher order term which contains two operators for electron in lead must be included. Lacroix suggested

the decoupled approximation:

$$\langle\langle c_{k\sigma}c_{q-\sigma}d_{-\sigma}^+, d_{\sigma}^+ \rangle\rangle \approx -\langle d_{-\sigma}^+c_{q-\sigma} \rangle \langle\langle c_{k\sigma}, d_{\sigma}^+ \rangle\rangle \quad (2.66)$$

$$\langle\langle c_{q-\sigma}^+c_{k\sigma}d_{-\sigma}, d_{\sigma}^+ \rangle\rangle \approx -\langle c_{q-\sigma}^+d_{-\sigma} \rangle \langle\langle c_{k\sigma}, d_{\sigma}^+ \rangle\rangle \quad (2.67)$$

$$\langle\langle c_{q-\sigma}^+c_{k-\sigma}d_{\sigma}, d_{\sigma}^+ \rangle\rangle \approx \langle c_{q-\sigma}^+c_{k-\sigma} \rangle \langle\langle d_{\sigma}, d_{\sigma}^+ \rangle\rangle \quad (2.68)$$

can be employed for the temperature higher than or near the Kondo temperature.

For the temperature is higher than or near Kondo temperature, $T \sim T_K$, the Eq.(2.67) and Eq.(2.68) are the higher order terms and can be ignored for $T \sim T_K$. This approximation is called the high temperature Lacroix's decoupled approximation. For temperature $T \ll T_K$, both Eq.(2.67) and Eq.(2.68) must be considered. And more higher order terms have to be included as temperature is lower.



CHAPTER 3

ANDERSON MODEL WITH SPIN-FLIP ASSOCIATED TUNNELING

Recently, many theoretical and experimental researches related to electron spin were studied. Owing to the progress in nanofabrication and microelectronic techniques, devices based on the electron spin, such as the spin memory[38], spin transistor[39] and electron spin based quantum computer[40],[41] may be realized very soon. These devices are related to the spin polarization orientation or spin flip effect. Usually, the spin flip effect occurs in the scattering processes. The scattering processes may be caused by the magnetic impurities, magnons, domain walls at the interface or electrode[42] or may be due to the interaction with phonon[43], or photon field[44]. In addition to the scattering processes, the spin flip may take place when the electron transports between different spin state regions. One of the instances is that the electron transports between the Rashba quantum dot and ferromagnetic lead. The Rashba effect might be observed in InAs semiconductors. The eigen state of the Rashba Hamiltonian is the superposition of the spin state $|\uparrow\rangle$ and $|\downarrow\rangle$ i.e. $|\pm\rangle = \frac{1}{\sqrt{2}}(e^{i\theta/2} |\uparrow\rangle \pm e^{-i\theta/2} |\downarrow\rangle)$ [41]. It is known that the off-diagonal terms of the tunneling amplitude matrix and coupling constant are nonzero and

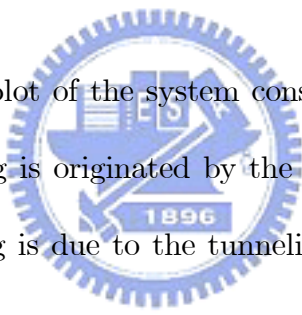
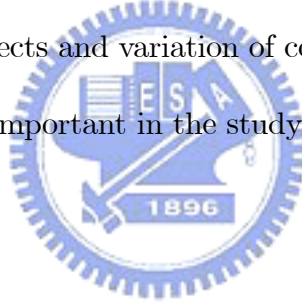


Figure 3.1: The Schematic plot of the system considered in this work. (a) The spin flip associated tunneling is originated by the impurity scattering. (b) The spin flip associated tunneling is due to the tunneling between the different spin states.

the spin flip associated tunneling appears in the system[45]. The sketch of the spin-flip associated tunneling through a quantum system is shown in Fig.3.1.

The spin flip associated tunneling effect could cause some special behaviors in electric properties of the material. The intradot spin flip effect was found to shift the resonant energy ε_0 of the quantum dot to $\varepsilon_0 \pm R$, where R is the spin flip scattering amplitude[45]. Sergueev et. al.[46] studied the spin flip associated

tunneling through a quantum dot and described the spin valve effect. The spin valve effect caused by the transport between different spin states manifests that the resistance depends on the direction (in parallel or anti-parallel) of the magnetization of two ferromagnetic (FM) metals[46][47][48][49]. Zhu and Balatsky studied the spin flip associated tunneling through a local nuclear spin precessing in a magnetic field to simulate the conductance oscillation observed in STM experiment[50]. They included the off-diagonal process and concluded that the conductance of the system can be modified obviously. F. Guinea pointed out that the elastic spin flip effects give rise to a temperature-independent reduction of the magnetoresistance while the inelastic spin-flip processes give rise to a temperature dependent nonohmic effects and variation of conductance[42]. As mentioned above, the spin flip effect is important in the study of spin electronic devices and thus is worth to be explored.



In the spin-based devices such as the spin based quantum computer which may be operated at low temperature, the correlation between the electron in quantum dot and the conduction electron in reservoir is important because the correlation will cause a peak of density of state (DOS) in the vicinity of Fermi level for temperature $T \leq T_K$, where T_K is Kondo temperature. Anderson impurity model, which describes the correlation due to on-site Coulomb interaction and the direct tunneling between the conduction band and the local spin state in magnetic impurity, is also employed to describe the quantum dot (QD) system[51].

The correlation interaction causes a sharp peak in the vicinity of Fermi level for temperature below T_K . The electron in impurity may tunnel out of the impurity site to occupy a "virtual state", and then to be replaced by an electron from the metal[21][52]. This process can effectively "flip" the spin of impurity. Schrieffer and Wolff have shown that, in the limit of strong on-site Coulomb interaction, Anderson impurity model is equivalent to the s-d model when the impurity level ε_0 is well below the Fermi level and Kondo effect is obtained in this limit[22]. In the original Anderson impurity model, the electron spin does not flip during the process of tunneling between the impurity and the electron reservoir. In this work, we consider the electron spin flips during the tunneling process, i.e. the spin flip associated coupling constant $\Gamma_\alpha^{\bar{\sigma}\sigma} = 2\pi \sum_{k,s,\alpha \in L,R} V_{k\alpha s,\bar{\sigma}}^* V_{k\alpha s,\sigma} \times \delta(\omega - \varepsilon_{k\alpha s})$ where $\sigma(s)$ is the spin state of electron in QD (lead) and $\bar{\sigma} \neq \sigma$ is included in our study. The effects on the density of state and the conductance of quantum dot system versus the strength of the spin flip coupling will be discussed. Comparing to the original Anderson model, the spin flip associated tunneling effect is expected to contribute additional self-energy which may modify the local density of state (LDOS, or the diagonal part $-2 \text{Im} G_{\sigma\sigma}^r$). The conductance depends strongly on the profile of the spectral function, and the off-diagonal part, $-2 \text{Im} G_{\bar{\sigma}\sigma}^r$, of which may change sign in the vicinity of peak position of DOS. Therefore, the off-diagonal spectral function is expected to modify the conductance. In other words, the conductance may be modified by the spin flip associated tunneling.

Instead of studying the mechanism of the spin flip effect, we will study the spin flip effect in a phenomenological way. The tunneling coupling constant will be assumed the same as that proposed in ref.[50].

3.1 Model and Formalism

The Hamiltonian of the system considered in this work can be written as:

$$H_d = \sum_{\sigma} \varepsilon_{\sigma} d_{\sigma}^{\dagger} d_{\sigma} + U n_{\sigma} n_{\bar{\sigma}} \quad (3.1)$$

$$H_C = \sum_{\substack{k_{\alpha s} \\ \alpha \in L, R}} \varepsilon_{k_{\alpha s}} c_{k_{\alpha s}}^{\dagger} c_{k_{\alpha s}}$$

$$H_T = \sum_{k_{\alpha s}} V_{k_{\alpha s}, \sigma}^* d_{\sigma}^{\dagger} c_{k_{\alpha s}} + V_{k_{\alpha s}, \sigma} c_{k_{\alpha s}}^{\dagger} d_{\sigma}$$

where d_{σ}^{\dagger} (d_{σ}) is the creation (annihilation) operator of the electron with spin state σ in the dot, and $c_{k_{\alpha s}}^{\dagger}$ ($c_{k_{\alpha s}}$) is the creation (annihilation) operator of an electron with momentum k and spin state s in α lead (where $\alpha \in L, R$). Note that the spin states s and σ are not necessary in the same eigenstate, for example the spin state σ in QD may be the eigen state of Rashba and the spin state s in the lead may be the pure spin up or spin down state. The energy $\varepsilon_{k_{\alpha s}}$ is the single particle energy of conduction electron in α lead. U is the intradot Coulomb interaction. The electron tunneling between the lead and dot can be described by the tunneling matrix $V_{k_{\alpha s}, \sigma}$. As shown in Ref.[50], the coupling constant between QD and the lead can be expressed by $\Gamma_{\alpha}^{\bar{\sigma}\sigma} = 2\pi \sum_{k, s, \alpha \in L, R} V_{k_{\alpha s}, \bar{\sigma}}^* V_{k_{\alpha s}, \sigma} \times \delta(\omega - \varepsilon_{k_{\alpha s}})$. The spin-flip coupling constant is set to be symmetric for the state $\sigma(\bar{\sigma})$ flipped

into the state $\bar{\sigma}(\sigma)$, i.e. $\Gamma_{\alpha}^{\bar{\sigma}\sigma} = \Gamma_{\alpha}^{\sigma\bar{\sigma}} = \Gamma_{\alpha}^s$. And the normal coupling constant $\Gamma_{\alpha}^{\sigma\sigma} = 2\pi \sum_{k,s,\alpha \in L,R} V_{k\alpha s,\sigma}^* V_{k\alpha s,\sigma} \times \delta(\omega - \varepsilon_{k\alpha s})$ is assumed to be spin independent, i.e. $\Gamma_{\alpha}^{\sigma\sigma} = \Gamma_{\alpha}^{\bar{\sigma}\bar{\sigma}} = \Gamma_{\alpha}^n$. In this paper, we use the notion $\bar{\sigma}$ to stand for spin being not equal to σ while σ' being equal to or not equal to σ .

The Green function \mathbf{G} corresponding to spin flip associated tunneling effect of noninteracting system can be written as:

$$\begin{aligned} \begin{bmatrix} G_{\sigma\sigma} & G_{\sigma\bar{\sigma}} \\ G_{\bar{\sigma}\sigma} & G_{\bar{\sigma}\bar{\sigma}} \end{bmatrix} &= \begin{bmatrix} G_{\sigma\sigma}^0 & 0 \\ 0 & G_{\bar{\sigma}\bar{\sigma}}^0 \end{bmatrix} + \begin{bmatrix} G_{\sigma\sigma}^0 & 0 \\ 0 & G_{\bar{\sigma}\bar{\sigma}}^0 \end{bmatrix} \begin{bmatrix} \Sigma_{\sigma\sigma} & \Sigma_{\sigma\bar{\sigma}} \\ \Sigma_{\bar{\sigma}\sigma} & \Sigma_{\bar{\sigma}\bar{\sigma}} \end{bmatrix} \begin{bmatrix} G_{\sigma\sigma} & G_{\sigma\bar{\sigma}} \\ G_{\bar{\sigma}\sigma} & G_{\bar{\sigma}\bar{\sigma}} \end{bmatrix} \\ &= \begin{bmatrix} [(G_{\sigma\sigma}^0)^{-1} - \Sigma_{\sigma\sigma} - \Sigma_{\sigma\bar{\sigma}} \tilde{G}_{\bar{\sigma}\bar{\sigma}}^0 \Sigma_{\bar{\sigma}\sigma}]^{-1} & \tilde{G}_{\sigma\sigma}^0 \Sigma_{\sigma\bar{\sigma}} G_{\bar{\sigma}\bar{\sigma}} \\ \tilde{G}_{\bar{\sigma}\bar{\sigma}}^0 \Sigma_{\bar{\sigma}\sigma} G_{\sigma\sigma} & [(G_{\bar{\sigma}\bar{\sigma}}^0)^{-1} - \Sigma_{\bar{\sigma}\bar{\sigma}} - \Sigma_{\bar{\sigma}\sigma} \tilde{G}_{\sigma\sigma}^0 \Sigma_{\sigma\sigma'}]^{-1} \end{bmatrix} \end{aligned} \quad (3.2)$$

where the self-energy $\Sigma_{\sigma\sigma}$ is caused by the tunneling without spin-flip associated and the self-energy $\Sigma_{\bar{\sigma}\bar{\sigma}}$ is caused by the spin-flip associated tunneling. $\Sigma_{\bar{\sigma}\sigma}$ flips spin σ to spin $\bar{\sigma}$ during the electron transports between the lead and the dot. $G_{\sigma\sigma}^0$ is the free particle Green function and $\tilde{G}_{\sigma\sigma}^0 = (\omega - \varepsilon_{\sigma} - \Sigma_{\sigma\sigma})^{-1}$ is Green function of electron in QD with spin state σ perturbed by tunneling effect. The detailed derivation of Eq.(3.2) is shown in Appendix A.

If the intradot Coulomb interaction is included, the Kondo effect occurs when $T \leq T_K$. There are many approaches to solve the problem, such as equation of motion (EOM) method[25][26][27][28][47] noncrossing-approximation approach[29][48], or renormalization group method[49][26][30]. The equation of motion method will

be used to solve the Green function of the interaction system in this work. In the processes of the EOM, the two-particle correlation function (or Green function) arises from the two-particle on-site Coulomb interaction and needs to be decoupled. The accuracy of EOM method depends on the decoupling scheme. One of the compact way to decouple the two-particle correlation function to single-particle correlation function is the decoupling scheme introduced by Lacroix for high temperature (i.e. $T \geq T_K$). The high temperature Lacroix's decoupling approximation at low temperatures ($T < T_K$) gives only qualitative solution and is even quantitatively correct at high temperatures ($T \geq T_K$)[46][26]. The EOM and Lacroix's high temperature decoupling scheme are popularly adopted by many authors. In this work, we will use the high temperature Lacroix decoupling approximation to decouple the two-particle Green function.

Consider the spin flip associated tunneling effect and the intradot particle-particle interaction is assumed to be Coulomb interaction. By using the method of equation of motion in Green function \mathbf{G} , one obtains

$$\begin{aligned}
 & \begin{bmatrix} (\omega - \varepsilon_\sigma)G_{\sigma\sigma} & (\omega - \varepsilon_\sigma)G_{\sigma\bar{\sigma}} \\ (\omega - \varepsilon_{\bar{\sigma}})G_{\bar{\sigma}\sigma} & (\omega - \varepsilon_{\bar{\sigma}})G_{\bar{\sigma}\bar{\sigma}} \end{bmatrix} \\
 &= \begin{bmatrix} 1 & 0 \\ 0 & 1 \end{bmatrix} + \begin{bmatrix} \Sigma_{\sigma\sigma}^{Tn} & \Sigma_{\sigma\bar{\sigma}}^{Ts} \\ \Sigma_{\bar{\sigma}\sigma}^{Ts} & \Sigma_{\bar{\sigma}\bar{\sigma}}^{Tn} \end{bmatrix} \begin{bmatrix} G_{\sigma\sigma} & G_{\sigma\bar{\sigma}} \\ G_{\bar{\sigma}\sigma} & G_{\bar{\sigma}\bar{\sigma}} \end{bmatrix} + U \begin{bmatrix} G_{\sigma\sigma}^{(2)} & G_{\sigma\bar{\sigma}}^{(2)} \\ G_{\bar{\sigma}\sigma}^{(2)} & G_{\bar{\sigma}\bar{\sigma}}^{(2)} \end{bmatrix}
 \end{aligned} \tag{3.3}$$

where $G_{\sigma\bar{\sigma}} \equiv (-i) \langle T \{ d_\sigma, d_{\bar{\sigma}}^+ \} \rangle$ and $G_{\sigma\sigma}^{(2)} \equiv (-i) \langle T \{ d_\sigma n_{\bar{\sigma}}, d_\sigma^+ \} \rangle$. The Green function $G_{\sigma\sigma}^{(2)}$ is the two particle Green function corresponding to particle-particle

interaction (Coulomb interaction) which relates the Kondo effect. Using the EOM

in $\mathbf{G}^{(2)}$, we obtain:

$$\begin{aligned}
& \begin{bmatrix} (\omega - \varepsilon_\sigma - U)G_{\sigma\sigma}^{(2)} & (\omega - \varepsilon_\sigma - U)G_{\sigma\bar{\sigma}}^{(2)} \\ (\omega - \varepsilon_{\bar{\sigma}} - U)G_{\bar{\sigma}\sigma}^{(2)} & (\omega - \varepsilon_{\bar{\sigma}} - U)G_{\bar{\sigma}\bar{\sigma}}^{(2)} \end{bmatrix} \\
& = \begin{bmatrix} \langle n_{\bar{\sigma}} \rangle & 0 \\ 0 & \langle n_\sigma \rangle \end{bmatrix} + \\
& \sum_{k\alpha s} \begin{bmatrix} V_{k\alpha s, \sigma}^*(-i) \langle T \{ c_{k\alpha s}^+ d_{\bar{\sigma}}^+ d_\sigma^+ \} \rangle & V_{k\alpha s, \sigma}^*(-i) \langle T \{ c_{k\alpha s}^+ d_{\bar{\sigma}}^+ d_\sigma^+ \} \rangle \\ V_{k\alpha s, \bar{\sigma}}^*(-i) \langle T \{ c_{k\alpha s}^+ d_\sigma^+ d_\sigma^+ \} \rangle & V_{k\alpha s, \bar{\sigma}}^*(-i) \langle T \{ c_{k\alpha s}^+ d_\sigma^+ d_\sigma^+ \} \rangle \end{bmatrix} \\
& + \sum_{k\alpha s} \begin{bmatrix} V_{k\alpha s, \bar{\sigma}}(-i) \langle T \{ c_{k\alpha s}^+ d_\sigma d_\sigma, d_\sigma^+ \} \rangle & V_{k\alpha s, \bar{\sigma}}(-i) \langle T \{ c_{k\alpha s}^+ d_\sigma d_\sigma, d_\sigma^+ \} \rangle \\ V_{k\alpha s, \sigma}(-i) \langle T \{ c_{k\alpha s}^+ d_{\bar{\sigma}} d_\sigma, d_\sigma^+ \} \rangle & V_{k\alpha s, \sigma}(-i) \langle T \{ c_{k\alpha s}^+ d_{\bar{\sigma}} d_\sigma, d_\sigma^+ \} \rangle \end{bmatrix} \\
& - \sum_{k\alpha s} \begin{bmatrix} V_{k\alpha s, \bar{\sigma}}^*(-i) \langle T \{ c_{k\alpha s}^+ d_\sigma^+ d_\sigma^+ \} \rangle & V_{k\alpha s, \bar{\sigma}}^*(-i) \langle T \{ c_{k\alpha s}^+ d_\sigma^+ d_\sigma^+ \} \rangle \\ V_{k\alpha s, \sigma}^*(-i) \langle T \{ c_{k\alpha s}^+ d_\sigma^+ d_\sigma^+ \} \rangle & V_{k\alpha s, \sigma}^*(-i) \langle T \{ c_{k\alpha s}^+ d_\sigma^+ d_\sigma^+ \} \rangle \end{bmatrix}
\end{aligned} \tag{3.4}$$

In general there are four one-particle Green functions ($G_{\sigma\sigma}$, $G_{\sigma\bar{\sigma}}$, $G_{\bar{\sigma}\sigma}$ and $G_{\bar{\sigma}\bar{\sigma}}$)

and four two-particle Green functions ($G_{\sigma\sigma}^{(2)}$, $G_{\sigma\bar{\sigma}}^{(2)}$, $G_{\bar{\sigma}\sigma}^{(2)}$ and $G_{\bar{\sigma}\bar{\sigma}}^{(2)}$) in our system.

Contrast with Eq.(3.3), the equation of Green function $\mathbf{G}^{(2)}$ can be assumed as:

$$\begin{aligned}
& \begin{bmatrix} (\omega - \varepsilon_\sigma - U)G_{\sigma\sigma}^{(2)} & (\omega - \varepsilon_\sigma - U)G_{\sigma\bar{\sigma}}^{(2)} \\ (\omega - \varepsilon_{\bar{\sigma}} - U)G_{\bar{\sigma}\sigma}^{(2)} & (\omega - \varepsilon_{\bar{\sigma}} - U)G_{\bar{\sigma}\bar{\sigma}}^{(2)} \end{bmatrix} \\
& = \begin{bmatrix} \langle n_{\bar{\sigma}} \rangle & 0 \\ 0 & \langle n_\sigma \rangle \end{bmatrix} + \begin{bmatrix} X_{\sigma\sigma}^{(2)} & X_{\sigma\bar{\sigma}}^{(2)} \\ X_{\bar{\sigma}\sigma}^{(2)} & X_{\bar{\sigma}\bar{\sigma}}^{(2)} \end{bmatrix} \begin{bmatrix} G_{\sigma\sigma} & G_{\sigma\bar{\sigma}} \\ G_{\bar{\sigma}\sigma} & G_{\bar{\sigma}\bar{\sigma}} \end{bmatrix} + \begin{bmatrix} Y_{\sigma\sigma}^{(2)} & Y_{\sigma\bar{\sigma}}^{(2)} \\ Y_{\bar{\sigma}\sigma}^{(2)} & Y_{\bar{\sigma}\bar{\sigma}}^{(2)} \end{bmatrix} \begin{bmatrix} G_{\sigma\sigma}^{(2)} & G_{\sigma\bar{\sigma}}^{(2)} \\ G_{\bar{\sigma}\sigma}^{(2)} & G_{\bar{\sigma}\bar{\sigma}}^{(2)} \end{bmatrix}
\end{aligned} \tag{3.5}$$

In order to simplify the problem, we consider infinite U limit. Under infinite U

limit, the off-diagonal term of $\mathbf{Y}^{(2)}$ can be ignored (the detailed derivation will be

given in appendix B). The Eq.(3.5) can be rewritten as:

$$\begin{aligned} & \begin{bmatrix} G_{\sigma\sigma}^{(2)} & G_{\sigma\bar{\sigma}}^{(2)} \\ G_{\bar{\sigma}\sigma}^{(2)} & G_{\bar{\sigma}\bar{\sigma}}^{(2)} \end{bmatrix} \\ &= \begin{bmatrix} g_{\sigma\sigma}^{0(2)} \langle n_{\bar{\sigma}} \rangle & 0 \\ 0 & g_{\sigma\bar{\sigma}}^{0(2)} \langle n_{\sigma} \rangle \end{bmatrix} + \begin{bmatrix} g_{\sigma\sigma}^{0(2)} (X_{\sigma\sigma}^{(2)} G_{\sigma\sigma} + X_{\sigma\bar{\sigma}}^{(2)} G_{\bar{\sigma}\sigma}) & g_{\sigma\sigma}^{0(2)} (X_{\sigma\bar{\sigma}}^{(2)} G_{\bar{\sigma}\bar{\sigma}} + X_{\sigma\sigma}^{(2)} G_{\sigma\bar{\sigma}}) \\ g_{\sigma\bar{\sigma}}^{0(2)} (X_{\bar{\sigma}\sigma}^{(2)} G_{\sigma\sigma} + X_{\bar{\sigma}\bar{\sigma}}^{(2)} G_{\bar{\sigma}\sigma}) & g_{\sigma\bar{\sigma}}^{0(2)} (X_{\bar{\sigma}\bar{\sigma}}^{(2)} G_{\sigma\bar{\sigma}} + X_{\bar{\sigma}\sigma}^{(2)} G_{\bar{\sigma}\bar{\sigma}}) \end{bmatrix} \end{aligned}$$

where $g_{\sigma\sigma}^{0(2)} \equiv (\omega - \varepsilon_{\sigma} - Y_{\sigma\sigma} - U)^{-1}$ and $g_{\sigma\bar{\sigma}}^{0(2)} \equiv (\omega - \varepsilon_{\bar{\sigma}} - Y_{\bar{\sigma}\bar{\sigma}} - U)^{-1}$. Substitute

$\mathbf{G}^{(2)}$ into \mathbf{G} , one obtains:

$$\begin{aligned} & \begin{bmatrix} (\omega - \varepsilon_{\sigma}) G_{\sigma\sigma} & (\omega - \varepsilon_{\sigma}) G_{\sigma\bar{\sigma}} \\ (\omega - \varepsilon_{\bar{\sigma}}) G_{\bar{\sigma}\sigma} & (\omega - \varepsilon_{\bar{\sigma}}) G_{\bar{\sigma}\bar{\sigma}} \end{bmatrix} \\ &= \begin{bmatrix} 1 + U g_{\sigma\sigma}^{0(2)} \langle n_{\bar{\sigma}} \rangle & 0 \\ 0 & 1 + U g_{\sigma\bar{\sigma}}^{0(2)} \langle n_{\sigma} \rangle \end{bmatrix} + \begin{bmatrix} \Sigma_{\sigma\sigma}^T + U g_{\sigma\sigma}^{0(2)} X_{\sigma\sigma}^{(2)} & \Sigma_{\sigma\bar{\sigma}}^T + U g_{\sigma\sigma}^{0(2)} X_{\sigma\bar{\sigma}}^{(2)} \\ \Sigma_{\bar{\sigma}\sigma}^T + U g_{\sigma\bar{\sigma}}^{0(2)} X_{\bar{\sigma}\sigma}^{(2)} & \Sigma_{\bar{\sigma}\bar{\sigma}}^T + U g_{\sigma\bar{\sigma}}^{0(2)} X_{\bar{\sigma}\bar{\sigma}}^{(2)} \end{bmatrix} \begin{bmatrix} G_{\sigma\sigma} & G_{\sigma\bar{\sigma}} \\ G_{\bar{\sigma}\sigma} & G_{\bar{\sigma}\bar{\sigma}} \end{bmatrix} \\ &\equiv \begin{bmatrix} 1 + U g_{\sigma\sigma}^{0(2)} \langle n_{\bar{\sigma}} \rangle & 0 \\ 0 & 1 + U g_{\sigma\bar{\sigma}}^{0(2)} \langle n_{\sigma} \rangle \end{bmatrix} + \begin{bmatrix} \Sigma_{\sigma\sigma}^{tot} & \Sigma_{\sigma\bar{\sigma}}^{tot} \\ \Sigma_{\bar{\sigma}\sigma}^{tot} & \Sigma_{\bar{\sigma}\bar{\sigma}}^{tot} \end{bmatrix} \begin{bmatrix} G_{\sigma\sigma} & G_{\sigma\bar{\sigma}} \\ G_{\bar{\sigma}\sigma} & G_{\bar{\sigma}\bar{\sigma}} \end{bmatrix} \end{aligned}$$

Under the infinite U limit, $U \mathbf{g}^{0(2)} \sim -1$ and $\Sigma^{tot} = \Sigma^T - \mathbf{X}^{(2)}$. Compare to

Eq.(3.2) (after some algebra), one obtains:

$$\begin{aligned} & \begin{bmatrix} G_{\sigma\sigma} & G_{\sigma\bar{\sigma}} \\ G_{\bar{\sigma}\sigma} & G_{\bar{\sigma}\bar{\sigma}} \end{bmatrix} \tag{3.6} \\ &= \begin{bmatrix} (1 - \langle n_{\bar{\sigma}} \rangle) [(\tilde{G}_{\sigma\sigma}^0)^{-1} - \Sigma_{\sigma\bar{\sigma}}^{tot} \tilde{G}_{\bar{\sigma}\bar{\sigma}}^0 \Sigma_{\bar{\sigma}\sigma}^{tot}]^{-1} & \tilde{G}_{\sigma\sigma}^0 \Sigma_{\sigma\bar{\sigma}}^{tot} G_{\bar{\sigma}\bar{\sigma}} \\ \tilde{G}_{\bar{\sigma}\bar{\sigma}}^0 \Sigma_{\bar{\sigma}\sigma}^{tot} G_{\sigma\sigma} & (1 - \langle n_{\sigma} \rangle) [(\tilde{G}_{\bar{\sigma}\bar{\sigma}}^0)^{-1} - \Sigma_{\bar{\sigma}\sigma}^{tot} \tilde{G}_{\sigma\sigma}^0 \Sigma_{\sigma\sigma}^{tot}]^{-1} \end{bmatrix} \end{aligned}$$

In Eq.(3.6) $\tilde{G}_{\sigma\sigma}^0 \equiv (\omega - \varepsilon_{\sigma} - \Sigma_{\sigma\sigma}^{tot})^{-1}$ and $\tilde{G}_{\bar{\sigma}\bar{\sigma}}^0 \equiv (\omega - \varepsilon_{\bar{\sigma}} - \Sigma_{\bar{\sigma}\bar{\sigma}}^{tot})^{-1}$. Compare $\tilde{G}_{\sigma\sigma}^0$

with Eq.(3) in ref[26]

$$G_{\sigma\sigma} = \frac{1 - \langle n_{\bar{\sigma}} \rangle}{\omega - \varepsilon_{\sigma} - \Sigma_{0\sigma} - \Sigma_{1\sigma}} \quad (3.7)$$

which is the Green function corresponding to original Anderson model and set $\mathbf{X}^{(2)} \equiv -\Sigma_{1\sigma}$. $\tilde{\mathbf{G}}^0$ is the same as Green function corresponding to the original Anderson Hamiltonian except the factor $(1 - \langle n_{\bar{\sigma}} \rangle)$. $\tilde{\mathbf{G}}^0$ can be regarded as the Green function of the quasiparticle of Anderson Hamiltonian without spin flip effect. Now, the remaining problem is to obtain $\mathbf{X}^{(2)}$ and $\mathbf{Y}^{(2)}$. The detailed derivation and results are presented in Appendix B.

The form of Eq.(3.6) is the same as that of the Eq.(3.2) except the self-energy $\mathbf{X}^{(2)}$ which relates to Kondo effect. The physical picture of the Green function (Eq.(3.6)) can be interpreted as follows: $\tilde{\mathbf{G}}^0$ is the Green function corresponding to Anderson Hamiltonian without spin-flip effect, i.e. it is the form of Green function as shown in Eq.(3) of Ref.[26]. $G_{\sigma\sigma}$ in Eq.(3.6), for example, represents the corresponding σ state quasiparticle of Anderson Hamiltonian which is scattered between the σ and $\bar{\sigma}$ states and causes the self-energy $\Sigma_{\sigma\bar{\sigma}}^{tot} \tilde{G}_{\bar{\sigma}\sigma}^0 \Sigma_{\bar{\sigma}\sigma}^{tot}$. $\Sigma_{\sigma\sigma}^{tot}$ contains two terms: the self-energy $\Sigma_{\sigma\sigma}^T$ corresponding to the scattering via the normal channel and the self-energy $X_{\bar{\sigma}\sigma}^{(2)}$ corresponding to the scattering via the Kondo channel. The normal channel scattering is energy and temperature independent. Since the Kondo effect is strongly dependent on the temperature and causes a Kondo resonant peak in the vicinity of the Fermi level of lead, the Kondo channel scattering is strongly dependent on the temperature and dominates the scattering

with energy in the vicinity of Fermi energy of lead.

Since the transport problem in quantum dot system may be a nonequilibrium problem, we will employ the nonequilibrium Green function method and the transport equation developed by Wingreen et. al. to calculate the particle number and conductance[17]. To evaluate the Eq.(3.6) numerically, one has to determine the particle number $\langle n_\sigma \rangle$ and the expectation value $\langle d_\sigma^+ d_{\bar{\sigma}} \rangle$ by self-consistent method. In order to calculate the expectation values $\langle n_\sigma \rangle$ and $\langle d_\sigma^+ d_{\bar{\sigma}} \rangle$, the corresponding lesser Green function $G_{\sigma\sigma}^<$ and $G_{\bar{\sigma}\sigma}^<$ must be solved first, i.e. $\langle n_\sigma \rangle = -i \int \frac{d\varepsilon}{2\pi} G_{\sigma\sigma}^<$ and $\langle d_\sigma^+ d_{\bar{\sigma}} \rangle = -i \int \frac{d\varepsilon}{2\pi} G_{\bar{\sigma}\sigma}^<$. In this work, we use the method proposed by Sun and Guo which is able to solve the lesser Green function of interacting system exactly for the steady state problem[53]. The detailed derivation processes are shown in appendix C.



3.2 Result and Discussion

In the following discussion, all energy scales are normalized to the normal tunneling coupling constant $\Gamma_\alpha^n = 1$. The resonant energy of quantum dot is set as $\varepsilon_0 = -5$. The Fermi level of the lead E_F is set to be zero for the equilibrium situation. The temperature is normalization to Kondo temperature T_K which is calculated by the exact expression obtained by Haldane $T_K \approx (D\Gamma)^{1/2} \exp(\pi(\varepsilon_0 - E_F)/(2\Gamma)) \approx 0.004$ [23] with the halfwidth $D = 100$ and $\Gamma = \Gamma_L^n + \Gamma_R^n$.

Since the high temperature Lacroix's decoupling approximation at low temper-

atures ($T < T_K$) gives only qualitative solution and is even quantitatively correct at high temperatures ($T > T_K$), thus, we consider the situation with temperature near Kondo temperature i.e. $T = 10T_K$, $1T_K$ and $0.1T_K$ and a normal limit $T = 100T_K$, of which the Kondo effect can be ignored for comparison[54]. The spectral function (or local density of state, LDOS when $\bar{\sigma} = \sigma$) $A_{\bar{\sigma}\sigma}(\omega) = -2\text{Im} G_{\bar{\sigma}\sigma}^r$ in equilibrium situation is calculated in terms of the strength of spin-flip associated tunneling which is described by the spin-flip coupling constant Γ^s . As previous discussion, the quasiparticle of Anderson Hamiltonian is scattered by the normal channel and the Kondo channel. The self-energy Σ^T due to normal channel scattering is independent of the energy and the temperature, thus the electron can be scattered by the normal channel in arbitrary energy and temperature. Contrast to the normal channel, the Kondo effect channel is energy dependent and the strength is increased logarithmically in the vicinity of Fermi level when $T \leq T_K$. Thus, the self-energy corresponding to Kondo channel $\mathbf{X}^{(2)}$ is sensitive to temperature and energy. It can be expected that the Kondo channel dominates the scattering due to spin flip associated tunneling effect in the vicinity of Fermi level when $T \leq T_K$. The normal channel scattering dominates the spin flip effect for electrons with energies far away from the Fermi level or $T > T_K$. As shown in Fig.3.2, the LDOS in the region far away from the Fermi level is temperature independent. It implies that the electron with energy far away from the Fermi level is mainly scattered by the normal channel. Fig.3.3 shows the detailed plot

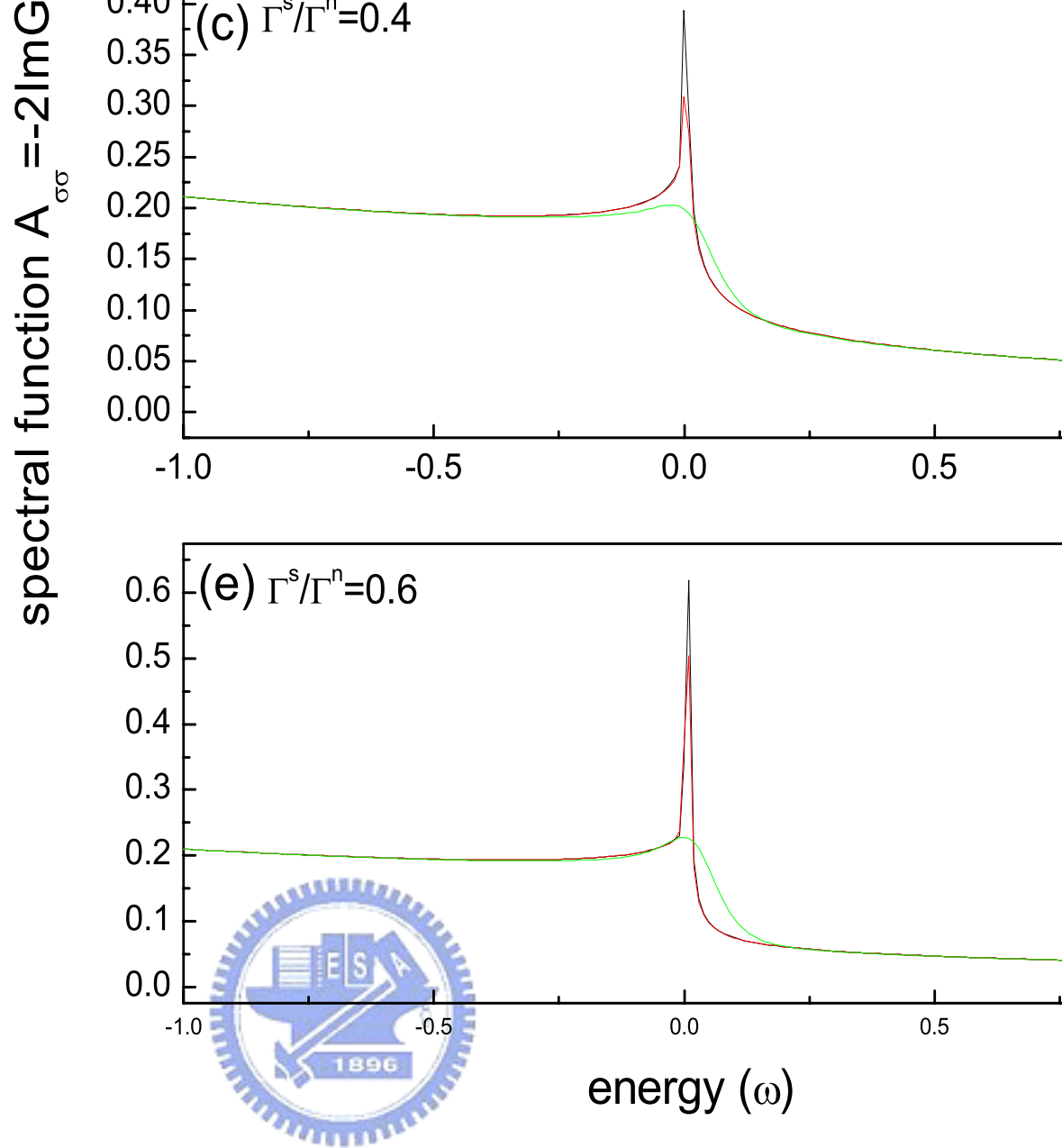


Figure 3.2: The plot of spectral function as function of ω with temperature $T = 10T_K, 1T_K$ and $T = 0.1T$.

of LDOS with energy in the vicinity of Fermi level. The spectral functions for $T = 100T_K$, i.e. the normal case, are shown in Fig.3.3.(a),(b) (dash lines). The spin-flip scattering via normal channel affects the diagonal part spectrum function $A_{\sigma\sigma}$ (or LDOS) very slightly for the case of $T = 100T_K$ (normal limit). But the dependence of the off-diagonal spectrum function $A_{\bar{\sigma}\sigma}$ on spin-flip scattering via classical channel is stronger than $A_{\sigma\sigma}$. When the temperature is decreased to the order of Kondo temperature ($T = 10T_K$ and $T = 1T_K$ in our case), the Kondo effect becomes obvious and the Kondo resonance peak grows logarithmically. As Fig.3.3(a),(b) (solid line) and (c),(d) show, it is obvious that the LDOS with energy near Fermi level is strongly dependent on temperature when temperature is close to the Kondo temperature. Therefore, it implies that the scattering in the region near Fermi level is dominated by the Kondo channel. When the temperature is below the Kondo temperature ($T = 0.1T_K$ in our case), the scattering via Kondo channel is prominent. As shown in Fig.3.3(e) and (f), there are two major effects due to the spin-flip associated tunneling via Kondo channel. The amplitude of the Kondo resonance peak is increased as Γ^s is increased, i.e. the Kondo resonance peak is enhanced by the spin flip associated tunneling effect. Besides the increasing of the peak height, the spin flip tunneling also causes the blue shift of Kondo resonance. These effects become stronger as the temperature is decreased. Note that the enhancement and shift of Kondo resonance peak due to spin-flip associated tunneling will affect the conductance. Since the off-diagonal

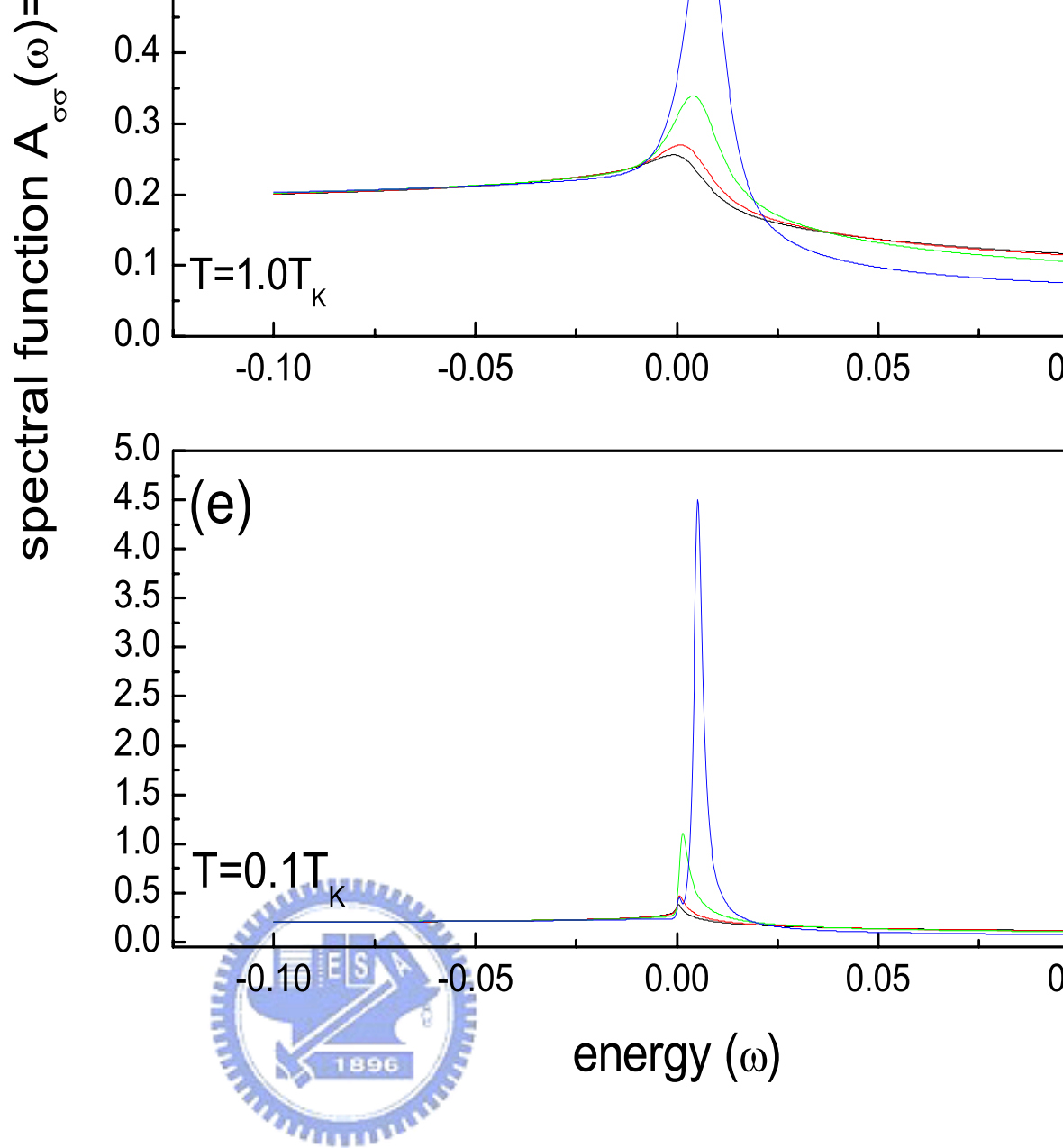


Figure 3.3: The detailed plot of spectral function in the vicinity of the Fermi level as function of ω (a) $T = 100T_K$ and $10T_K$ (b) $T = 1T_K$ (c) $T = 0.1T_K$ with various $\Gamma_\alpha^s/\Gamma_\alpha^n$.

Green function is $G_{\bar{\sigma}\sigma} = \tilde{G}_{\bar{\sigma}\sigma}^0 \Sigma_{\bar{\sigma}\sigma}^{tot} G_{\sigma\sigma}$, the profile of off-diagonal spectral function $A_{\bar{\sigma}\sigma}$ is similar to the diagonal spectral function $A_{\sigma\sigma}$ but with opposite sign. It is worth to note that for the case of $T \geq T_K$, the decrease (more negative) of $A_{\bar{\sigma}\sigma}$ is faster than the increase of $A_{\sigma\sigma}$. This phenomenon is the main reason of suppression of conductance for $T \geq T_K$.

The conductance g^c for the equilibrium case is calculated by Eq.(3) of Ref.[50]. For equilibrium situation, the current is contributed from the electron with energy near the Fermi level of leads. Thus, the equilibrium conductance reflects the properties of Kondo resonance peak with energy in vicinity of Fermi level of leads. Fig.3.4 shows the equilibrium conductance versus the spin flip coupling constant Γ^s . One can find that for $\Gamma^s = 0$, the total conductance g_{tot}^c is increased as the temperature is decreased, since the Kondo resonance peak is enhanced as the temperature is decreased. For the case of $T = 100T_K$, the Kondo effect can be ignored and the scattering is dominated by the normal channel. As previous discussion, the decrease of $A_{\bar{\sigma}\sigma}$ is faster than the increase of $A_{\sigma\sigma}$ as Γ^s is increased, hence the total conductance g_{tot}^c is dominated by the off-diagonal part conductance $g_{\sigma\bar{\sigma}}^c$ and decreased as Γ^s is increased. For the cases of $T = 10T_K$ ($1.0T_K$) the Kondo effect appears, however it is not obvious. One can find that $g_{\sigma\sigma}^c$ is increased slightly as Γ^s is increased for $\Gamma^s > 0.3\Gamma^n$ ($0.1\Gamma^n$). This phenomena reflects the enhancement of Kondo resonance peak due to spin-flip effect via Kondo channel as discussed previously. Similar to the case of $T = 100T_K$, the total conductance

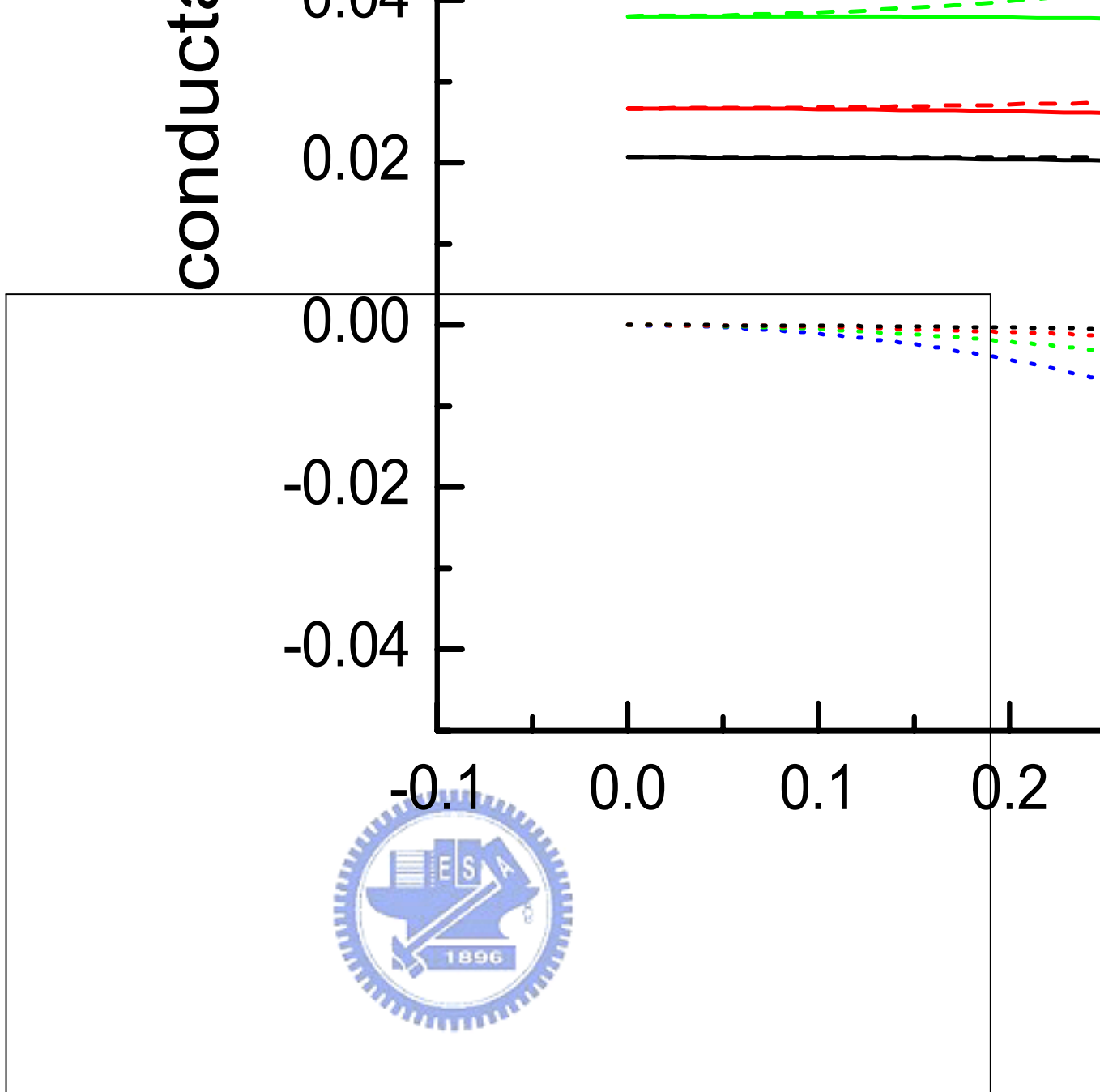


Figure 3.4: The equilibrium conductance versus $\Gamma_\alpha^s/\Gamma_\alpha^n$ at various temperatures. The dash line is the diagonal part. The dot line is the off-diagonal part. And the solid line is the total conductance. The blue line is $T = 100T_K$, the green line $T = 10T_K$, the red line is $T = 1T_K$ and The black line is $T = 0.1T_K$

is dominated by off-diagonal conductance and decreased as Γ^s is increased. For the case of $T = 0.1T_K$, the effect due to spin-flip scattering via the Kondo channel becomes more prominent. The diagonal part $g_{\sigma\sigma}^c$ contains peak enhanced and peak shift effects due to spin flip via Kondo channel. For $\Gamma^s < 0.48$, the peak enhanced effect is dominated and $g_{\sigma\sigma}^c$ increased as Γ^s is increased. For $\Gamma^s > 0.48$, the peak shift effect is dominated and thus the peak height is shifted out of the vicinity of Fermi level of leads, and thus there are only fewer electrons contribute to the conductance, hence $g_{\sigma\sigma}^c$ is decreased. The profile of off-diagonal spectral function $A_{\bar{\sigma}\sigma}$ is similar to that of $A_{\sigma\sigma}$ except the opposite sign, thus the behavior of off-diagonal part conductance is similar to the diagonal part except the sign. For $T = 0.1T_K$ the total conductance is dominated by $g_{\sigma\sigma}^c$. In the region dominated by the peak enhanced effect, i.e. $\Gamma^s < 0.48$, the total conductance is slightly increased as Γ^s is increased. In the region dominated by peak shift effect, the total conductance decreased as Γ^s is increased. Note that the conductance is suppressed rapidly for the case of $T = 0.1T_K$ when $\Gamma^s > 0.48$. The rapid decreasing of conductance is caused by the peak shift effect due to spin-flip scattering.

For the nonequilibrium case, a quantum dot connected to two leads with different Fermi level is studied. The Fermi level is set as zero when the bias voltage is zero. When the bias voltage V_b is applied, the Fermi levels of the leads are $E_F^R = -V_b/2$ and $E_F^L = V_b/2$. The nonequilibrium differential conductance is defined as $g^c = \Delta J / \Delta V_b$, where the current J is calculated by the method of Ref.[17]. The

nonequilibrium differential conductance is shown in Fig.3.5. Since the applied bias is symmetry, the conductance is symmetry for $V_{bias} > 0$ and $V_{bias} < 0$, as shown in Fig.3.6(a) and (b). Follow the same reason, the nonequilibrium differential conductance is decreased as Γ_s is increased for the cases of $T \geq T_K$. In the region $|V_{bias}| > 0.25$ the conductance is temperature insensitive. It implies that the nonequilibrium differential conductance for $|V_{bias}| > 0.25$ is dominated by the scattering via normal channel, the behavior of differential conductance is similar to the equilibrium case for $T > T_K$. Hence, for $|V_{bias}| > 0.25$, differential conductance is decreased as Γ^s is increased. In the region with energy near Fermi level, i.e. $|V_{bias}| < 0.25$, the Kondo effect is more important when $T < T_k$. This is because that the Kondo effect influences LDOS when the electron energy is near Fermi level only. The nonequilibrium differential conductance is influenced strongly by Kondo effect when bias voltage $|V_{bias}| \sim 0$ for $T \leq T_k$. Fig.3.5(b) shows the detailed plot of the nonequilibrium differential conductance with bias voltage $|V_{bias}| < 0.05$. The variation of the conductance for $|V_{bias}| \sim 0$ is similar to the case of $|V_{bias}| \gg 0$ when $T > T_k$ (the dotted line in Fig.3.5(b)) and the scattering is via the normal channel. As the temperature is decreased to $T \sim T_k$, the influence due to Kondo effect becomes important and the Kondo resonance peak is prominent. Hence, the conductance is larger than the one for $T > T_k$. For $T = T_k$ (the dash line in Fig.3.5(b)), the quantity of conductance suppression due to the spin flip associated tunneling is similar to that in large bias voltage region.

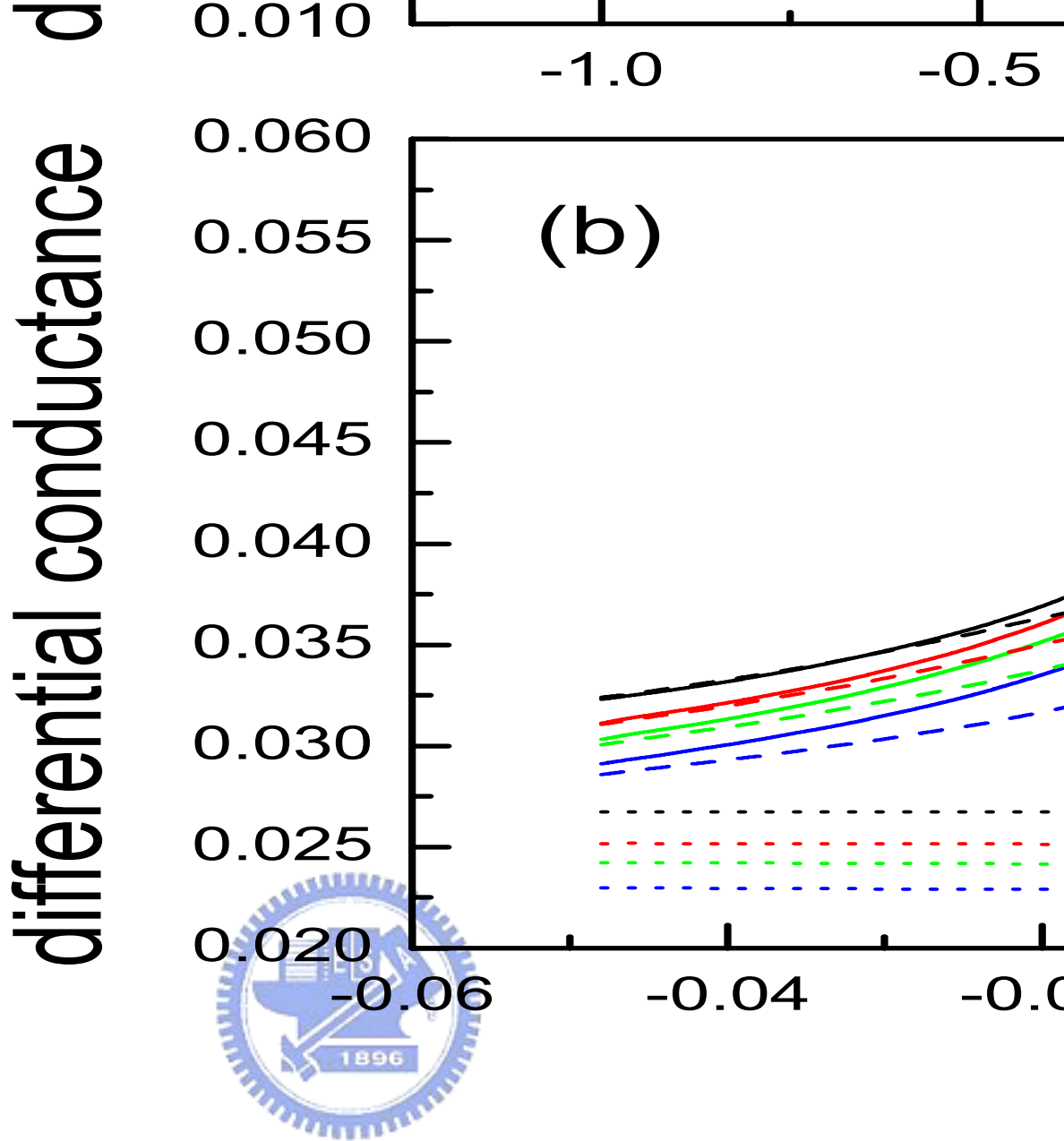


Figure 3.5: Fig.5 (a) The differential conductance versus bias voltage with various $\Gamma_{\alpha}^s/\Gamma_{\alpha}^n$ for different temperature. (b) The detailed plot of (a) with energy in vicinity of Fermi level.

The suppression of conductance is due to the decrease of $g_{\sigma\bar{\sigma}}^c$ as Γ^s is increased. The prominent of conductance reflects the prominent Kondo resonance peak of LDOS. When $T \leq T_k$ (the solid line in Fig.3.4(b)), the influence of peak shift of Kondo resonance becomes important. As the case of equilibrium, the $g_{\sigma\sigma}^c$ is strongly suppressed by the shift of Kondo resonance peak when Γ_s is large. As a result, the total conductance is suppressed rapidly when $\Gamma^s > 0.4$ and causes a valley when $\Gamma^s = 0.6$. Fig.3.6.(a),(b) shows the spectral function for $T = 0.1T_K$ and $V_{bias} = 10^{-3}$. One can find that the LDOS within the Fermi level of leads is increased as Γ^s is increased when $\Gamma^s < 0.6$. This explains the differential conductance is increased as Γ^s is increased when $\Gamma^s < 0.6$ and $T = 0.1T_K$ in the vicinity of $V_{bias} = 0$. For $\Gamma^s = 0.6$, the peak shift effect shifts the peak height out of the region between Fermi level of leads and the total LDOS within the Fermi level of leads is fewer than the LDOS for $\Gamma^s < 0.6$. Hence, differential conductance appears slightly when $V_{bias} \sim 0$ for $T = 0.1T_K$ and $\Gamma^s = 0.6$. This tip of conductance occurs when $T < T_k$ in the vicinity of Fermi level of leads, therefore, this phenomenon is mainly originated from the scattering via Kondo channel.

3.3 Summary

In summary, we study the spin flip associated tunneling in Anderson model. The total effect can be interpreted as follows. As the Eq.(3.6) shows, the quasi-

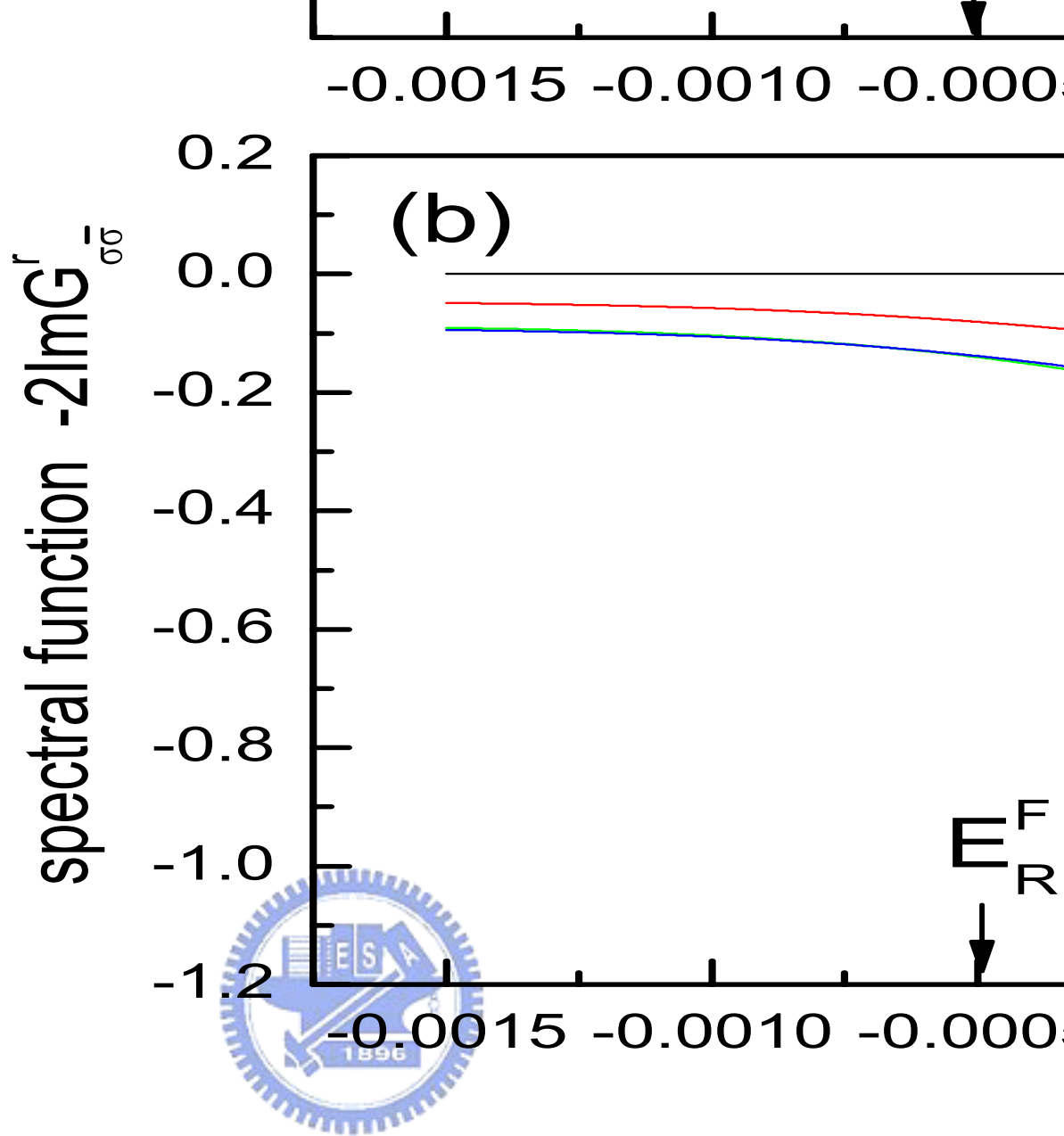


Figure 3.6: The nonequilibrium spectral function for the case of $V_{bias} = -10^{-3}$ with various $\Gamma_{\alpha}^s/\Gamma_{\alpha}^n$.

particle described by Anderson Hamiltonian is scattered via normal channel and the Kondo channel. The normal channel dominates the scattering of the electrons with energy far away from the Fermi level of the lead. The electrons with energy near Fermi level of the leads are mainly scattered by Kondo channel when $T \leq T_k$. Note that, only the infinite U limit approximation is used in Eq.(3.6), i.e. the Eq.(3.6) is a general form for Anderson model with spin flip associated tunneling in infinite U limit and does not relate to the decouple method. The spin flip associated tunneling via the Kondo channel causes two main effects. One is the enhancement of Kondo resonance peak, the other is the blue shift of the Kondo resonance peak. When temperature $T = 10T_K$ and $T = 1.0T_K$, the Kondo resonance peak is obviously enhanced by spin flip associated tunneling effect, but the blue shift of Kondo resonance peak is not obvious. This effect is reflected on the conductance. The enhancement of the Kondo resonant peak causes the increases of diagonal part of conductance $g_{\sigma\sigma}$ and decreases the off-diagonal part of conductance $g_{\bar{\sigma}\sigma}$ (more negative). Since the decrease of the off-diagonal part conductance is stronger than the increase of diagonal part of conductance, as a result the total conductance is suppressed by spin flip associated tunneling. The conductance due to off-diagonal processes is negative and can not be neglected. As the temperature is lower, the blue shift of Kondo resonance peak becomes important. When $T \leq T_k$ and the spin flip associated coupling constant Γ_s is large enough, the blue shift of Kondo resonance peak will cause a strong suppres-

sion of the diagonal part of conductance and the total conductance is suppressed rapidly. The conductance suppressed due to the shift of Kondo resonance peak is ascribed to the Kondo channel mainly, since the effect occurs as $T < T_K$. The high temperature Lacroix's decoupling approximation is used to decouple the two particle correlation function (or Green function). Our result is quantitatively correct when $T > T_K$. The Kondo resonance peak is slightly enhanced and blue shifted as $T \geq T_K$. On the contrary, the Kondo resonance peak is enhanced prominently and blue shifted obviously in the case of $T = 0.1T_k$. Although the decoupling approximation only gives qualitative result for $T < T_K$, the conductance can be suppressed strongly by the spin flip associated tunneling effect for $T < T_K$.



3.4 Appendix A

At the first, we derive the general form of Green function for spin flip system. Assume that the lowest order self-energies corresponding to the non-spin-flip transition processes $\sigma \rightarrow \sigma$ and $\bar{\sigma} \rightarrow \bar{\sigma}$ (the diagonal terms) are $\Sigma_{\sigma\sigma}$ and $\Sigma_{\bar{\sigma}\bar{\sigma}}$. And the lowest order self-energies corresponding to spin flip transition processes $\bar{\sigma} \rightarrow \sigma$ and $\sigma \rightarrow \bar{\sigma}$ (the diagonal terms) are $\Sigma_{\sigma\bar{\sigma}}$ and $\Sigma_{\bar{\sigma}\sigma}$. The typical Dyson equation

can be expressed as :

$$\begin{aligned}
\begin{bmatrix} G_{\sigma\sigma} & G_{\sigma\bar{\sigma}} \\ G_{\bar{\sigma}\sigma} & G_{\bar{\sigma}\bar{\sigma}} \end{bmatrix} &= \begin{bmatrix} G_{\sigma\sigma}^0 & 0 \\ 0 & G_{\bar{\sigma}\bar{\sigma}}^0 \end{bmatrix} + \begin{bmatrix} G_{\sigma\sigma}^0 & 0 \\ 0 & G_{\bar{\sigma}\bar{\sigma}}^0 \end{bmatrix} \begin{bmatrix} \Sigma_{\sigma\sigma} & \Sigma_{\sigma\bar{\sigma}} \\ \Sigma_{\bar{\sigma}\sigma} & \Sigma_{\bar{\sigma}\bar{\sigma}} \end{bmatrix} \begin{bmatrix} G_{\sigma\sigma} & G_{\sigma\bar{\sigma}} \\ G_{\bar{\sigma}\sigma} & G_{\bar{\sigma}\bar{\sigma}} \end{bmatrix} \\
&= \begin{bmatrix} G_{\sigma\sigma}^0 & 0 \\ 0 & G_{\bar{\sigma}\bar{\sigma}}^0 \end{bmatrix} + \begin{bmatrix} G_{\sigma\sigma}^0 \Sigma_{\sigma\sigma} G_{\sigma\sigma} + G_{\sigma\sigma}^0 \Sigma_{\sigma\bar{\sigma}} G_{\bar{\sigma}\sigma} & G_{\sigma\sigma}^0 \Sigma_{\sigma\sigma} G_{\sigma\bar{\sigma}} + G_{\sigma\sigma}^0 \Sigma_{\sigma\bar{\sigma}} G_{\bar{\sigma}\bar{\sigma}} \\ G_{\bar{\sigma}\bar{\sigma}}^0 \Sigma_{\bar{\sigma}\sigma} G_{\sigma\sigma} + G_{\bar{\sigma}\bar{\sigma}}^0 \Sigma_{\bar{\sigma}\bar{\sigma}} G_{\bar{\sigma}\sigma} & G_{\bar{\sigma}\bar{\sigma}}^0 \Sigma_{\bar{\sigma}\sigma} G_{\sigma\bar{\sigma}} + G_{\bar{\sigma}\bar{\sigma}}^0 \Sigma_{\bar{\sigma}\bar{\sigma}} G_{\bar{\sigma}\bar{\sigma}} \end{bmatrix}
\end{aligned} \tag{3.8}$$

The off-diagonal terms can be rewritten as $G_{\sigma\bar{\sigma}} = \tilde{G}_{\sigma\sigma}^0 \Sigma_{\sigma\bar{\sigma}} G_{\bar{\sigma}\bar{\sigma}}$ and $G_{\bar{\sigma}\sigma} = \tilde{G}_{\bar{\sigma}\bar{\sigma}}^0 \Sigma_{\bar{\sigma}\sigma} G_{\sigma\sigma}$

where $\tilde{G}_{\sigma\sigma}^0 \equiv [(G_{\sigma\sigma}^0)^{-1} - \Sigma_{\sigma\sigma}]^{-1}$ and $\tilde{G}_{\bar{\sigma}\bar{\sigma}}^0 \equiv [(G_{\bar{\sigma}\bar{\sigma}}^0)^{-1} - \Sigma_{\bar{\sigma}\bar{\sigma}}]^{-1}$. Substitute these

expressions of $G_{\sigma\bar{\sigma}}$ and $G_{\bar{\sigma}\sigma}$ into the diagonal term, the Eq.(3.8) becomes:

$$\begin{bmatrix} G_{\sigma\sigma} & G_{\sigma\bar{\sigma}} \\ G_{\bar{\sigma}\sigma} & G_{\bar{\sigma}\bar{\sigma}} \end{bmatrix} = \begin{bmatrix} [(G_{\sigma\sigma}^0)^{-1} - \Sigma_{\sigma\sigma} - \Sigma_{\sigma\bar{\sigma}} \tilde{G}_{\bar{\sigma}\bar{\sigma}}^0 \Sigma_{\bar{\sigma}\sigma}]^{-1} & G_{\sigma\bar{\sigma}} = \tilde{G}_{\sigma\sigma}^0 \Sigma_{\sigma\bar{\sigma}} G_{\bar{\sigma}\bar{\sigma}} \\ \tilde{G}_{\bar{\sigma}\bar{\sigma}}^0 \Sigma_{\bar{\sigma}\sigma} G_{\sigma\sigma} & [(G_{\bar{\sigma}\bar{\sigma}}^0)^{-1} - \Sigma_{\bar{\sigma}\bar{\sigma}} - \Sigma_{\bar{\sigma}\sigma} \tilde{G}_{\sigma\sigma}^0 \Sigma_{\sigma\sigma'}]^{-1} \end{bmatrix} \tag{3.9}$$

The equation Eq.(3.9) is the same as Eq.(5a) and Eq.(5b) in ref.[50] exactly.

3.5 Appendix B

In order to solve Eq.(3.4), one has to decouple the two correlation functions $\langle T \{ c_{k_{\alpha}s}^+ d_{\bar{\sigma}}^+ d_{\sigma}^+ \} \rangle$, $\langle T \{ c_{k_{\alpha}s}^+ d_{\sigma} d_{\bar{\sigma}} d_{\sigma}^+ \} \rangle$ and $\langle T \{ c_{k_{\alpha}s} d_{\bar{\sigma}}^+ d_{\sigma}^+ \} \rangle$ etc.. The decoupling scheme proposed by Lacroix at high temperature limit:

$$\langle T \{ c_{k_{\alpha}s}^+(t) c_{k_{\beta}s'}(t) d_{\bar{\sigma}}^+(t), d_{\sigma}^+(t') \} \rangle = \delta_{k_{\alpha}, k_{\beta}} \delta_{s, s'} f(\varepsilon_{k_{\alpha}s}) \langle T \{ d_{\bar{\sigma}}^+(t), d_{\sigma}^+(t') \} \rangle \tag{3.10}$$

$$\langle T \{ c_{k_{\alpha}s}^+(t) c_{k_{\beta}s'}(t) d_{\sigma}(t), d_{\sigma}^+(t') \} \rangle = \delta_{k_{\alpha}, k_{\beta}} \delta_{s, s'} f(\varepsilon_{k_{\alpha}s}) \langle T \{ d_{\sigma}(t), d_{\sigma}^+(t') \} \rangle$$

$$\langle T \{ c_{k_{\alpha}s}(t) c_{k_{\beta}s'}(t) d_{\sigma}^+(t), d_{\sigma}^+(t') \} \rangle = \langle T \{ c_{k_{\alpha}s}(t) c_{k_{\beta}s'}(t) d_{\bar{\sigma}}^+(t), d_{\sigma}^+(t') \} \rangle = 0$$

is used. For example, consider the term $\langle c_{k_{\alpha s}} d_{\bar{\sigma}}^{\pm} d_{\sigma}, d_{\sigma}^{\pm} \rangle$ of Eq.(3.4). Using the EOM method, and Lacroix's high temperature decoupling approximation, one obtains:

$$\begin{aligned}
& (\omega - \varepsilon_{k_{\alpha s}} - \varepsilon_{\sigma} + \varepsilon_{\bar{\sigma}}) \langle T \{ c_{k_{\alpha s}} d_{\bar{\sigma}}^{\pm} d_{\sigma}, d_{\sigma}^{\pm} \} \rangle \quad (3.11) \\
&= V_{k_{\alpha s}, \sigma} \langle T \{ d_{\sigma} d_{\bar{\sigma}}^{\pm} d_{\sigma}, d_{\bar{\sigma}}^{\pm} \} \rangle + V_{k_{\alpha s}, \bar{\sigma}} \langle T \{ d_{\bar{\sigma}} d_{\bar{\sigma}}^{\pm} d_{\sigma}, d_{\sigma}^{\pm} \} \rangle - \sum_{q_{\alpha s'}} V_{q_{\alpha s'}, \bar{\sigma}} \langle T \{ c_{k_{\alpha s}} c_{q_{\alpha s'}}^{\pm} d_{\sigma}, d_{\sigma}^{\pm} \} \rangle \\
&= - \langle d_{\bar{\sigma}}^{\pm} d_{\sigma} \rangle V_{k_{\alpha s}, \sigma} (i) G_{\sigma\sigma} + V_{k_{\alpha s}, \bar{\sigma}} (i) (G_{\sigma\sigma} - G_{\sigma\sigma}^{(2)}) - \sum_{q_{\alpha s'}} V_{q_{\alpha s'}, \bar{\sigma}} \langle c_{k_{\alpha s}} c_{q_{\alpha s'}}^{\pm} \rangle (i) G_{\sigma\sigma} \delta_{k_{\alpha s}, q_{\alpha s'}}
\end{aligned}$$

,thus

$$\begin{aligned}
- \sum_{k_{\alpha s}} V_{k_{\alpha s}, \bar{\sigma}}^* (-i) \langle c_{k_{\alpha s}} d_{\bar{\sigma}}^{\pm} d_{\sigma}, d_{\sigma}^{\pm} \rangle &= \langle d_{\bar{\sigma}}^{\pm} d_{\sigma} \rangle \sum_{k_{\alpha s}} \frac{V_{k_{\alpha s}, \bar{\sigma}}^* V_{k_{\alpha s}, \sigma}}{\omega - \varepsilon_{k_{\alpha s}} - \varepsilon_{\sigma} + \varepsilon_{\bar{\sigma}}} G_{\sigma\sigma} \quad (3.12) \\
&+ \sum_{k_{\alpha s}} \frac{|V_{k_{\alpha s}, \bar{\sigma}}|^2}{\omega - \varepsilon_{k_{\alpha s}} - \varepsilon_{\sigma} + \varepsilon_{\bar{\sigma}}} (G_{\sigma\sigma}^{(2)} - G_{\sigma\sigma}) \\
&+ \sum_{k_{\alpha s}} \frac{|V_{k_{\alpha s}, \bar{\sigma}}|^2}{\omega - \varepsilon_{k_{\alpha s}} - \varepsilon_{\sigma} + \varepsilon_{\bar{\sigma}}} (1 - f_{\alpha}(\varepsilon_{k_{\alpha s}})) G_{\sigma\sigma}
\end{aligned}$$

in the same way, the $\langle T \{ c_{k_{\alpha s}} d_{\bar{\sigma}}^{\pm} d_{\sigma}, d_{\bar{\sigma}}^{\pm} \} \rangle$ term of Eq.(3.4) is:

$$\begin{aligned}
& \sum_{k_{\alpha s}} V_{k_{\alpha s}, \sigma}^* (-i) \langle T \{ c_{k_{\alpha s}} d_{\bar{\sigma}}^{\pm} d_{\sigma}, d_{\bar{\sigma}}^{\pm} \} \rangle \quad (3.13) \\
&= \sum_{k_{\alpha s}} \frac{|V_{k_{\alpha s}, \sigma}|^2}{\omega - \varepsilon_{k_{\alpha s}}} G_{\sigma\sigma}^{(2)} - \langle n_{\bar{\sigma}} \rangle \frac{V_{k_{\alpha s}, \sigma}^* V_{k_{\alpha s}, \bar{\sigma}}}{\omega - \varepsilon_{k_{\alpha s}}} G_{\bar{\sigma}\sigma} + \frac{V_{k_{\alpha s}, \sigma}^* V_{k_{\alpha s}, \bar{\sigma}}}{\omega - \varepsilon_{k_{\alpha s}}} f_{\alpha}(\varepsilon_{k_{\alpha s}}) G_{\bar{\sigma}\sigma}
\end{aligned}$$

and the $\langle T \{ c_{k_{\alpha s}}^{\pm} d_{\sigma} d_{\bar{\sigma}}, d_{\sigma}^{\pm} \} \rangle$ term is

$$\begin{aligned}
& \sum_{k_{\alpha s}} V_{k_{\alpha s}, \bar{\sigma}}^* (-i) \langle T \{ c_{k_{\alpha s}}^{\pm} d_{\sigma} d_{\bar{\sigma}}, d_{\sigma}^{\pm} \} \rangle \quad (3.14) \\
&= \sum_{k_{\alpha s}} - \frac{|V_{k_{\alpha s}, \sigma}|^2}{\omega + \varepsilon_{k_{\alpha s}} - \varepsilon_{\sigma} - \varepsilon_{\bar{\sigma}} - U} G_{\bar{\sigma}\sigma}^{(2)} - \frac{|V_{k_{\alpha s}, \sigma}|^2}{\omega + \varepsilon_{k_{\alpha s}} - \varepsilon_{\sigma} - \varepsilon_{\bar{\sigma}} - U} G_{\sigma\sigma}^{(2)} \\
&+ \sum_{k_{\alpha s}} \frac{|V_{k_{\alpha s}, \sigma}|^2}{\omega + \varepsilon_{k_{\alpha s}} - \varepsilon_{\sigma} - \varepsilon_{\bar{\sigma}} - U} f_{\alpha}(\varepsilon_{k_{\alpha s}}) G_{\bar{\sigma}\sigma} + \frac{V_{k_{\alpha s}, \bar{\sigma}}^* V_{k_{\alpha s}, \sigma}}{\omega + \varepsilon_{k_{\alpha s}} - \varepsilon_{\sigma} - \varepsilon_{\bar{\sigma}} - U} f_{\alpha}(\varepsilon_{k_{\alpha s}}) G_{\sigma\sigma}
\end{aligned}$$

Under the infinite U limit, the Eq.(3.14) is zero. Compare to Eq.(3.5), The self-energy $Y_{\sigma\bar{\sigma}}^{(2)}$ transfers $G_{\sigma\bar{\sigma}}^{(2)}$ to $G_{\sigma\sigma}^{(2)}$, we can recognize that $Y_{\sigma\bar{\sigma}}^{(2)} = \sum_{k_{\alpha}s} -\frac{|V_{k_{\alpha}s,\sigma}|^2}{\omega + \varepsilon_{k_{\alpha}s} - \varepsilon_{\sigma} - \varepsilon_{\bar{\sigma}} - U}$ and can be ignored under the infinite U limit. Hence the Green function $G_{\sigma\bar{\sigma}}^{(2)}$ is found as:

$$\begin{aligned}
(\omega - \varepsilon_{\sigma} - U)G_{\sigma\bar{\sigma}}^{(2)}(\omega) &= n_{\bar{\sigma}} \tag{3.15} \\
&+ \sum_{k_{\alpha}s} \frac{|V_{k_{\alpha}s,\sigma}|^2}{\omega - \varepsilon_{k_{\alpha}s}} G_{\sigma\bar{\sigma}}^{(2)} - \langle n_{\bar{\sigma}} \rangle \frac{V_{k_{\alpha}s,\sigma}^* V_{k_{\alpha}s,\bar{\sigma}}}{\omega - \varepsilon_{k_{\alpha}s}} G_{\bar{\sigma}\sigma} + \frac{V_{k_{\alpha}s,\sigma}^* V_{k_{\alpha}s,\bar{\sigma}}}{\omega - \varepsilon_{k_{\alpha}s}} f_{\alpha}(\varepsilon_{k_{\alpha}s}) G_{\bar{\sigma}\sigma} \\
&+ \langle d_{\bar{\sigma}}^{\dagger} d_{\sigma} \rangle \sum_{k_{\alpha}s} \frac{V_{k_{\alpha}s,\bar{\sigma}}^* V_{k_{\alpha}s,\sigma}}{\omega - \varepsilon_{k_{\alpha}s} - \varepsilon_{\sigma} + \varepsilon_{\bar{\sigma}}} G_{\sigma\sigma} + \frac{|V_{k_{\alpha}s,\bar{\sigma}}|^2}{\omega - \varepsilon_{k_{\alpha}s} - \varepsilon_{\sigma} + \varepsilon_{\bar{\sigma}}} (G_{\sigma\bar{\sigma}}^{(2)} - G_{\sigma\sigma}) \\
&+ \frac{|V_{k_{\alpha}s,\bar{\sigma}}|^2}{\omega - \varepsilon_{k_{\alpha}s} - \varepsilon_{\sigma} + \varepsilon_{\bar{\sigma}}} (1 - f_{\alpha}(\varepsilon_{k_{\alpha}s})) G_{\sigma\sigma} \\
&\equiv Y_{\sigma\bar{\sigma}}^{(2)} G_{\sigma\bar{\sigma}}^{(2)} + X_{\sigma\bar{\sigma}}^{(2)} G_{\sigma\sigma} + X_{\sigma\bar{\sigma}}^{(2)} G_{\bar{\sigma}\sigma}
\end{aligned}$$

where

$$\begin{aligned}
Y_{\sigma\bar{\sigma}}^{(2)} &\equiv \sum_{k_{\alpha}s} \frac{|V_{k_{\alpha}s,\sigma}|^2}{\omega - \varepsilon_{k_{\alpha}s}} + \frac{|V_{k_{\alpha}s,\bar{\sigma}}|^2}{\omega - \varepsilon_{k_{\alpha}s} - \varepsilon_{\sigma} + \varepsilon_{\bar{\sigma}}} \tag{3.16} \\
X_{\sigma\bar{\sigma}}^{(2)} &\equiv \sum_{k_{\alpha}s} \langle d_{\bar{\sigma}}^{\dagger} d_{\sigma} \rangle \frac{V_{k_{\alpha}s,\bar{\sigma}}^* V_{k_{\alpha}s,\sigma}}{\omega - \varepsilon_{k_{\alpha}s} - \varepsilon_{\sigma} + \varepsilon_{\bar{\sigma}}} - \frac{|V_{k_{\alpha}s,\bar{\sigma}}|^2}{\omega - \varepsilon_{k_{\alpha}s} - \varepsilon_{\sigma} + \varepsilon_{\bar{\sigma}}} f_{\alpha}(\varepsilon_{k_{\alpha}s}) \\
X_{\sigma\bar{\sigma}}^{(2)} &= \sum_{k_{\alpha}s} -\langle n_{\bar{\sigma}} \rangle \frac{V_{k_{\alpha}s,\sigma}^* V_{k_{\alpha}s,\bar{\sigma}}}{\omega - \varepsilon_{k_{\alpha}s}} + \frac{V_{k_{\alpha}s,\sigma}^* V_{k_{\alpha}s,\bar{\sigma}}}{\omega - \varepsilon_{k_{\alpha}s}} f_{\alpha}(\varepsilon_{k_{\alpha}s})
\end{aligned}$$

3.6 Appendix C

In this appendix, we will show the detailed derivation of the expression of $\langle n_{\sigma} \rangle$ and $\langle n_{\bar{\sigma}} \rangle$. We follow the derivation proposed by Sun and Guo. Since the system considered in this paper is steady state, the first derivation of the expectation values of $\langle d_{\sigma}^{\dagger} d_{\sigma} \rangle$ and $\langle d_{\bar{\sigma}}^{\dagger} d_{\bar{\sigma}} \rangle$ over time is zero, i.e. $\langle i \frac{\partial}{\partial t} [d_{\sigma}^{\dagger} d_{\sigma}] \rangle = 0$. Use the

equation of motion method, one can find the time evolution of particle number

$\langle d_\sigma^+ d_\sigma \rangle$ as:

Hence,

$$\left\langle i \frac{\partial}{\partial t} [d_\sigma^+ d_\sigma] \right\rangle = \sum_{k\alpha s} -V_{k\alpha s, \sigma} \langle c_{k\alpha s}^+ d_\sigma \rangle + V_{k\alpha s, \sigma}^* \langle d_\sigma^+ c_{k\alpha s} \rangle = 0 \quad (3.17)$$

where $\langle c_{k\alpha s}^+ d_\sigma \rangle = -i \int \frac{d\varepsilon}{2\pi} G_{\sigma, k\alpha s}^<(\varepsilon)$ and $\langle d_\sigma^+ c_{k\alpha s} \rangle = -i \int \frac{d\varepsilon}{2\pi} G_{k\alpha s, \sigma}^<(\varepsilon)$. The lesser Green function $G_{\sigma, k\alpha s}^<(\varepsilon)$ and $G_{k\alpha s, \sigma}^<(\varepsilon)$ can be easily calculated by the Dyson expansion and Langreth theorem. In order to calculate the lesser Green function, the contour ordered Green function must be found first. The contour Green function $G_{k\alpha s, \sigma}(t, t')$ is:

$$\begin{aligned} G_{k\alpha s, \sigma}(t, t') &= -iT \langle c_{k\alpha s}(t) d_\sigma^+(t') \rangle \\ &= (-i)^2 T \int d\tau (V_{k\alpha s, \sigma} \langle c_{k\alpha s}(t) c_{k\alpha s}^+(\tau) \rangle \langle d_\sigma d_\sigma^+(t') \rangle + V_{k\alpha s, \bar{\sigma}} \langle c_{k\alpha s}(t) c_{k\alpha s}^+(\tau) \rangle \langle d_{\bar{\sigma}} d_{\bar{\sigma}}^+(t') \rangle) \\ &= T \int d\tau [V_{k\alpha s, \sigma} g_{k\alpha s}(t, \tau) G_{\sigma\sigma}(\tau, t') + V_{k\alpha s, \bar{\sigma}} g_{k\alpha s}(t, \tau) G_{\bar{\sigma}\bar{\sigma}}(\tau, t')] \end{aligned} \quad (3.18)$$

Then, using the Fourier transformation and Langreth theorem, the lesser Green function $G_{k\alpha s, \sigma}^<$

$$G_{k\alpha s, \sigma}^< = V_{k\alpha s, \sigma} (g_{k\alpha s}^r G_{\sigma\sigma}^< + g_{k\alpha s}^< G_{\sigma\sigma}^a) + V_{k\alpha s, \bar{\sigma}} (g_{k\alpha s}^r G_{\bar{\sigma}\bar{\sigma}}^< + g_{k\alpha s}^< G_{\bar{\sigma}\bar{\sigma}}^a) \quad (3.19)$$

In the same way, the lesser Green function $G_{\sigma, k\alpha s}^<$ is:

$$G_{\sigma, k\alpha s}^< = V_{k\alpha s, \sigma}^* (G_{\sigma\sigma}^r g_{k\alpha s}^< + G_{\sigma\sigma}^< g_{k\alpha s}^a) + V_{k\alpha s, \bar{\sigma}}^* (G_{\bar{\sigma}\bar{\sigma}}^r g_{k\alpha s}^< + G_{\bar{\sigma}\bar{\sigma}}^< g_{k\alpha s}^a) \quad (3.20)$$

Substitute Eq.(3.19) and Eq.(3.20) into Eq.(3.17), one can obtain:

$$\begin{aligned} & \sum_{k_{\alpha s}} \int \frac{d\varepsilon}{2\pi} V_{k_{\alpha s},\sigma}^* V_{k_{\alpha s},\sigma} [G_{\sigma\sigma}^r g_{k_{\alpha s}}^<(\varepsilon) + G_{\sigma\sigma}^<(\varepsilon) g_{k_{\alpha s}}^a(\varepsilon)] + V_{k_{\alpha s},\bar{\sigma}}^* V_{k_{\alpha s},\bar{\sigma}} [G_{\sigma\bar{\sigma}}^r(\varepsilon) g_{k_{\alpha s}}^< + G_{\sigma\bar{\sigma}}^<(\varepsilon) g_{k_{\alpha s}}^a] \\ & = \sum_{k_{\alpha s}} \int \frac{d\varepsilon}{2\pi} V_{k_{\alpha s},\sigma}^* V_{k_{\alpha s},\sigma} [g_{k_{\alpha s}}^r G_{\sigma\sigma}^< + g_{k_{\alpha s}}^< G_{\sigma\sigma}^a] + V_{k_{\alpha s},\bar{\sigma}}^* V_{k_{\alpha s},\bar{\sigma}} [g_{k_{\alpha s}}^r G_{\sigma\bar{\sigma}}^< + g_{k_{\alpha s}}^< G_{\sigma\bar{\sigma}}^a] \end{aligned} \quad (3.21)$$

Using the relations: $\sum_{k_{\alpha s}} V_{k_{\alpha s},\sigma}^* V_{k_{\alpha s},\sigma} g_{k_{\alpha s}}^{r,a} = \sum_{\alpha} \mp i \frac{\Gamma_{\alpha}}{2}$, $\sum_{k_{\alpha s}} V_{k_{\alpha s},\bar{\sigma}}^* V_{k_{\alpha s},\bar{\sigma}} g_{k_{\alpha s}}^{r,a} = \sum_{\alpha} \mp i \frac{\Gamma_{\alpha}}{2}$, $\sum_{k_{\alpha s}} V_{k_{\alpha s},\sigma}^* V_{k_{\alpha s},\sigma} g_{k_{\alpha s}}^<(\varepsilon) = i \sum_{\alpha} \Gamma_{\alpha} f_{\alpha}(\varepsilon)$ and $\sum_{k_{\alpha s}} V_{k_{\alpha s},\bar{\sigma}}^* V_{k_{\alpha s},\bar{\sigma}} g_{k_{\alpha s}}^<(\varepsilon) = i \sum_{\alpha} \Gamma_{\alpha} f_{\alpha}(\varepsilon)$. And after some simple algebra, one finds :

$$\begin{aligned} (\Gamma_n^2 - \Gamma_s^2) \int \frac{d\varepsilon}{2\pi} G_{\sigma\sigma}^<(\varepsilon) &= \Gamma_n \left[\sum_{\alpha} -i \Gamma_n^{\alpha} \int \frac{d\varepsilon}{2\pi} f_{\alpha}(\varepsilon) [2 \text{Im} G_{\sigma\sigma}^r(\varepsilon)] - i \Gamma_s^{\alpha} \int \frac{d\varepsilon}{2\pi} f_{\alpha}(\varepsilon) [2 \text{Im} G_{\sigma\bar{\sigma}}^r(\varepsilon)] \right] \\ & - \Gamma_s \left[\sum_{\alpha} -i \Gamma_s^{\alpha} \int \frac{d\varepsilon}{2\pi} f_{\alpha}(\varepsilon) [2 \text{Im} G_{\sigma\sigma}^r(\varepsilon)] - i \Gamma_n^{\alpha} \int \frac{d\varepsilon}{2\pi} f_{\alpha}(\varepsilon) [2 \text{Im} G_{\sigma\bar{\sigma}}^r(\varepsilon)] \right] \end{aligned} \quad (3.22)$$

where $\Gamma_n = \sum_{\alpha} \Gamma_n^{\alpha}$ and $\Gamma_s = \sum_{\alpha} \Gamma_s^{\alpha}$. In Eq.(3.22), we have used the relation $G_{\sigma\bar{\sigma}}^{r,a,<}(\varepsilon) = G_{\sigma\bar{\sigma}}^{r,a,<}(\varepsilon)$ since the spin states are degenerate in QD. In the same way for treating $\langle i \frac{\partial}{\partial t} [d_{\sigma}^{\dagger} d_{\sigma}] \rangle = 0$, with the condition $\langle i \frac{\partial}{\partial t} [d_{\bar{\sigma}}^{\dagger} d_{\bar{\sigma}}] \rangle = 0$, one obtains the relation

$$\begin{aligned} (\Gamma_n^2 - \Gamma_s^2) \int \frac{d\varepsilon}{2\pi} G_{\sigma\bar{\sigma}}^<(\varepsilon) &= \Gamma_n \left[\sum_{\alpha} -i \Gamma_n^{\alpha} \int \frac{d\varepsilon}{2\pi} f_{\alpha}(\varepsilon) [2 \text{Im} G_{\sigma\sigma}^r(\varepsilon)] - i \Gamma_n^{\alpha} \int \frac{d\varepsilon}{2\pi} f_{\alpha}(\varepsilon) [2 \text{Im} G_{\sigma\bar{\sigma}}^r(\varepsilon)] \right] \\ & - \Gamma_s \left[\sum_{\alpha} -i \Gamma_n^{\alpha} \int \frac{d\varepsilon}{2\pi} f_{\alpha}(\varepsilon) [2 \text{Im} G_{\sigma\sigma}^r(\varepsilon)] - i \Gamma_s^{\alpha} \int \frac{d\varepsilon}{2\pi} f_{\alpha}(\varepsilon) [2 \text{Im} G_{\sigma\bar{\sigma}}^r(\varepsilon)] \right] \end{aligned} \quad (3.23)$$

Since the retarded (advanced) Green functions have been solved, the equation of $\int \frac{d\varepsilon}{2\pi} G_{\sigma\sigma}^<(\varepsilon)$ and $\int \frac{d\varepsilon}{2\pi} G_{\bar{\sigma}\bar{\sigma}}^<(\varepsilon)$ can be solved also. The results can be checked by taking the equilibrium limit, i.e. $f_R(\varepsilon) = f_L(\varepsilon) = f(\varepsilon)$

$$\langle n_\sigma \rangle = -i \int \frac{d\varepsilon}{2\pi} G_{\sigma\sigma}^<(\varepsilon) = \int \frac{d\varepsilon}{2\pi} f_\alpha(\varepsilon) [-2 \text{Im} G_{\sigma\sigma}^r(\varepsilon)] \quad (3.24)$$

and

$$\langle d_\sigma^\pm d_\sigma \rangle = -i \int \frac{d\varepsilon}{2\pi} G_{\sigma\sigma}^<(\varepsilon) = \int \frac{d\varepsilon}{2\pi} f_\alpha(\varepsilon) [-2 \text{Im} G_{\sigma\sigma}^r(\varepsilon)] \quad (3.25)$$

The Eq.(3.24) and Eq.(3.25) show that Eq.(3.22) and Eq.(3.23) obey the fluctuation dissipation theorem at equilibrium limit.

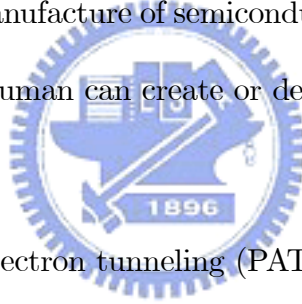
$$\begin{aligned} & \Gamma_n \int \frac{d\varepsilon}{2\pi} G_{\sigma\sigma}^<(\varepsilon) + \Gamma_s \int \frac{d\varepsilon}{2\pi} G_{\bar{\sigma}\bar{\sigma}}^<(\varepsilon) \\ &= \sum_\alpha -\Gamma_n^\alpha \int \frac{d\varepsilon}{2\pi} f_\alpha(\varepsilon) [G_{\sigma\sigma}^r(\varepsilon) - G_{\sigma\sigma}^a(\varepsilon)] - \Gamma_s^\alpha \int \frac{d\varepsilon}{2\pi} f_\alpha(\varepsilon) [G_{\bar{\sigma}\bar{\sigma}}^r(\varepsilon) - G_{\bar{\sigma}\bar{\sigma}}^a(\varepsilon)] \end{aligned} \quad (3.26)$$

$$\begin{aligned} & \Gamma_s \int \frac{d\varepsilon}{2\pi} G_{\sigma\sigma}^<(\varepsilon) + \Gamma_n \int \frac{d\varepsilon}{2\pi} G_{\bar{\sigma}\bar{\sigma}}^<(\varepsilon) \\ &= \sum_\alpha -\Gamma_s^\alpha \int \frac{d\varepsilon}{2\pi} f_\alpha(\varepsilon) [G_{\sigma\sigma}^r(\varepsilon) - G_{\sigma\sigma}^a(\varepsilon)] - \Gamma_n^\alpha \int \frac{d\varepsilon}{2\pi} f_\alpha(\varepsilon) [G_{\bar{\sigma}\bar{\sigma}}^r(\varepsilon) - G_{\bar{\sigma}\bar{\sigma}}^a(\varepsilon)] \end{aligned} \quad (3.27)$$

CHAPTER 4

ELECTRON TRANSPORT THROUGH A DIPOLE-INTERACTION-DOUBLE-DOT SYSTEM UNDER NON-WEAK RESERVOIR COUPLING APPROXIMATION

Due to the progress of the manufacture of semiconductor device and the technique of microscopic experiment, human can create or detect (count) few photons by a semiconductor device[55].



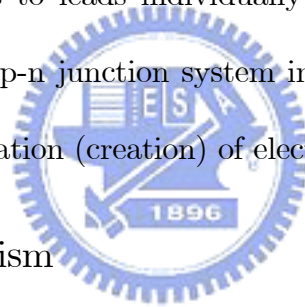
The photon-associated electron tunneling (PAT) through quantum dot (QD) attracts theoretical and experimental researchers in past decades. In a single level QD system, the energy of electron-photon interaction quasi-particle is found as $\varepsilon_{ph}^n = \varepsilon_0 \pm n\omega_{ph}$, where $n \in \text{integer}$ and ω_{ph} is the photon frequency[56]. For a two level QD system interacting with photon via dipole interaction, the electron-photon interaction quasi-particle energy is $\varepsilon_{ph,\pm}^n = (\varepsilon_a - \varepsilon_b \pm \omega_{ph} \pm \Omega_{Rabi})$, where $\Omega_{Rabi} = \sqrt{|\Delta f|^2 + (\varepsilon_a - \varepsilon_b - \omega_{ph})^2}$ is the Rabi frequency and $|\Delta f|^2$ relates to the coupling strength of electron-photon interaction[20]. In theoretical study, most of researchers first solved the electron-photon interaction state and then

coupled the electron-photon interaction state to leads, i.e. they described PAT in QD system by treating the quantum dot state as an electron-photon interaction quasi-particle and coupling the quasi-particle to the leads. This treatment is called weak reservoir coupling approximation[57]. However, the weak reservoir coupling approximation is appropriated only for the case in which the coupling constant of electron-photon interaction is much larger than the tunneling matrix between dot and lead. Under this approximation the electron photon interaction is treated as a main Hamiltonian and tunneling effect is treated as a perturbation. The higher order tunneling effect, such as the Kondo effect and co-tunneling effect, is usually ignored.



When the quantum dot is coupled to lead, the correlation between dot and lead, i.e. the Kondo effect, will appear when temperature of the system is below critical temperature, i.e. Kondo temperature[24]. When temperature is below Kondo temperature, a virtual state is constructed with energy at the vicinity of the Fermi level of lead. The Kondo effect in Anderson impurity model presents a sharp peak of the density of state, which is called the Kondo resonant peak. This Kondo resonant peak is in the vicinity of Fermi level when temperature below the Kondo temperature due to the electron correlation interaction between the electron in QD and lead.

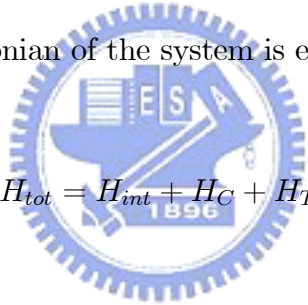
Figure 4.1: Fig.1 The Schematic plot of the system considered in this work. (a) The two-dot system couples to leads individually and interacts each other via dipole interaction. (b) The p-n junction system in which the photon is created (destroyed) by the recombination (creation) of electron-hole pair.



4.1 Model and Formalism

In this chapter, we consider a separate double-dot system in which the two dots interact with each other via photon field as shown in the Fig.4.1 . The conductance due to electron transport through each dot is studied. In order to simplify the problem, we ignore the interdot Coulomb interaction. This is because that the interdot Coulomb interaction just causes the charge energy of system which shifts the energy level of quantum dot and the effect to be described in this work is independent of Coulomb interaction. The neglect of the interdot Coulomb in-

teraction will not affect the main physical feature described in this work. The condition of the system is set as: the corresponding Kondo temperature is lower than the system temperature, hence the Kondo effect will be ignored. We also assume there is only one electron level (the ground state level) in each QD and the coupling constants between QDs and leads are the same ($\Gamma_m^\alpha = \Gamma/2 = 1/2$). The energy difference between QDs can be modulated by a controlling gate between the QDs. The QDs are assumed to interact with each other via photon field within the framework of dipole approximation. The QDs system can emit (absorb) a photon via annihilating (creating) an electron in higher energy QD (the dot2) and creates (annihilates) an electron in lower energy QD (the dot1) simultaneously. The Hamiltonian of the system is expressed as:



$$H_{tot} = H_{int} + H_C + H_T \quad (4.1)$$

where $H_C = \sum_{k_\alpha \in L, R, m \in 1, 2} \varepsilon_{k_\alpha, m} c_{k_\alpha, m}^\dagger c_{k_\alpha, m}$ is the Hamiltonian for the electron in lead, $H_T = \sum_{k_\alpha, m \in 1, 2} V_{k_\alpha, m}^* d_m^\dagger c_{k_\alpha, m} + h.c.$ is the tunneling Hamiltonian, and H_{int} is the Hamiltonian for the interaction region (dot region)

$$H_{int} = H_e + H_{ph} + H_{e-ph} \quad (4.2)$$

$$H_e = \sum_{m \in 1, 2} \varepsilon_m d_m^\dagger d_m$$

$$H_{ph} = \omega b^\dagger b$$

$$H_{e-p} = (M^* d_2^\dagger d_1 b + M d_1^\dagger d_2 b^\dagger)$$

where d_m^+ (d_m) is the creation (annihilation) operator of the electron with state m in QD ($m \in 1, 2$; 1 indicates the lower energy dot (leads) and 2 indicates the higher energy dot (leads)), $c_{k_\alpha}^+$ (c_{k_α}) is the creation (annihilation) operator of electron with momentum k in α lead (where $\alpha \in L, R$) and b^+ (b) is the creation (annihilation) operator of photon. The electron tunneling between the lead and dot is described by the tunneling matrix $V_{k_\alpha s, \sigma}$. The Hamiltonian H_{ep} corresponds to the electron-photon interaction. The electron-photon coupling coefficient $M = -\vec{p} \cdot \vec{E}$, where $\vec{p} = e \langle 2 | \vec{r} | 1 \rangle$, is the electron dipole transition matrix element and \vec{E} is the strength of electric field of the photon field[19]. In order to simplify the model, the tunneling matrix between dots is incorporated into the electron-photon coupling coefficient M . M is assumed to be equal to Γ for the non-weak reservoir coupling limit. In order to avoid the Kondo effect, we consider the case of $U_{inter} \gg (\varepsilon_{F,m} - \varepsilon_m)$ and $(\varepsilon_{F,m} - \varepsilon_m) \gg \Gamma$, where U_{inter} is the interdot Coulomb interaction. In this case the Kondo temperature maybe lower than the system temperature and the Kondo effect may be ignored.

Since the non-weak reservoir coupling is considered in this work, we use the equation of motion method to study the electron-photon interaction and tunneling effect at the same time. Using the equation of motion method, the time evolution of the electron and photon field operators can be expressed as:

$$i\dot{d}_2 = \varepsilon_2 d_2 + M^* d_1 b + \sum_{k_\alpha} V_{2,k_\alpha}^* c_{k_\alpha} \quad (4.3)$$

$$id_2^+ = -\varepsilon_2 d_2^+ - M d_1^+ b^+ - \sum_{k_\alpha} V_{k_\alpha,1} c_{k_\alpha}^+ \quad (4.4)$$

$$id_1 = \varepsilon_1 d_1 + M d_2 b^+ + \sum_{k_\alpha} V_{k_\alpha,1}^* c_{k_\alpha} \quad (4.5)$$

$$id_1^+ = -\varepsilon_1 d_1^+ - M^* d_2^+ b - \sum_{k_\alpha} V_{k_\alpha,1} c_{k_\alpha}^+ \quad (4.6)$$

$$ic_{k_\alpha,m} = \varepsilon_{k_\alpha} c_{k_\alpha} + V_{k_\alpha,m} d_m \quad (4.7)$$

$$ic_{k_\alpha,m}^+ = -\varepsilon_{k_\alpha} c_{k_\alpha,m}^+ - V_{m,k_\alpha}^* d_m^+ \quad (4.8)$$

$$ib = \omega_{ph} b + M d_1^+ d_2 \quad (4.9)$$

$$ib^+ = -\omega_{ph} b^+ - M^* d_2^+ d_1 \quad (4.10)$$

By using Fourier transform and Eq.(4.3), we find the Green function G_{11} satisfies:

$$(\omega - \varepsilon_1 - \Sigma_1^T) G_{11} = 1 + M \langle\langle d_2 b^+; d_1^+ \rangle\rangle \quad (4.11)$$

and $\langle\langle d_2 b^+; d_1^+ \rangle\rangle$ satisfies:

$$\begin{aligned} & (\omega - \varepsilon_2 + \omega_{ph} - \Sigma_2^T) \langle\langle d_2 b^+; d_1^+ \rangle\rangle \quad (4.12) \\ & = M^*(1 + n_{ph}) \langle\langle d_1; d_1^+ \rangle\rangle - M^* \langle\langle d_2 d_2^+ d_1; d_1^+ \rangle\rangle - \sum_{k_\alpha,2} \frac{M^* V_{k_\alpha,2}^*}{\omega - \varepsilon_{k_\alpha,2} + \omega_{ph}} \langle\langle c_{k_\alpha,2} d_2^+ d_1; d_1^+ \rangle\rangle \end{aligned}$$

In this work, the terms with order higher than $|V_{k_\alpha,m}|^2 |M|^2$ will be ignored. Thus, we need to collect the second and the third terms with $M^* |V_{k_\alpha,2}^*|^2$. By the EOM method, we find:

$$\begin{aligned} & \sum_{k_\alpha,2} \frac{M^* V_{k_\alpha,2}^*}{\omega - \varepsilon_{k_\alpha,2} + \omega_{ph}} \langle\langle c_{k_\alpha,2} d_2^+ d_1; d_1^+ \rangle\rangle \quad (4.13) \\ & = -\frac{M^*}{\Delta} \sum_{k_\alpha,2} |V_{k_\alpha,2}^*|^2 \left[\frac{1}{(\omega - \varepsilon_{k_\alpha,2} + \omega_{ph})} - \frac{1}{(\omega - \varepsilon_{k_\alpha,2} + \omega_{ph} + \Delta)} \right] \\ & \quad [(1 - f(\varepsilon_{k_\alpha,2})) G_{11} - \langle\langle d_2 d_2^+ d_1; d_1^+ \rangle\rangle] \quad (4.14) \end{aligned}$$

With the help of the equation $\sum_{k_{1\alpha}} f_{FD}(\varepsilon_{k_\alpha}) \frac{|V_{k_\alpha}|^2}{\omega - \varepsilon_{k_\alpha} + i\delta} = \sum_{\alpha} -\frac{i\Gamma_{\alpha}}{2} - \frac{\Gamma_{\alpha}}{\pi} \ln \frac{[(\omega - \varepsilon_F)^2 + (\pi T)^2]^{1/2}}{|\omega - \varepsilon_F + D|}$

and taking the wideband approximation, the first term is found as:[58]

$$\begin{aligned} & \sum_{k_{\alpha,2}} |V_{k_{\alpha,2}}^*|^2 \left[\frac{1}{(\omega - \varepsilon_{k_{\alpha,2}} + \omega_{ph})} - \frac{1}{(\omega - \varepsilon_{k_{\alpha,2}} + \omega_{ph} + \Delta)} \right] (1 - f(\varepsilon_{k_{\alpha,2}})) \quad (4.15) \\ &= \frac{\Gamma_2}{2\pi} \ln \frac{(\omega - \varepsilon_2^F + \omega_{ph})^2 + (\pi T)^2}{(\omega - \varepsilon_2^F + \omega_{ph} + \Delta)^2 + (\pi T)^2} \end{aligned}$$

In a similar way, one can obtain

$$\begin{aligned} & M^* \langle \langle d_2 d_2^+ d_1; d_1^+ \rangle \rangle \quad (4.16) \\ &= -\frac{M^*}{(\omega - \varepsilon_1 - \Sigma_1^T - 2\Sigma_2^T)} \frac{\Gamma_2}{2\pi} \ln \frac{(\omega - \varepsilon_1 - \varepsilon_2^F + \varepsilon_2)^2 + (\pi T)^2}{(\omega - \varepsilon_1 + \varepsilon_{\varepsilon_2^F} - \varepsilon_2)^2 + (\pi T)^2} G_{11} \end{aligned}$$

Thus,

$$\begin{aligned} & (\omega - \varepsilon_2 + \omega_{ph} - \Sigma_2^T) \langle \langle d_2 b^+; d_1^+ \rangle \rangle \quad (4.17) \\ &= M^* (1 + n_{ph}) G_{11} \\ &+ \frac{\Gamma_2}{2\pi} \left[\frac{M^*}{(\omega - \varepsilon_1 - \Sigma_1^T - 2\Sigma_2^T)} \ln \frac{(\omega - \varepsilon_1 - \varepsilon_2^F + \varepsilon_2)^2 + (\pi T)^2}{(\omega - \varepsilon_1 + \varepsilon_{\varepsilon_2^F} - \varepsilon_2)^2 + (\pi T)^2} \right. \\ &+ \left. \frac{M^*}{\Delta} \ln \frac{(\omega - \varepsilon_2^F + \omega_{ph})^2 + (\pi T)^2}{(\omega - \varepsilon_2^F + \omega_{ph} + \Delta)^2 + (\pi T)^2} \right] G_{11} \end{aligned}$$

Substitute Eq.(4.17) into Eq.(4.12), we obtain Green G_{11} :

$$G_{11} = \frac{1}{(\omega - \varepsilon_1 - \Sigma_1^T) - \frac{|M^*|^2}{(\omega - \varepsilon_1 - \Delta - \Sigma_2^T)} (n_{ph} + 1) - \Sigma_{1a} - \Sigma_{1b}} \quad (4.18)$$

where

$$\Sigma_{1a} = \frac{|M^*|^2 \Gamma_2}{2\pi(\omega - \varepsilon_1 - \Delta - \Sigma_2^T)} \frac{1}{\Delta} \ln \frac{(\omega - \varepsilon_2^F + \omega_{ph})^2 + (\pi T)^2}{(\omega - \varepsilon_2^F + \omega_{ph} + \Delta)^2 + (\pi T)^2} \quad (4.19)$$

$$\Sigma_{1b} = \frac{|M^*|^2 \Gamma_2}{2\pi(\omega - \varepsilon_1 - \Delta - \Sigma_2^T)} \frac{1}{(\omega - \varepsilon_1 - \Sigma_1^T - 2\Sigma_2^T)} \ln \frac{(\omega - \varepsilon_1 - \varepsilon_2^F + \varepsilon_2)^2 + (\pi T)^2}{(\omega - \varepsilon_1 + \varepsilon_2^F - \varepsilon_2)^2 + (\pi T)^2} \quad (4.20)$$

Similarly, the Green function of QD2 can be obtained as:

$$G_{22} = \frac{1}{(\omega - \varepsilon_2 - \Sigma_2^T) - \frac{|M^*|^2}{(\omega - \varepsilon_2 + \Delta - \Sigma_1^T)} n_{ph} - \Sigma_{2a} - \Sigma_{2b}} \quad (4.21)$$

where

$$\Sigma_{2a} = \frac{|M^*|^2 \Gamma_1}{2\pi(\omega - \varepsilon_2 + \Delta - \Sigma_1^T)} \frac{1}{\Delta} \ln \frac{(\omega - \varepsilon_1^F - \omega_{ph})^2 + (\pi T)^2}{(\omega - \varepsilon_1^F - \omega_{ph} - \Delta)^2 + (\pi T)^2} \quad (4.22)$$

$$\Sigma_{2b} = \frac{|M^*|^2 \Gamma_1}{2\pi(\omega - \varepsilon_2 + \Delta - \Sigma_1^T)} \frac{1}{(\omega - \varepsilon_2 - \Sigma_2^T - 2\Sigma_1^T)} \ln \frac{(\omega - \varepsilon_2 - \varepsilon_1^F + \varepsilon_1)^2 + (\pi T)^2}{(\omega - \varepsilon_2 + \varepsilon_1^F - \varepsilon_1)^2 + (\pi T)^2} \quad (4.23)$$

We assume that the lead-dot coupling constant is the same in the considered system. The Green function of QD1 and QD2 can be rewritten as

$$G_{11} = \frac{(\omega - \varepsilon_1^0 - \Delta + i\frac{\Gamma}{2})}{(\omega - \varepsilon_1^-)(\omega - \varepsilon_1^+) + i\Gamma(\omega - \varepsilon_1^0 - \frac{\Delta}{2})} \quad (4.24)$$

$$G_{22} = \frac{(\omega - \varepsilon_2 + \Delta + i\frac{\Gamma}{2})}{(\omega - \varepsilon_2^-)(\omega - \varepsilon_2^+) + i\Gamma(\omega - \varepsilon_2^0 + \frac{\Delta}{2})} \quad (4.25)$$

where

$$\varepsilon_m^\pm = \varepsilon_m + (-1)^{m-1} \frac{\Delta}{2} \pm \frac{\sqrt{\Delta^2 + 4\Sigma_m'^2}}{2}; m = 1, 2 \quad (4.26)$$

$$\Sigma_1'^2 = \frac{\Gamma^2}{4} \quad (4.27)$$

$$\begin{aligned} &+ |M|^2 [(n_{ph}) \\ &+ \frac{\Gamma}{2\pi} \frac{1}{\Delta} \ln \frac{(\omega - \varepsilon_2^F + \omega_{ph})^2 + (\pi T)^2}{(\omega - \varepsilon_2^F + \omega_{ph} + \Delta)^2 + (\pi T)^2} \\ &+ \frac{\Gamma}{2\pi} \frac{1}{(\omega - \varepsilon_1 - \Sigma_1^T - 2\Sigma_2^T)} \ln \frac{(\omega - \varepsilon_1 - \varepsilon_2^F + \varepsilon_2)^2 + (\pi T)^2}{(\omega - \varepsilon_1 + \varepsilon_2^F - \varepsilon_2)^2 + (\pi T)^2}] \end{aligned}$$

$$\begin{aligned}
\Sigma_2'^2 &= \frac{\Gamma^2}{4} \\
&+ |M|^2 [(n_{ph} + 1) \\
&+ \frac{\Gamma}{2\pi} \frac{1}{\Delta} \ln \frac{(\omega - \varepsilon_1^F - \omega_{ph} - \Delta)^2 + (\pi T)^2}{(\omega - \varepsilon_1^F - \omega_{ph})^2 + (\pi T)^2} \\
&+ \frac{\Gamma}{2\pi} \frac{1}{(\omega - \varepsilon_2 - \Sigma_2^T - 2\Sigma_1^T)} \ln \frac{(\omega - \varepsilon_2 - \varepsilon_1^F + \varepsilon_1)^2 + (\pi T)^2}{(\omega - \varepsilon_2 + \varepsilon_1^F - \varepsilon_1)^2 + (\pi T)^2}]
\end{aligned} \tag{4.28}$$

The first term in the square bracket of the term $\Sigma_m'^2$ contains photon number n_{ph} , and is related to the Rabi oscillation effect. The second and third terms which contains the logarithm term relates to the correlation between the m th QD and the m th lead ($m \neq m', m, m' \in 1, 2$), i.e. the correlation of dot and nonconnected-lead. Since the large value of $\varepsilon_m^F - \varepsilon_F$ is chosen, the third term can be ignored.

The physical picture mechanism of the dot-nonconnected-lead correlation can be explained as follow. The electron in dot1 (low energy dot) is excited to dot2 (higher energy dot) with an energy close to $\varepsilon_1^F + \omega_{ph}$ via absorbing a photon and tunneling into lead. Simultaneously, there is an electron in lead2 tunneling into dot2 with energy at vicinity of Fermi energy of lead2 and transits into dot1 via emitting a photon. The main effect of the term $\Sigma_m'^2$ depends on the competition between Rabi oscillation and the dot-nonconnected-lead correlation effect. If the detuning factor Δ (which determinates the strength of the dot-nonconnected-lead correlation) is large, then the term $\Sigma_m'^2$ is dominated by Rabi oscillation effect. In this situation, the correlation between QD and nonconnected-lead can be ignored. The dot-nonconnected-lead correlation is important when the detuning factor Δ is small. There is a critical detuning factor Δ_C which determines the impor-

tance of dot-nonconnected-lead correlation. Besides the frequency of photon filed (the detuning factor), the dot-nonconnected-lead correlation also depends on the temperature. From Eq.(4.27) and Eq.(4.28), it can be expected that the dot-nonconnected-lead correlation will be weak and the self-energy Σ'_m is dominated by the Rabi oscillation effect when temperature is higher than a critical temperature T_C^{ph} . From Eq.(4.19) and Eq.(4.20), it can be expected that the critical temperature T_C^{ph} can be chosen as $\pi T_C^{ph} = |\Delta|$. Hence the dot-nonconnected-lead correlation becomes weak when $T > T_C^{ph}$. From Eq.(4.26), we define the critical detuning factor for the dot-nonconnected-lead correlation. Assume the resonance state corresponding to the dot-nonconnected-lead of dot1 is $\varepsilon_1^{\prime\pm}$. For the case of $|\varepsilon_1^{\prime\pm} - \varepsilon_m| \gg |\Delta|$, the Eq.(4.26) for $\omega = \varepsilon_1^{\prime\pm}$ is

$$(\varepsilon_1^{\prime\pm} - \varepsilon_1)^2 = \Sigma_1^{\prime 2} > 0 \quad (4.29)$$

where the condition $|\Sigma_1^{\prime 2}| \gg |\Delta|$ is used, since $|\Sigma_1^{\prime 2}|$ grows logarithmically at the vicinity of $\varepsilon_1^{\prime\pm}$. Choose $\varepsilon_1^{\prime\pm} = \varepsilon_2^F - \omega_{ph} - \Delta$ which is the singular point of $\Sigma_1^{\prime 2}$ when $T = 0$ and give the positive value of $\Sigma_1^{\prime 2}$. Using the condition $\pi T_C^{ph} = |\Delta_C|$, we determine the critical detuning factor Δ_C as

$$\Delta_C = \frac{\Gamma}{\pi} \frac{|M|^2}{(\varepsilon_2^F - \varepsilon_2)^2 - |M|^2 (n_{ph}) - \frac{\Gamma^2}{4}} \ln 2 \quad (4.30)$$

There is a large value of Δ_C corresponding the condition $(\varepsilon_2^F - \varepsilon_2)^2 - |M|^2 (n_{ph}) - \frac{\Gamma^2}{4} = 0$. From Eq.(4.27), the dot-nonconnected-lead correlation disappears when Δ_C is large. Hence, the condition $(\varepsilon_2^F - \varepsilon_2)^2 - |M|^2 (n_{ph}) - \frac{\Gamma^2}{4} = 0$ is not the solution corresponding to the dot-nonconnected-lead correlation as discussed in case of

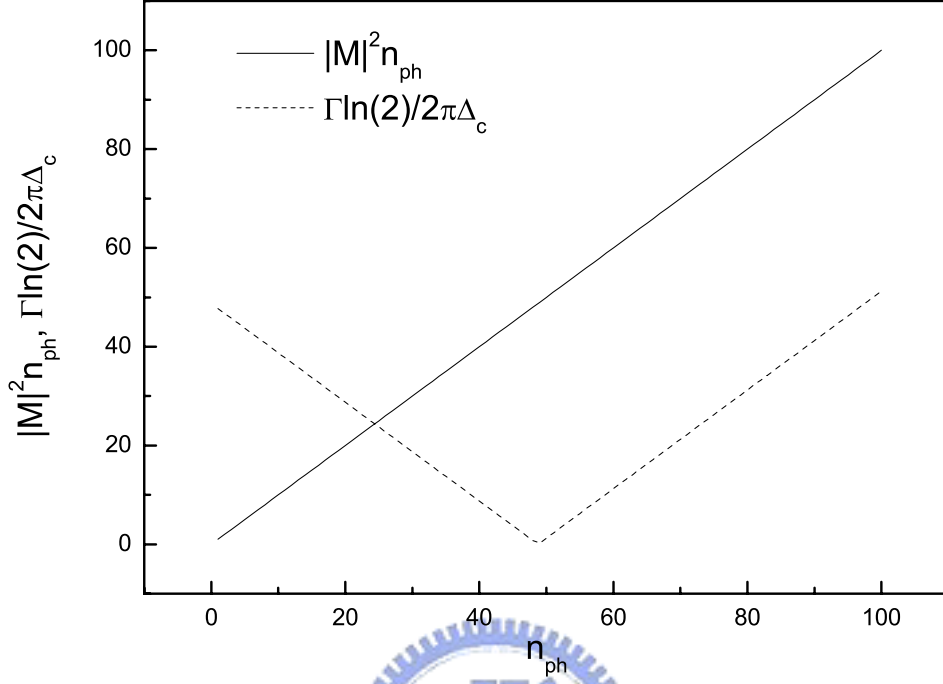


Figure 4.2: The plot of the Rabi oscillation term and dot-non-connected-lead correlation term in Eq.(4.27) with $|M|^2 = \Gamma = 1$ and $(\varepsilon_m^F - \varepsilon_m) = 5$.

large Δ_C . Fig.4.2 shows the plot of Rabi oscillation term ($|M|^2 n_{ph}$) and dot-non-connected-lead term ($\frac{\Gamma}{2\pi} \frac{1}{\Delta} \ln \frac{(\omega - \varepsilon_2^F + \omega_{ph})^2 + (\pi T)^2}{(\omega - \varepsilon_2^F + \omega_{ph} + \Delta)^2 + (\pi T)^2}$) in Eq.(4.27) when $\omega = \varepsilon_2^F - \omega_{ph}$, $\Delta = \Delta_C(n_{ph})$ and $T = T_C$ with versus n_{ph} for the case of $|M|^2 = \Gamma = 1$ and $\varepsilon_m^F - \varepsilon_m = 7\Gamma$. It is obviously that the dot-nonconnected-lead correlation effect is

disappear when $n_{ph} \approx 50$ and Eq.(4.27) is dominated by the dot-nonconnected-leadcorrelation when $n_{ph} \ll 50$ or $n_{ph} \gg 50$. Fig.4.3 shows the spectral func-

tion $A_i(\omega) = -2\text{Im} G_{ii}(\omega)$ for dot1 versus photon number n_{ph} when $T = T_C$ and $\Delta = \Delta_C$. (In follow discussion about the spectral function, the energies of system are set as $\varepsilon_1 = -5$, $\varepsilon_2 = 5$, $\varepsilon_1^F = 2$ and $\varepsilon_1^F = 12$.) Note that the peak corresponding to dot-nonconnected-lead correlation disappears when $n_{ph} = 49$. The detuning factor is inverse proportional to the photon number when the photon number is larger than the one corresponding to the large solution of Δ . For large $|M|^2$, $|\Delta|$ is inverse proportional to the strength of electron-photon interaction and photon number, and T_C will be decreased with the increasing of $|M|^2$ and n_{ph} . The bandwidth Γ due to the tunneling effect between dot and lead is an important quantity in the dot-nonconnected-lead correlation effect. Γ provides a detuning factor to cause the dot-non-connected lead correlation at finite temperature. It can be expected that the critical temperature and detuning is decreased with the decreasing of tunneling bandwidth.

The fig.4.4 shows the spectrum function with various detuning factor Δ for temperature $T = T_c$ for photon number $n_{ph} = 9$. It shows that the dot-nonconnected-lead correlation disappears when $\Delta > \Delta_c$. For $\Delta \leq \Delta_c$ there are two peaks corresponding to the dot-nonconnected lead correlation at the vicinity of Fermi energy of leads which reflect the poles corresponding to dot-nonconnected-lead correlation of Green function. Fig.4.5 shows the spectral function for various temperature. It shows that the QD1-lead2 correlation effect disappears when temperature T (the detuning factor Δ) is higher than the critical temperature T_C (the detuning

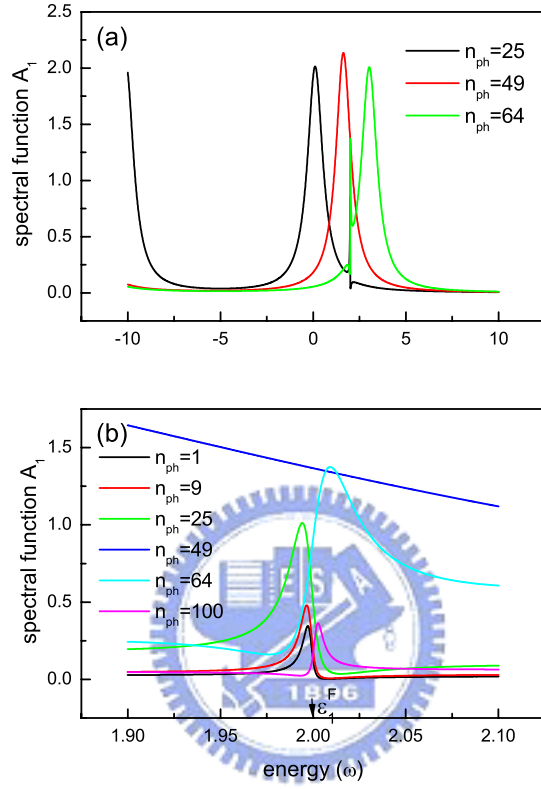


Figure 4.3: The plot of spectral function of dot1 versus photon number n_{ph} . (a) The spectral function includes the Rabi oscillation effect. (b) The detail plot with the energy at the vicinity of $\omega = \varepsilon_1^F$ which is the peak position corresponding to dot-nonconnected-lead correlation

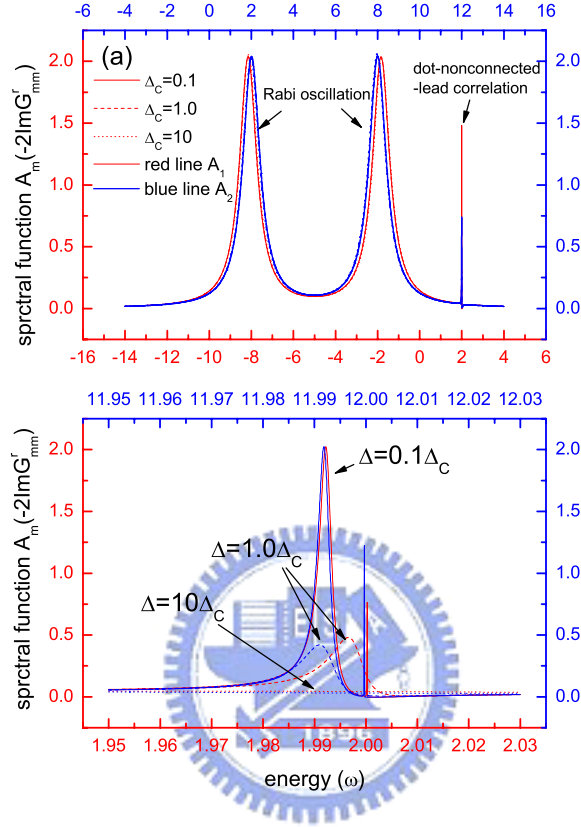


Figure 4.4: The spectral function A_m with various detuning factor for $n_{ph} = 9$ and $T = T_C$. The red (blue) line represent the spectral function of dot1 (dot2). (a) Include the peaks corresponding to Rabi frequency and the dot-nonconnected-lead correlation. (b) The dot-nonconnected-lead peak at the vicinity of Fermi energy of leads.

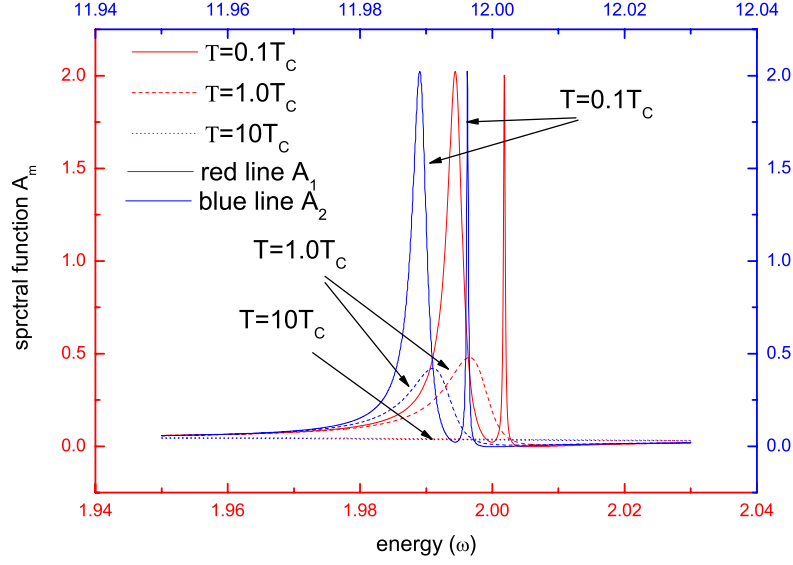


Figure 4.5: The spectral function A_m with various temperature for $n_{ph} = 9$ and $\Delta = \Delta_C$ with energy at vicinity of Fermi energy of leads. The red (blue) line represent the spectral function of dot1 (dot2).

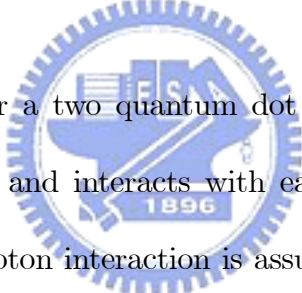
factor Δ_C).

The conductance due to electron transport through dot m is calculated by the equation:

$$g_m = \frac{e^2}{\hbar} \Gamma \int \frac{d\omega}{2\pi} f'_{FD}(\omega) \text{Im} G_m^r(\omega) \quad (4.31)$$

Since the peak height of the spectral function $A_m = -2 \text{Im} G_m^r$ of the QD m -lead m' correlation is dependent on the Fermi level of lead m' , the conductance g_1 contributed from the QD1-lead2 correlation channel is dependent on the Fermi

level of lead1 and lead2. Fig.4.6 shows the conductance of QD1 versus the Fermi level of lead2. The Fermi level of lead2 is modified as $\varepsilon_2^F = \varepsilon_2 + \Delta\varepsilon$. It shows that the peak height of the conductance corresponding to the dot1-lead2 correlation locates at $\varepsilon_1^F = \varepsilon_1 + \Delta\varepsilon$. The conductance with Fermi level of lead1 far away from $\varepsilon_1 + \Delta\varepsilon$ is dominated by Rabi oscillation and is independent of the Fermi level of lead2. Since the image part of self energy is dependent on the energy, the peak height is decreased with increasing of the energy difference from the resonance energy of dot2. One can find that the peak height is decreased with the increasing of $\Delta\varepsilon$ which reflects the energy dependent of the image part of denominator in Eq.(4.24) and Eq.(4.25).



In summary, we consider a two quantum dot system in which each dot is coupled to lead individually and interacts with each other via electron-photon interaction. The electron-photon interaction is assumed in as the dipole approximation. The strength of electron-photon interaction is considered as the same order as the dot-lead coupling, i.e. the weak reservoir coupling approximation is no longer hold. The correlation between quantum dot and non-connected-lead is constructed via the electron-photon interaction and the image part of self-energy is energy dependent. There is a critical temperature $T_C^{ph} = |\Delta|/\pi$ for the dot-nonconnected-lead correlation via dipole interaction in the two-dot system considered in this work. Besides the critical temperature, there is a critical detuning factor Δ_C for the dot-nonconnected-lead correlation. The correlation between dot

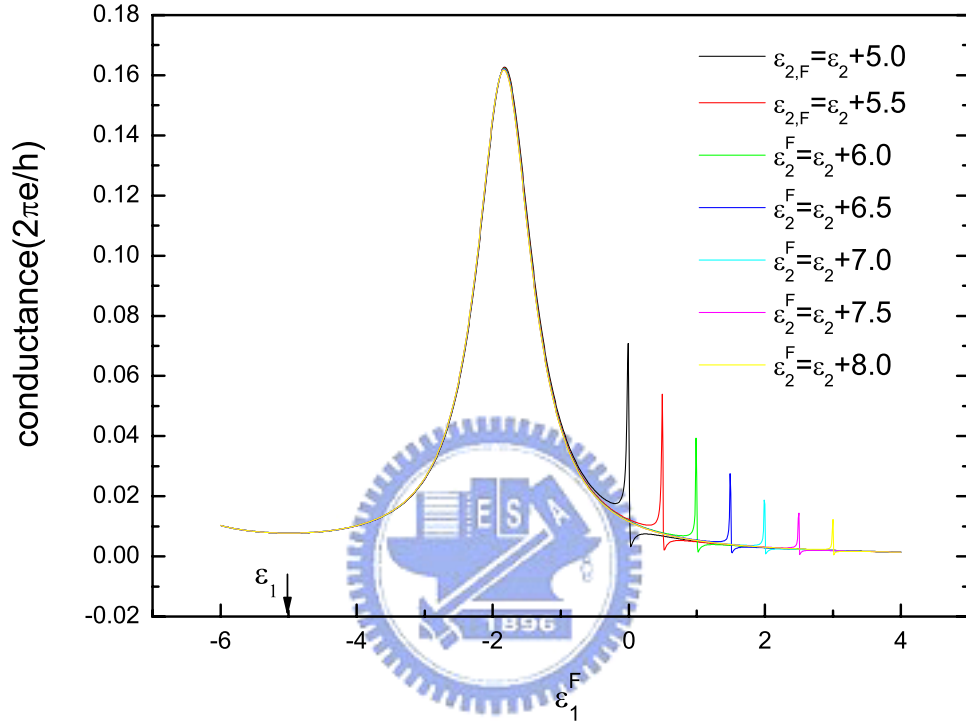


Figure 4.6: The equilibrium conductance (zero bias) for dot1 as function of Fermi energy ε_1^F . The resonant energy of dot1 is set as $\varepsilon_1 = -5$ and dot2 is set as $\varepsilon_2 = 5$. The Fermi energy of lead2 is set as $\varepsilon_2^F = \varepsilon_2 + \Delta\varepsilon$.

and non-connected lead disappears and the interaction between dots is dominated by Rabi oscillation effect mainly when the temperature of the system T is higher than T_C^{ph} or detuning factor Δ is larger than Δ_C . The correlation between dot and non-connected lead is obviously pronounced when T is below T_C^{ph} and Δ is smaller than Δ_C . When the correlation between dot and nonconnected-lead is established, the spectrum function of electron in dot with energy in the vicinity of $\omega = \varepsilon_2^F - \omega_{ph}$ will grow logarithmically. The absolute value of critical detuning factor $|\Delta_C|$ is proportional to the dot-lead coupling constant Γ reflects that the requirement of the strength of dot-lead coupling for the correlation between dot and non-connected lead. The self-energy originated from the dot-nonconnected-lead correlation is small as Γ is small. As shown in Eq.(4.30) absolute value of critical detuning factor $|\Delta_C|$ is inverse proportional to $(\varepsilon_m^F - \varepsilon_m)^2$ for the case of few photon number or is inverse proportional to n_{ph} for the case of large photon number. And the critical temperature T_C^{ph} is defined as $T_C^{ph} = |\Delta|/\pi$. Since the Kondo temperature is exponential decreased with $(\varepsilon_m^F - \varepsilon_m)$, hence, one can find a suitable condition that $T_C^{ph} > T_K$, in which the Kondo effect is disappeared. As the Fig.4.2 shows, for small photon number, the correlation between dot and non-connected lead is important. In the case consider in this work, if the energy difference between dot1 and dot2 is set as $10meV(\sim 2500GHz)$ which is roughly equal to the required energy of photon field, the critical detuning factor Δ_C will be $0.056meV(\sim 14GHz)$, and the critical temperature is $225mK$ for the case of

$n_{ph} = 9$ and $\varepsilon_m^F - \varepsilon_m = 7meV$ as considered in this work. This condition can be achieved easily in experiment. Note that, unlike the Kondo temperature, the critical temperature of dot-nonconnected-lead correlation via dipole interaction is inverse proportional to $(\varepsilon_m^F - \varepsilon_m)^2$. Hence one can choose a suitable Fermi energy of lead that the corresponding Kondo temperature T_K is much smaller than the critical temperature T_C^{ph} so that the dot-nonconnected-lead correlation appears while Kondo effect is nonobvious. In our system, $T_K = 1.7 \times 10^{-4}\Gamma$ and $T_C^{ph} = 0.0018\Gamma$ for $\Delta = \Delta_C$. [23] The key argument in our model is that the dot-lead coupling does not too weak and the electron-photon interaction between dots is not much strong. Since the strength of electron-photon interaction is a trigonometric function of the inter-distance of the dots or the wavelength of photon field, the weak dipole interaction will be implemented by choosing a suitable distance of the dots or the wavelength of the photon field. [59] Furthermore, although we model the dipole interaction between two dots as the electron excitation (decay) and photon absorption (emitting), the system may be constructed in p-n dot junction system embedded in a microcavity as shown in Fig.4.1.(b). The electron decay (excited) process in the two-dot system is replaced by the electron-hole recombination (electron-hole pair creation) in p-n dot junction and the emitted (absorbed) photon.

CHAPTER 5

SUMMARY

In chapter 3, we consider the Anderson model with spin flip associated tunneling in quantum dot system. Under the effect of spin flip associated tunneling, the quantum dot state can be regarded as the original Anderson model quasiparticle state scattered via the normal spin-flip channel and Kondo spin-flip channel. For the temperature higher than the Kondo temperature, the spin-flip scattering is dominated by the normal channel. The normal channel spin-flip scattering enhances the amplitude of spectral function. The diagonal part spectral function is increased (more positive) and off-diagonal part spectral function is decreased (more negative) as the strength of the spin-flip associated tunneling is increased. Since the decrease of the strength of off-diagonal part spectral function is stronger than the increase of the diagonal part, the conductance is thus decreased as the strength of spin-flip associated tunneling effect is increased. When the temperature is below Kondo temperature, the effect of spin-flip associated tunneling is dominated by the Kondo channel. The Kondo channel spin-flip scattering enhances the peak height and causes the blue shift of Kondo resonance peak. The behavior of conductance is dominated by the competition between the peak height enhancement and the blue shift effect. When the spin-flip associated tunneling

is weak, the enhancement of peak height is the main effect. The diagonal part spectral function is increased and stronger than the decrease of the diagonal part as the strength of spin-flip associated tunneling is increased. Hence, the conductance is increased as the strength of spin-flip associated tunneling is increased. When the spin-flip associated tunneling is strong, the blue shift is the main effect. The peak of Kondo resonance is shifted out of the vicinity of Fermi level of lead. Hence the conductance is decreased as the strength spin-flip is increased. The conductance is dominated by the diagonal part spectral function when temperature is higher than Kondo temperature and scattering is dominated by the normal channel. Contrast to the case of temperature higher than Kondo temperature, the conductance is dominated by the diagonal part spectral function when the temperature is lower than Kondo temperature and spin-flip scattering is dominated by the Kondo channel.



In chapter 4, We consider a double-dot system and studied the dot-nonconnected-lead correlation induced by the electron-photon interaction. We find that there is a critical temperature $T_C = |\Delta|/\pi$ and a critical detuning factor Δ_C . The dot-nonconnected-lead is constructed when $T < T_C$ and $\Delta < \Delta_C$ and the spectral function will grow logarithmically at the neighborhood of $\omega = \varepsilon_{2(1)}^F - (+)\omega_{ph}$ for dot 1(2). Owing to the dot-nonconnected-lead correlation, the conductance will be affected by the Fermi level of nonconnected-lead. For example, the conductance due to electron transport between lead1 through dot1 will show a peak corresponding

to the dot-nonconnected-lead correlation at the neighborhood of $\varepsilon_2^F - \omega_{ph}$. The critical detuning factor Δ_C is inversely proportional to the photon number when photon number is large, hence the critical detuning factor and critical temperature are very small when photon number is large.

Acknowledgement 1 This work is supported by the National Science Council of Taiwan under grant numbers NSC 89-2112-M-009-065, NSC 90-2112-M-009-026, NSC 91-2120-M-009-002, NSC 92-2120-M-009-010, NSC 94-2120-M-009-002.



CHAPTER 6

FUTURE WORKS

In the Anderson model with spin-flip tunneling effect, the resonant energy may be shifted to a renormalized energy due to the spin-flip associated tunneling effect. The effect of energy shift will affect the peak position of Kondo resonance peak and modify the conductance. This effect is one of the important effects in FM (ferromagnetic)-dot-FM system [46][47][48][49]. One can compare the effect due to the spin-flip scattering and the energy. Besides, the high temperature Lacroix's decouple scheme is used in this dissertation. As it is well known the high temperature Lacroix's decouple scheme is suitable quantitatively only when the temperature is below the Kondo temperature. For more accurate calculation or lower temperature case, more higher order terms must be included or other more accurate or rigorous methods must be used.

In the electron-photon induced dot-nonconnected-lead correlation effect, the on-site and interdot Kondo effect are not included in our calculation. Although one may choose a suitable condition under which the Kondo effect disappears, however, the study on the competition between the Kondo effect and the electron-photon interaction including dot-nonconnected-lead correlation is absolutely worth to be explored in future.

BIBLIOGRAPHY

- [1] M. A. Reed, J. N. Randall, R. J. Aggarwal, R. J. Matyi, T. M. Moore, and A. E. Wetsel, *Phys. Rev. Lett.* 60 ,535 (1988)
- [2] R.C. Ashoori; *Nature* 379, 413 (1996).
- [3] S. Tarucha, D. G. Austing, T. Honda, R. J. van der Hage, and L. P. Kouwenhoven, *Phys. Rev. Lett.* 77, 3613 (1996); L. P. Kouwenhoven, T. H. Oosterkamp, M. W. S. Danoesastro, M. Eto, D. G. Austing, T. Honda, S. Tarucha, *Science*, Vol 278, 1788, 1997.
- [4] R. C. Ashoori, H. L. Stormer, J. S. Weiner, L. N. Pfeiffer, K. W. Baldwin, and K. W. West ; *Phys. Rev. Lett.* 71, 613 (1993).
- [5] Tokura Y, Kouwenhoven LP, Austing DG, Tarucha S; *Physica B*, 246, 83 (1998).
- [6] Sara M. Cronenwett, Tjerk H. Oosterkamp, and Leo P. Kouwenhoven, *Science* 281, 540 (1998).
- [7] Takeshi Inoshita, *Science* 281, 526 (1998); W. G. van der Wiel, S. De Franceschi, T. Fujisawa, J. M. Elzerman, S. Tarucha, and L. P. Kouwenhoven, *ibid.* 289, 2105 (2000); D. Goldhaber-Gordon, Hadas Shtrikman, D. Mahalu, David Abusch-Magder, U. Meirav, and M. A. Kastner, *Nature (London)* 391, 156 (1998); D. Goldhaber-Gordon, J. Gores, M. A. Kastner, Hadas Shtrikman, D. Mahalu, and U. Meirav, *Phys. Rev. Lett.* 81, 5225 (1998).

- [8] S. Sasaki, S. De Franceschi, J. M. Elzerman, W. G. van der Wiel, M. Eto, S. Tarucha, and L. P. Kouwenhoven, *Nature (London)* 405, 764 (2000).
- [9] Ned S. Wingreen and Yigal Meir, *Phys. Rev. B.* 49, 11040 (1994).
- [10] L. P. Kouwenhoven, N.C. van der Vaart, A.T. Johnson, W. Kool, C.J.P.M. Harmans, J.G. Williamson, A.A.M. Staring, and C.T. Foxon, *Z. Phys. Rev. B* 85, 367 (1991).
- [11] Photon assisted tunneling in quantum dots, edited by W.G. Van Der Wiel, T.H. Oosterkamp, S. De Franceschi, C.J.P. M. Harmans and L.P. Kouwenhoven.
- [12] M. Switkes, C.M. Marcus, K. Campman, and A.C. Gossard, to be published in *Science*, (March 1999).
- [13] L.P. Kouwenhoven, A.T. Johnson, N.C. van der Vaart, C.J.P.M. Harmans and C.T. Foxon, *Phys. Rev. Lett.* 67, 1626 (1991); and *Zeitschrift fur Physik* 85, 381 (1991).
- [14] P. K. Tien and J. P. Gordon, *Phys. Rev.* 129, 647 (1963).
- [15] T. H. Oosterkamp, L. P. Kouwenhoven, A. E. A. Koolen, N. C. van der Vaart, and C. J. P. M. Harmans, *Phys. Rev. B* 78, 1536 (1997).
- [16] D. Sokolovski, *Phys. Rev. B* 37, 4201 (1988); P. Johansson, *Phys. Rev. B* 41, 9892 (1990).
- [17] Antti-Pekka Jauho, Ned S. Wingreen and Yigal Meir, *Phys. Rev. B* 50, 5528 (1994).
- [18] C. L. Foden and D. M. Whittaker, *Phys. Rev. B* 58, 12617 (1998).

- [19] edited by Marlan O. Scully et al. (Cambridge University Press, Cambridge, 1997).
- [20] Ph. Brune, C. Bryder, and H. Schoeller, Phys. Rev. B 56, 4730 (1997); K.C. Lin and D.S. Chuu, Phys. Rev. B 64, 235320 (2001).
- [21] P.W. Anderson, Phys. Rev. 124, 41 (1961).
- [22] Schrieffer J R and Wolff P A, Phys. Rev. 149, 491 (1966).
- [23] F. D. M. Haldane, Phys. Rev. Lett. 40, 416 (1978)
- [24] D. V. Averin and A. N. Korotkov, Zh. Eksp. Teor. Fiz. 97, 927 (1990) [Sov. Phys. JETP 70, 937 (1990)]; C. W. J. Beenakker, Phys. Rev. B 44, 1646 (1991).; Ned S. Wingreen and Yigal Meir, Phys. Rev. B 49 11040 (1994).
- [25] C. Lacroix, J. Phys. F: Metal Phys. 11, 2389 (1981).
- [26] Yigal Meir, Ned S. Wingreen and Patrick A. Lee, Phys. Rev. Lett. 70, 2601 (1993).
- [27] Kicheon Kang and B. I. Min, Phys. Rev. B 52, 10689 (1995).
- [28] Hong-Gang Luo, Ju-Jian Ying and Shun-Jin Wang, Phys. Rev. B 59, 9710 (1999).
- [29] Ned S. Wingreen and Yigal Meir, Phys. Rev. B 49, 11040 (1994).
- [30] T. A. Costi, A. C. Hewson, and V. Zlatic, J. Phys.: Condens. Matter 6, 2519 (1994).

- [31] H.G. Luo, J.J. Ying and S.J. Wang, Phys. Rev. B 59, 9710 (1999).
- [32] Alexander L. Fetter & John Dirk Walecka, Quantum Theory of Many-particle System (McGraw-Hill, 1995), pp.59.
- [33] Joseph L. Briman et al., Quantum Theory of Many-body System (Springer, 1998), p.75.
- [34] Gerald D. Mahan, Many-particle Physics 2nd edition (Plenum Press, 1990), p.85~87.
- [35] G.C. Wick, Phys. Rev. 80, 268 (1950).
- [36] Langreth D.C., in Linear and Nonlinear Electron Transport in Solids, ed. by Devreese J.T., Van Doren E (Plenum, New York).
- [37] P. W. Anderson, Phys. Rev. 124, 41 (1961).
- [38] M. Dax, Semicond. Int. 20, 84 (1997).
- [39] H. X. Tang, F. G. Monzon, Ron Lifshitz, M. C. Cross, and M. L. Roukes, Phys. Rev. B. 61, 4437(2000); X. F. Wang, P. Vasilopoulos, and F. M. Peeters, Phys. Rev. B 65, 165217 (2002).
- [40] B. E. Kane, Nature (London) 393, 133 (1998).
- [41] S. Bandyopadhyay, Phys. Rev. B 61, 13813 (2000).
- [42] F. Guinea, Phys. Rev. B 58, 9212(1998)
- [43] A. V. Akimov, A. V. Scherbakov, D. R. Yakovlev, W. Ossau, L. W.

Molenkamp, T. Wojtowicz, J. Kossut, S. Tatarenko, and J. Cibert, *Physica B* 316–317, 41 (2002).

[44] F. T. Vasko and O. Keller, *Phys. Rev. B* 58, 15666 (1998).

[45] P. Zhang, Q.K. Xue, Y.P. Wang and X.C. Xie, *Phys. Rev. Lett.* 89, 286803 (2002).

[46] N. Sergueev, Qing-feng Sun, Hong Guo, B. G. Wang and Jian Wang, *Phys. Rev. B* 65, 165303 (2002).

[47] J. Martinek, Y. Utsumi, H. Imamura, J. Barnas, S. Maekawa, J. König, and G. Schön, *Phys. Rev. Lett.* 91, 127203 (2003).

[48] Bing Dong, H L Cui, S Y Liu and X L Lei ,*J. Phys.: Condens. Matter* 15 8435(2003).

[49] J. Martinek, M. Sindel, L. Borda, J. Barnas, J. König, G. Schön and J. von Delft, *Phys. Rev. Lett.* 91 247202 (2003).

[50] Jian-Xin Zhu and A. V. Balatsky, *Phys. Rev. Lett.* 89, 286802 (2002).

[51] L. I. Glazman and M. E. Raikh, *Pis'ma Zh. Eksp. Teor. Fiz.* 47, 378 (1988) [*JETP Lett.* 47, 452 (1988)]; Tai Kai Ng and Patrick A. Lee, *Phys. Rev. Lett.* 61, 1768 (1988).

[52] L. Kouwenhoven and L. Glazman, *Phys. World* 14, 33 (2001).

[53] Qing-feng Sun and Hong Guo, *Phys. Rev. B* 66, 155308 (2002).

[54] The temperature interested in ref[26] is in an order of 2 lower than Kondo temperature, however, the temperature considered in our work is about one tenth

of Kondo temperature, Therefore, our decoupling approach should sound reasonable.

- [55] Jelena Vuckovic, David Fattal, Charles Santori, Glenn S. Solomon and Yoshihisa Yamamoto)Appl. Phys. Lett. 82,26 (2003)
- [56] P.K. Tien and J.P. Gordon, Phys. Rev. 129, 647 (1963); C.L. Foden and D.M. Whittaker, Phys. Rev. B 58 12617 (1998); Qing-feng Sun, Jain Wang, and Tsung-han Lin, Phys. Rev. B 58, 13007 (1998).
- [57] D.V. Averin, Yu. V. Nazarov, in Single Charge Tunneling, Vol. 294 of NATO ASI Series B, editrd by H. Grabert and M.H. Devoret (Plenum Press, New York, 1991), Cahp. 6 p.217.
- [58] AlbaTheumann, Phys. Rev. 178, 978 (1969)
- [59] R. G. DeVoe and R. G. Brewer, Phys Rev. Lett. 76, 2049 (1996).



VITA

PERSONAL DATA

Name: Kao-Chin Lin

Brithday: April 23, 1970

PUBLICATION

1. Quantum mechanical approach for photon-associated electron tunneling through a quantum dot, *Physical Review B*, Vol.64, 235320, (2001).
2. Ballistic transport through coupled T-shaped quantum wires *Physica B*, Vol.348, 56-65 (2004).
3. Spin-flip transport through an interacting quantum dot, *Soild state communi-cations*, Vol.134, 831-865 (2005).
4. Anderson model with spin-flip associated tunneling. (will appear in *Physics Review B*).
5. Electron transport through a dipole-interaction-double-dot system under non-weak reservoir coupling approximation (in preparation).

